Nanoscale

REVIEW

View Article Online
View Journal | View Issue

Cite this: *Nanoscale*, 2025, **17**, 4906

NH_2-MIL-125(Ti) and its functional nanomaterials – a versatile platform in the photocatalytic arena

Priyanka Priyadarshini, Anshumika Mishra, Susanginee Nayak and Kulamani Parida *

Titanium (Ti)-based MOFs are promising materials known for their porosity, stability, diverse valence states, and a lower conduction band (CB) than Zr-MOFs. These features support stable ligand-to-metal charge transfer (LMCT) transitions under photoirradiation, enhancing photocatalytic performance. However, Ti-MOF structures remain a challenge owing to the highly volatile and hydrophilic nature of ionic Ti precursors. The discovery of MIL-125 marked a breakthrough in Ti-cluster coordination chemistry. Combining it with NH_2 chromophores to form NH_2-MIL-125 enhanced its structural design and extended its activity into the visible light region. This review delves into the high-performance photocatalytic properties of NH_2-MIL-125, focusing on its applications in H_2O_2 and H_2 production, CO_2 and N_2 reduction, drug and dye degradation, photocatalytic sensors, and organic transformation reactions. The discussion considers the influence of the Ti precursor, coordination environment, synthesis process, and charge transfer mechanisms. Numerous strategic methods have been discussed to improve the performance of NH_2-MIL-125 by incorporating linker modification, metal node modification, encapsulation of active species, and post-modification for enhancing light absorption ability, promoting charge separation, and improving photocatalytic efficiency. Moreover, future perspectives include methods to investigate how the efficiency of NH_2-MIL-125-based materials can be planned in promoting research by highlighting their versatility and potential impacts in the area of photocatalysis.

Received 14th September 2024,
Accepted 2nd January 2025

DOI: 10.1039/d4nr03774j

rsc.li/nanoscale

1. Introduction

The persistent challenges of energy exhaustion and environmental deterioration resulting from excessive fossil fuel use have long troubled humanity, prompting researchers to explore renewable, clean energy sources.[1] Harnessing sustainable solar energy to eliminate pollutants and generate power is widely acknowledged as an efficient and cost-effective strategy for environmental purification and addressing the energy crisis.[2] Mimicking the natural photosynthetic processes of green plants and microorganisms, photocatalysis has emerged as an eco-friendly and energy-efficient method to tackle energy and environmental challenges.[3] After the groundbreaking work of Fujishima and Honda, who utilized TiO_2, a photocatalyst for solar energy conversion, the field has seen significant advancements.[4] Numerous studies have concentrated on inorganic semiconductors, including metal oxides,[5] metal sulfides,[6] graphene,[7] quantum dots,[8] LDH,[9] perovskites[10] *etc.* Recently, the novel semiconductor graphitic carbon has attracted substantial research interest.[11] However, conventional photocatalysts typically suffer from a limited light absorption range, besides also having insufficient active sites and an increased rate of exciton pair recombination, which result in subpar performance. Therefore, there is an urgent need to develop well-grounded, high-performing catalysts that are receptive to light.

Metal–organic frameworks (MOFs), constructed from flexible organic ligands, metal ions, or well-elucidated secondary building units (SBUs), represent an innovative family of porous materials unveiled in the last decade.[12,13] MOFs stand out for their exceptional porosity, expansive surface area, well-ordered crystalline structure, and remarkable customizability, which allows the exploitation of inherent characteristics of organic ligands and metal clusters to produce a wide range of multifunctional MOFs.[14–16] The shape and extent of these organic ligands significantly influence the structure and symmetry of MOFs, while metal clusters impact their chemical stability and functional attributes, enabling the development of multifunctional materials.[17] Research on photoluminescence has indicated that metal clusters within MOFs function as quantum entities of inorganic semiconductors. Organic linkers act as sensing organs that activate the quantum entities through a linker to the metal charge transfer (LCCT) upon exposure to light.[18–21]

Centre for Nano Science and Nano Technology, S 'O' A (Deemed to be University), Bhubaneswar—751 030, Odisha, India. E-mail: kulamaniparida@soauniversity.ac.in, paridakulamani@yahoo.com

Combined with their structural analogy to zeolites, MOFs are promising for photocatalysis, compared with conventional semiconductors. In a MOF structure, the highest occupied molecular orbital (HOMO) of the organic linker can be easily tuned to optimize solar energy absorption. When excited, the electron can be transferred to a specific site within the MOF, such as the metal center or the lowest unoccupied molecular orbital (LUMO) of the organic linker.[22] The crystalline structure enables the optimization of the migration distance for photoexcited charges, with the travel distance and angles being governed by the arrangement of the constituent units.[23] MOFs offer significant advantages in photocatalysis: (i) the crystallinity of MOFs reduces the recombination of photogenerated electron holes (e^-–h^+), as structural defects often found in photocatalytic materials serve as recombination centers.[24,25] (ii) The extensive porosity of MOFs offers supplementary active sites and channels for transporting catalytic substrate, enabling swift transfer and utilization of exciton pairs.[26,27] (iii) MOFs' structural adaptability enables the incorporation of long-range wavelength-absorbing groups (*e.g.*, $-NH_2$) that act as organic bridging ligands. This enhancement broadens the light response spectrum and augments the generation of e^-/h^+ pairs upon illumination.[28] (iv) The adaptable compound structure of MOFs allows their easy integration with compounds like photosensitizers and co-catalysts, forming hetero or Schottky junction architectures. These structures aid in generating and separating photogenerated e^- and h^+.[29,30] Consequently, MOF-based photocatalysts are considered highly promising candidates for real-world applications in photocatalytic technology.

Among the many MOFs, most are built from divalent transition metal ions, resulting in open frameworks with good porosity but often poor stability in aqueous media. Increasing the metal ion charge and polarizing ability strengthens the metal–ligand interaction, enhancing the chemical stability and integrity of the coordination polymer.[31,32] While trivalent metal ions yield porous, water-stable MOFs, tetravalent ion-based MOFs are rare due to the high reactivity of such ions, often leading to oxides or amorphous coordination polymers. Zr(IV) is a notable exception, with UiO-66 (the first Zr-carboxylate MOF featuring a robust hexa-nuclear Zr-oxo-cluster) spurring significant advances in Zr(IV)-MOFs.[33] Higher-valence metals differ from lower-valence ones in their larger charge-to-ionic-radius ratio, making them more reactive and prone to oxygen affinity, resulting in multi-nuclear SBUs with high coordination numbers and greater framework robustness.[34,35] Titanium (Ti), situated immediately above zirconium in the periodic table, represents the ionic form of a typical tetravalent element. However, its significantly reduced ionic radius compared with Zr^{4+} gives Ti a stronger affinity for O_2. TiO_2 exhibits solubility only in immensely acidic conditions (pH < 0), and this stability is transferred to Ti-based MOFs constituting titanium oxo-carboxylate SBUs featuring robust Ti–O covalent bonds.[36] Therefore, titanium as a Ti^{4+} ion presents an appealing option for creating MOFs with excellent chemical stability, redox ability, and photocatalytic properties (Ti^{4+} can undergo photoreduction to Ti^{3+}). These features have led to swift advancement in Ti-based MOFs, with associated studies expanding significantly over the last decade.

Recently, Wei *et al.* developed a new Ti-MOF using an imine condensation-based covalent approach, which maintained the integrity of the titanium cluster structure, leading to enhanced crystallinity and thermal stability. This design reduced the bandgap and shifted the CB, boosting CO_2 reduction efficiency to 46 μmol g^{-1} h^{-1}, outperforming MOF-902.[37] Yao *et al.* synthesized LCU-505, a Ti-MOF incorporating a tetranuclear [Ti_2Tb_2] cluster and a tritopic ligand, combining titanium and terbium to enhance both structural stability and photocatalytic performance. The material exhibited a highly microporous framework with a BET surface area of 882.4 m^2 g^{-1}, providing large void spaces that are well-suited for gas adsorption.[38] Li *et al.* introduced a chelating coordination modulation (CCM) approach for synthesizing Ti-MOF single crystals. By employing chelating ligands, they stabilized the Ti center and controlled the formation of large single crystals with a stable octahedral structure. This method enabled the growth of high-quality Ti-MOFs with customized properties suitable for a range of applications.[39] Garcia-Baldovi *et al.* made a significant advancement in Ti-MOF photocatalysis with the development of MIP-177-LT, a titanium-oxo cluster-based Ti-MOF featuring formate-imprinted active sites. This design facilitated efficient hydrogen production from formic acid, achieving an impressive quantum yield of 22% in the UV region, significantly outperforming TiO_2 P25 in photocatalytic activity.[40] Additionally, a self-assembled TiO_2/Ti-BPDC-Pt heterojunction, constructed *via* surface pyrolytic reconstruction, demonstrated efficient charge separation and achieved high H_2 evolution rates of 12.4 mmol g^{-1} h^{-1}, greatly surpassing the performance of conventional TiO_2- or MOF-based systems.[41] Zhao *et al.* synthesized a 2D Ti-MOF featuring a honeycomb-like structure in which Ni atoms were anchored to Ti(IV)-oxo nodes. This arrangement created an efficient S-scheme charge transfer system when coupled with $BiVO_4$, resulting in a 66-fold enhancement in CO_2 photoconversion compared with pure $BiVO_4$, highlighting its potential for high-efficiency CO_2 reduction.[42] In 2024, Ti-MOF@DATp, a core–shell heterojunction material designed for the simultaneous photocatalytic reduction of U(VI) and oxidation of tetracycline, demonstrated exceptional photocatalytic performance, achieving 96% U(VI) removal and 90% tetracycline degradation. This underscored the multifunctional capability of Ti-MOFs for environmental remediation approaches.[43] Subsequently, the field has evolved gradually yet significantly, integrating new ideas and methodologies relative to other MOF-related research areas.

The identification of the exceptionally porous MIL-125 by Serre and co-workers, made from dicarboxylate linkers and Ti_8 clusters, sparked a surge in Ti-based MOF synthesis and expanded their photocatalytic applications.[44] The well-ordered 3D architecture of MIL-125 includes octahedral and tetrahedral cages—with attainable pore sizes of 12.55 and 6.13 Å, respectively. The MOF exhibits increased photonic sensitivity owing to the nature of titanium-oxo clusters, highlighting the ability of Ti-based MOFs for photocatalytic applications. This

titanium-based MOF stands out owing to exceptional adsorption, thermal stability, and the capacity to incorporate highly dense immobile Ti-sites within the porous framework.[45] However, a wide band gap (E_g ~ 3.72 eV) restricted its functions to the Ultraviolet (UV) spectrum.[44] Incorporating N-atoms by introducing –NH_2 groups to the organic linker narrows the photocatalyst's E_g and prevents crystal structure deterioration.[46] Fu and co-workers applied this strategy to engineer MIL-125 for UV photoresponse by substituting 2-amino terephthalate (NH_2-BDC) for BDC, creating the visible-light active NH_2-MIL-125.[47] NH_2-MIL-125(Ti) is attractive owing to its noticeable visible-light response, availability, and nontoxicity.[48] Composed of cyclic octamers of TiO_2 and ATA linkers, it is isostructural with MIL-125(Ti).[49] The –NH_2 group induces an LMCT band structure, enhancing light absorption,[50] with an auxiliary transition band up to 550 nm, extending its visible light activity.[51] The superior electron-donating characteristics of aromatic functional groups lead to the splitting of the valence band (VB) into a higher-energy occupying state. In contrast, the conduction band (CB), consisting of 2p and 3d orbitals of O and Ti, respectively, remains unaffected. This alteration leads to a narrower bandgap, extending the photocatalyst's photoresponse into the visible light spectrum.[50] NH_2-MIL-125(Ti), one among the initial Ti-based MOFs, was explored in photocatalysis, with applications in hydrogen generation,[52] organic pollutant degradation,[53] and CO_2 reduction.[54–56] It exhibits an E_g spanning from 2.5 to 2.6 eV (theoretical), making it highly suitable for visible-light semiconductor applications.[57] However, similar to most single-component photocatalysts, NH_2-MIL-125(Ti) faces challenges such as limited light response and high charge carrier recombination rates. Additionally, MOFs' poor stability and low electronic conductivity restrict their photocatalytic applications.[51] To surpass these constraints and enhance efficiency, the construction of heterojunction by integrating Ti-MOFs with other functional nanomaterials has gained traction.[50] This strategy can enhance the charge carrier's transfer rate, minimize the recombination, and boost overall light absorption intensity by pairing the MOF with narrow-band-gap semiconductor materials.[58–62] Furthermore, as a porous material, NH_2-MIL-125(Ti) can act as an adhesion carrier for other semiconductors, enhancing specific surface area and reducing composite agglomeration.[63] This porous structure facilitates charge conduction and reactive substance movement, such as pollutant or CO_2 molecule mass transfer.

Over the past twenty years, there has been a proliferation of MIL-based photocatalysts, with significant emphasis on materials based on NH_2-MIL-125(Ti). These materials have been engineered for applications such as CO_2 reduction, water splitting, pollutant degradation, and organic transformation, leveraging their efficient absorption of visible light and robust stability.[60,64,65] Numerous reviews have consolidated the applications of Ti-MOF-based photocatalysts.[66] Assi *et al.* highlighted the key Ti-MOFs and their potential photoredox capabilities,[67] while Yuan *et al.* comprehensively reviewed the structural arrangements, characteristics, and diverse applications of Ti-MOFs.[68] These extensive works highlight the rapid development and significant potential of MOF-based photocatalysts. However, no review has focused entirely on NH_2-MIL-125(Ti)-based semiconductor photocatalysts. Due to undefined bottlenecks in photocatalysis and outdated or incomplete reports on NH_2-MIL-125(Ti)-based photocatalysts, there is an urgent need for a comprehensive and timely systematic review on this topic. In this review, we comprehensively outline recent significant advancements in NH_2-MIL-125(Ti) MOFs, particularly the role they play in the photocatalytic arena and related mechanisms. This review discusses unique topological structures, synthetic routes of NH_2-MIL-125(Ti) MOF, and various strategies to enhance photocatalytic efficiency. Moreover, it tackles significant challenges in ongoing research and outlines prospects for future investigations. Besides establishing a foundational repository for NH_2-MIL-125(Ti), this comprehensive review also seeks to steer the blueprint and synthesis of Ti-based MOFs through an analysis of current frameworks. This methodology is poised to foster the exploration and advancement of more sophisticated MOF materials with possible applications within the discipline of photocatalysis. Scheme 1 illustrates the road map of the advancement of NH_2-MIL-125(Ti) and its functional nanohybrid materials in the photocatalytic arena.

2. Chemistry behind titanium cations

Synthesizing Ti-based MOFs remains a highly challenging endeavor in the MOF research field, with reported Ti-based MOFs being relatively scarce compared with those involving other metals, which have only been recently discovered. This scarcity can be attributed to the unique chemistry behind Ti-cations and the specific Ti-based complexes utilized as Ti precursors in MOF preparation. In this section, we aim to go deeper into the core issues surrounding the role played by titanium in MOF synthesis, present our perspective as to why titanium is less explored, and discuss how researchers are overcoming these challenges to produce more efficient Ti-MOFs.

The Ti(IV) ion is the most thermodynamically favored oxidation state, whereas Ti(III) can survive under reducing conditions, although it rapidly reverts to Ti(IV) when exposed to oxygen. However, Ti(IV) is susceptible to spontaneous hydrolysis in the presence of water, whether residual in solvents, intentionally added, or generated *in situ* during the reaction. This typically results in the formation of hefty multinuclear Ti-oxo clusters as secondary building units (SBUs), such as the octamer in MIL-125, along with the formation of amorphous TiO_2, even in highly acidic conditions. Due to its low electronegativity and high polarizability, TiO_2 can partially block the pores of the formed MOFs. The robust stability of TiO_2 makes it difficult to react with organic linkers, hindering the continuous formation of MOF architectures. This is illustrated in the titanium Pourbaix diagram (Fig. 1a), where Ti(IV) oxide predominates, and soluble molecular species are observed only in extremely acidic environments (pH < 0).[67] Selecting the appropriate titanium precursor and complexing ligand, along with

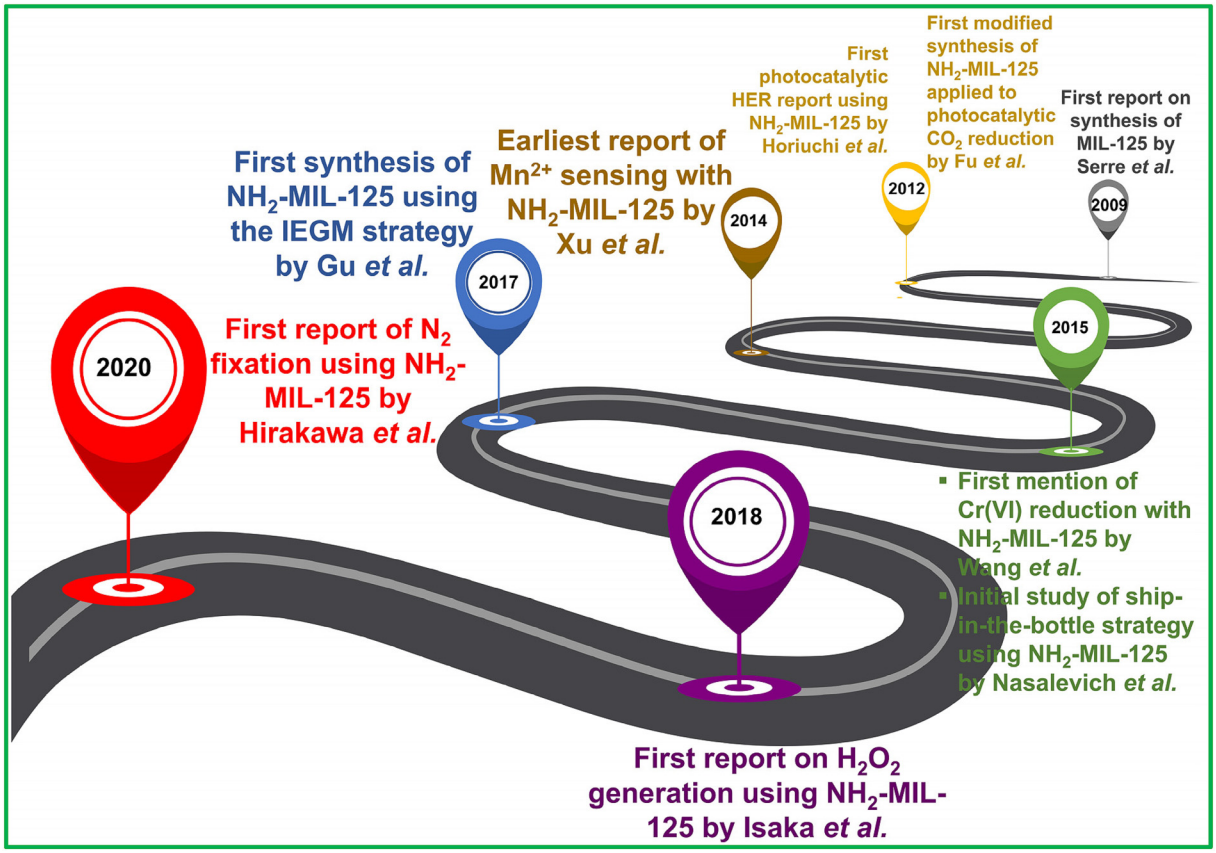

Scheme 1 Timeline of the advancement of NH_2-MIL-125(Ti) and its functional nanomaterials in photocatalysis to date.

the control of the pH of the media and the maintenance of a water-free condition, is critical for stabilizing Ti(IV) in solution and maintaining its reactivity. This shows that the greatest barrier in the field lies in maintaining a fine balance between stability and reactivity while working with titanium.

The titanium alkoxides, or $Ti(OR)_4$ (where R is an alkyl group), are the most frequently employed Ti precursors for MOF preparation. Hydrophobic alkoxy groups and steric hindrance reduce Ti^{4+} hydrolysis, with reactivity adjustable by altering the alkoxy chain.[66] Among these alkoxides, titanium isopropoxide ($Ti(iOPr)_4$) is frequently used for Ti-MOF synthesis as opposed to $TiCl_4$, which is highly volatile and produces a white mist of TiO_2 and HCl when exposed to humid air. Because of its vigorous hydrolysis and rapid release of HCl under optimal conditions, the use of $TiCl_4$ is uncommon.[71] In contrast, $Ti(iOPr)_4$, featuring hydrophobic alkoxide ligands attached to titanium centers, exhibits greater stability in air. Furthermore, Ti cations can form complexes with a variety of additional ligands (such as β-diketonates, carboxylates, phosphonates, catecholates, *etc.*), which, due to their bidentate nature, increase the coordination number and thereby enhance the stability of these species in aqueous environments. To prevent hydrolysis and improve the handling of the active titanium source, the entire synthesis process must be conducted in an inert glove box, presenting challenges for the overall procedure. As a result, while this approach is effective for synthesizing Ti-MOFs, its complexity has limited its widespread adoption. Alternatively, pre-forming Ti-oxo clusters can decelerate the nucleation and crystal formation reaction, thereby preventing hydrolysis. These clusters can either maintain their original structure or undergo rearrangement through association or dissociation during MOF synthesis.[72] The fact that Ti ions can exist in multiple oxidation states (Ti^{4+}/Ti^{3+}) and coordinate with a broad range of ligands only adds to the versatility of Ti in MOF chemistry.[67] From our perspective, the tendency of Ti-precursors to be unstable and extremely reactive represents an open question in the field. Substantial advances have been achieved in stabilizing Ti(IV) in solution by using conditions such as moisture-free conditions and inert atmospheres or by forming Ti-oxo clusters pre-synthesis to slow down hydrolysis kinetics. Much work, however, remains to be done to optimize these processes.

3. Coordination behavior of titanium ions

In designing and tailoring MOF structures and functions, understanding the coordination habits of metal ions—specifically how they coordinate with oxygen from carboxylates to

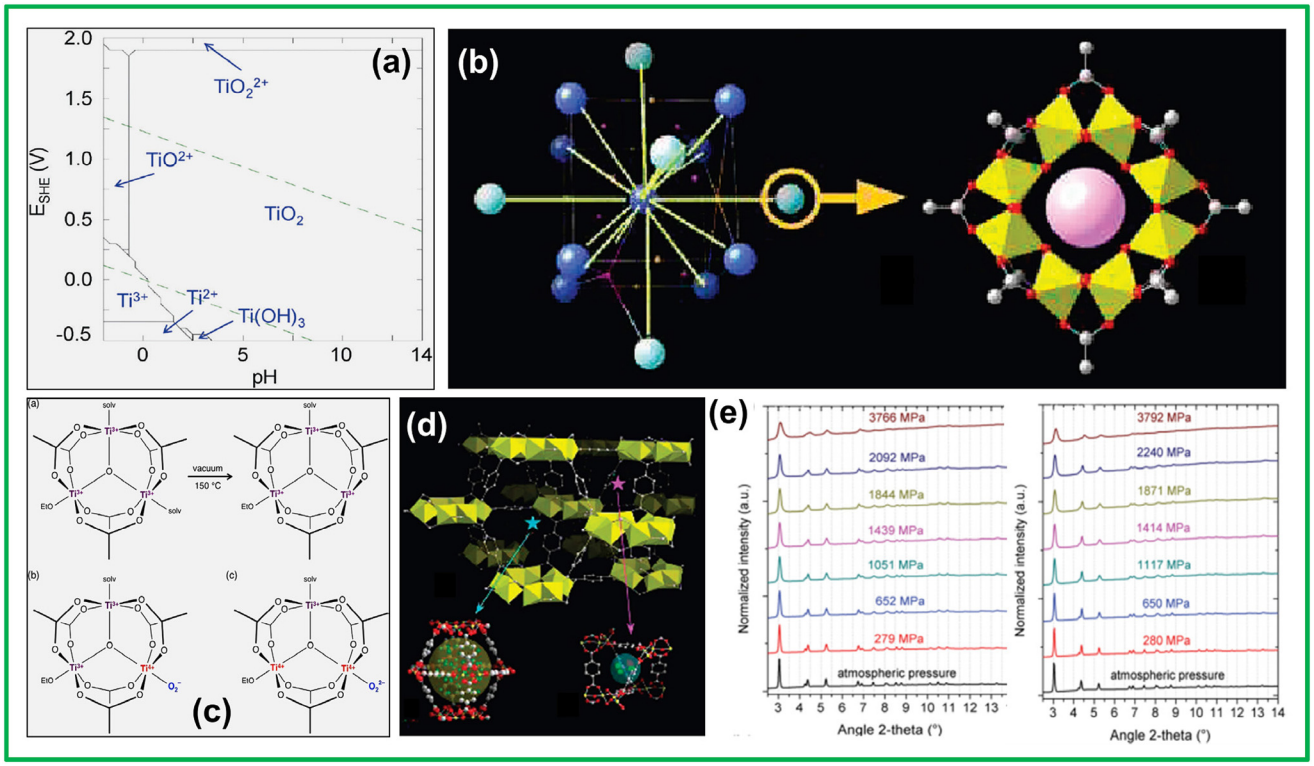

Fig. 1 (a) Pourbaix diagrams of titanium calculated for $[Ti^{4+}] = 10^{-3}$ mol L^{-1} at 25 °C using the Hydra and Medusa software. Green dashed lines: O_2/H_2O and H_2O/H_2 redox couples. Reprinted with permission from ref. 67. Copyright 2017 The Royal Society of Chemistry. (b) The perspective view of a centered cubic (cc) arrangement and the 12-fold coordination is shown by yellow lines. Purple and orange dots indicate the positions of the centers of the tetrahedral and octahedral vacancies and the view of the perforated cyclic octamer with edge- and corner-sharing Ti octahedra; it corresponds to the atom with an orange circle of the classical cc packing through the SBU augmentation. Reprinted with permission from ref. 47. Copyright 2009 American Chemical Society. (c) Illustration of the proposed composition of the Ti_3O clusters in 1 after heating at 150 °C under vacuum, reacting with O_2 to form titanium(IV) superoxide, and reacting with O_2 to form titanium(IV) peroxide. Reprinted with permission from ref. 69. Copyright 2015 American Chemical Society. (d) Perspective view of MIL-125 with the central octamer surrounded by 12 others; the pink and blue stars indicate the centers of the tetrahedral and octahedral vacancies in MIL-125, ball and stick representation of the octahedral vacancy, filled by water molecules (in green); the large yellow sphere represents the effective, accessible volume of the cage, and the tetrahedral vacancy. Reprinted with permission from ref. 47. Copyright 2009 American Chemical Society. (e) Powder X-ray diffraction patterns (λ = 0.694120 Å) were obtained for MIL-125(Ti) and NH_2-MIL-125(Ti) as a function of the applied pressure at room temperature. Reprinted with permission from ref. 70. Copyright 2015 The Royal Society of Chemistry.

form M–O–C clusters SBUs—is crucial for predicting topologies and structures.[73] The coordination geometry can vary significantly with different reaction systems. Titanium oxo clusters with nuclearities ranging from 2 to 52 have been observed, reflecting the challenges in controlling Ti ion chemistry.[33] Ti (IV) typically forms octahedrally coordinated TiO_6 units linked by μ_2-O or μ_3-O atoms, ensuing in variable Ti-oxo clusters. These clusters can vary even with a similar organic ligand under dissimilar synthetic environments. For instance, the $Ti_8O_8(OH)_4$ cluster in MIL-125 or NH_2-MIL-125 markedly differs from the $Ti_3(\mu_3\text{-O})$ cluster in its polymorph Ti-MIL-101. Such observations highlight the unpredictability and complexity associated with the working of Ti as a node in MOF structures.

One of the salient aspects of Ti-MOFs is their propensity to maintain very high symmetry, especially that of *in situ*-formed Ti-oxo clusters during solvothermal procedures. Most titanium cores, such as $Ti_8O_8(OH)_4$ of MIL-125/NH_2-MIL-125 and $Ti_3(\mu_3\text{-O})$ of Ti-MIL-101/Ti-MIL-100, exhibit high symmetry, laying the foundation for extremely symmetrical MOFs with arranged pore structure or channels (Fig. 1b and c).[47,69] These symmetrical structures represent a unique advantage of Ti-MOFs, as they offer both stability and versatility that can be fine-tuned to specific applications.

4. Structure of NH_2-MIL-125

When Ti cations react with polydentate carboxylate acids, they form massive Ti-oxo-carboxylate clusters characterized by high coordination numbers and nuclearity, leading to the diverse arrangement of the resulting Ti-MOFs. These clusters form due to the incomplete hydrolysis and subsequent polycondensation of metal forerunners, with H_2O derived through esterification of the carboxylate entity (not a part of the reaction) with alcohols, that is established from reacted Ti-alkoxides (*in situ*)

or deliberately added to solvent ones. The resulting clusters are composed of TiO_6 octahedra that are edge- and corner-sharing, interconnected through carboxylate linkers. This mechanism suggests that cluster formation is key to understanding the unique structural properties and functions of titanium-based MOFs like NH_2-MIL-125. The reactivity of titanium ions, their coordination preferences, and the behavior of precursor molecules all influence the resulting structure and material properties. This interplay defines the chemistry between titanium and organic ligands, determining the framework's strength and flexibility.

In 2009, Serre and colleagues reported the earliest porous crystalline carboxylate-based titanium-MOF, *i.e.*, MIL-125, which was tuned *via* a quick solvothermal approach.[47] The MIL-125 structure comprised $Ti_8O_8(OH)_4(COO)_{12}$ octamers (cyclic), comprising edge- and corner-sharing $TiO_5(OH)$ octahedra interconnected using ATA linkers (Fig. 1d). These SBUs were arranged in a centered cubic (cc) pattern, forming a quasi-cubic tetragonal lattice with an individual octamer having 12 adjacent SBUs. MIL-125(Ti) exhibited a rigid 3D interrelated porosity with two kinds of micropores, measuring 6 and 12.5 Å. Subsequently, the NH_2-functionalized correspondent NH_2-MIL-125 was efficaciously produced using the same linker, H_2ATA.[74] The inclusion of $-NH_2$ moieties in the organic ligands was unable to alter the MOF framework, and NH_2-MIL-125 was isostructural with the pristine MOF. The surface areas (BET & Langmuir) of NH_2-MIL-125 were 1302 and 1719 $m^2\ g^{-1}$, respectively, which were less than the theoretical value for the parent MIL-125(Ti) (approximately 2140 $m^2\ g^{-1}$). This reduction was probably a result of partial pore obstruction by the free ligand. Introducing functional groups such as $-NH_2$ to the organic ligands improved the chemical stability of the material. NH_2-MIL-125 was more stable to humidity than MIL-125, owing to the intramolecular hydrogen bonds between the amino groups and carboxylate oxygen atoms. This added stability may extend its applications into environments with varying moisture and temperature.

Furthermore, Yot *et al.* explored the framework practices of MIL-125 and aminated-MIL-125 under external stress using high-pressure PXRD (3.5 GPa) (Fig. 1e).[70] The materials exhibited a gradual and reversible reduction in crystallinity when subjected to pressure. This type of MOF material can incorporate a high density of immobilized Ti sites within porous structures and form isostructural MOFs, whose photoresponsive efficiency can be readily adjusted by integrating BDC derivatives. The potential for NH_2-MIL-125 to integrate a high density of immobilized Ti sites into its porous structure is significant for photocatalytic applications. The organic linkers can be adjusted to optimize the role played by titanium as an active site, thus allowing fine-tuning of Ti-MOFs for specific catalytic processes.

5. Synthesis procedures

The direct preparation of NH_2-MIL-125(Ti) is predominantly conducted through traditional hydrothermal or solvothermal methods. This approach involves dissolving or dispersing organic ligands and Ti precursors in appropriate solvents, which are then placed in a PTFE-lined steel autoclave or a sealed Pyrex vessel and thermally treated under high pressure for a duration that can range from several hours to days.

Initially, hydrothermal techniques were used to develop a range of titanophosphates[75–77] and oxalatotitanates,[78] although most of these were nonporous materials. Among these, the first porous Ti-MOF, MIL-91,[77] was notable. Serre and his team successfully produced the renowned prototypical titanium-MOF, MIL-125, in 2009. This synthesis marked the creation of the first-ever titanium-carboxylate-based MOF with high crystallinity and porosity, accomplished through a solvothermal method.[47] In this synthesis, $Ti(iOPr)_4$ reacted with terephthalic acid in a solvent blend of DMF and methanol at 423 K for 15 hours, resulting in a highly crystalline white powder identified as MIL-125(Ti). Perhaps the greatest drawback with MIL-125 is that it degrades fairly readily under extreme conditions (*e.g.*, high moisture and temperature variation). There lies the potential for even newer, more stable constructions, just as easily accessible from the laboratory bench, with comparable or even superior durability. The NH_2-functionalization of the MIL-125(Ti), denoted as NH_2-MIL-125 (Ti), is a good example of how minor modifications can improve its properties. It was synthesized by substituting terephthalic acid with 2-amino terephthalic acid in a comparable solvothermal procedure.[74]

The optimal selection of solvent is critical as it significantly impacts the crystallinity of the end products, often requiring a trial-and-error method to identify the optimal solvent combination. For example, although NH_2-MIL-125 can be synthesized with DMF and methanol, the material's properties can vary dramatically depending on the precise solvent ratio and conditions applied. This brings out a point: although solvothermal synthesis is very effective for most purposes, it is less accurate and reproducible compared with newer, more controlled methods.

The reaction mixture's pH impacts the organic linker's deprotonation process and affects the metal ions' coordination geometry. The ideal pH range favors the development of well-organized crystalline structures, while extreme pH values result in amorphous or less crystalline materials. Furthermore, the concentration of reactants is a critical factor in shaping the morphology of the resulting MOFs. For instance, regulating the concentration of the preliminary solution can change the morphological structure of NH_2-MIL-125 microcrystals from spherical dishes to octahedra (Fig. 2a).[79] The solvothermal reaction's length impacts the crystal development and the material's ultimate morphology. Prolonged reaction periods typically produce larger, well-structured crystals, while reduced time frames result in smaller, underdeveloped ones. This indicates that small changes in reactant concentrations and reaction conditions can significantly affect material properties, making careful optimization crucial.

While the solvothermal technique is the most predominant approach used for producing Ti-MOFs, optimizing conditions

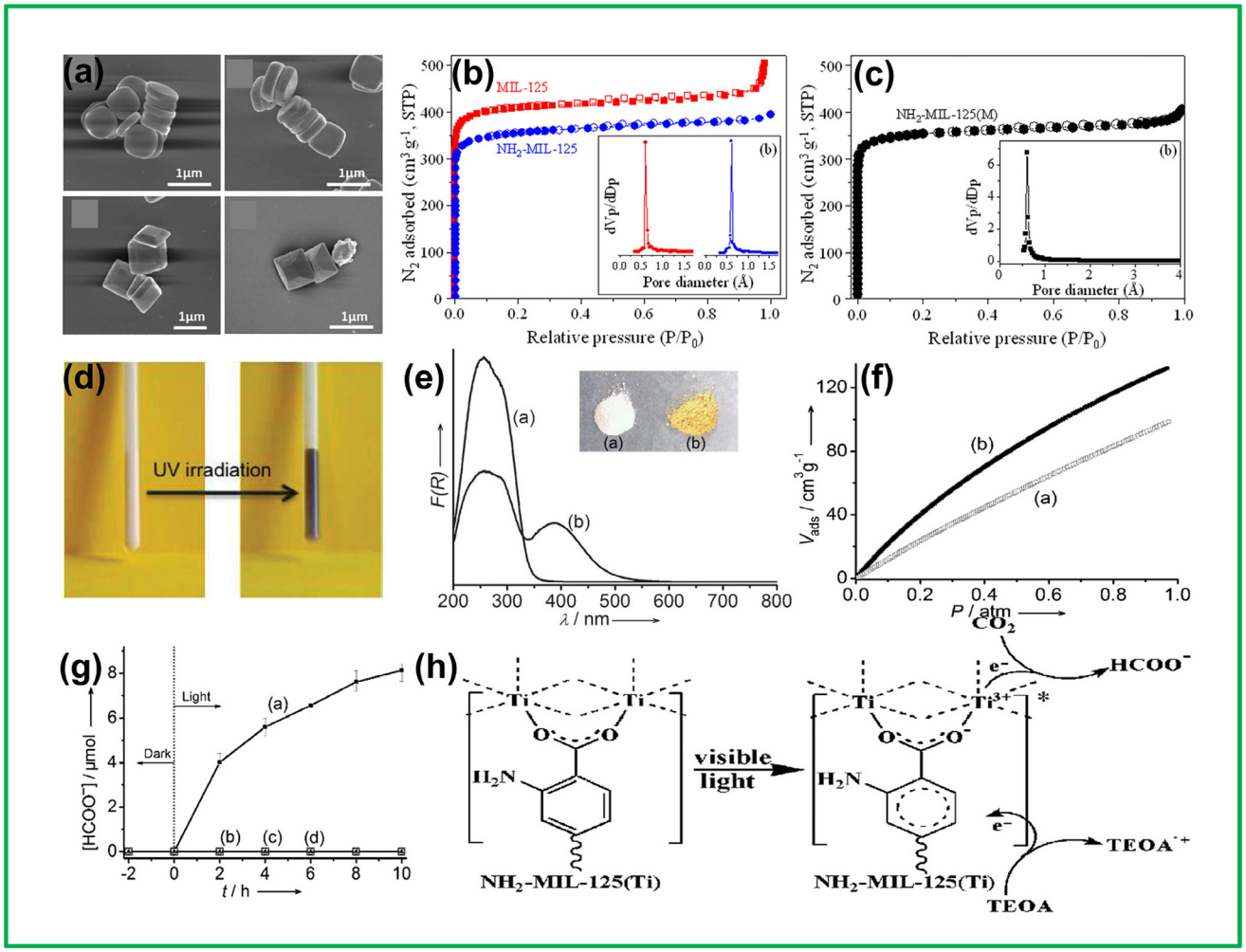

Fig. 2 (a) SEM images of NH_2-MIL-125(Ti) crystals synthesized with different total solvent volumes: 40 mL, 30 mL, 20 mL, and 15 mL. Reprinted with permission from ref. 79. Copyright 2014 The Royal Society of Chemistry. (b) N_2 adsorption–desorption isotherms at 77 K and (c) HK pore size distribution curves of MIL-125, NH_2-MIL-125, and NH_2-MIL-125(M) samples. Reprinted with permission from ref. 80. Copyright 2012 Elsevier B.V. (d) View of MIL-125 in a capillary filled with benzyl alcohol before and after UV irradiation. Reprinted with permission from ref. 47. Copyright 2009 American Chemical Society. (e) UV/Vis spectra of MIL-125(Ti) and NH_2-MIL-125(Ti). The inset shows the samples. (f) CO_2 adsorption isotherms (1 atm, 273 K) of MIL-125(Ti) and NH_2-MIL-125(Ti). (g) The amount of $HCOO^-$ produced as a function of the time of irradiation over NH_2-MIL-125(Ti) (■), MIL-125(Ti) (□), a mixture of TiO_2 and H_2ATA (○), and visible light irradiation without a sample (▲). (h) Proposed mechanism for the photocatalytic CO_2 reduction over NH_2-MIL-125(Ti) under visible light irradiation. Reprinted with permission from ref. 50. Copyright 2012 Wiley-VCH Verlag GmbH & Co.

for large-scale production remains a challenge. Hence, in addition to the conventional solvothermal approach, alternative technologies such as microwave[80,81] and ultrasonic[82] procedures have been employed for the facile fabrication of Ti-MOFs with high porosity. These techniques accelerate the process of crystallization, leading to reduced reaction times and temperatures. Ti-MOFs synthesized using these alternative approaches often exhibit varied particle shapes and sizes, which can significantly impact their characteristics. For instance, the rapid heating capability of microwave procedures was first used to formulate NH_2-MIL-125 through a solvothermal scheme.[80] This approach decreased the reaction time from 16 hours, typical in traditional solvothermal methods, to just 1 hour using microwave heating. PXRD confirmed that the resulting powders were phase-pure, with a typical particle size of 0.7 mm, which was less than that obtained *via* the solvothermal method. The lowering in particle size was attributed to the shortened reaction duration limiting particle growth and the speedy nucleation powered by the thermal process. The BET surface area of NH_2-MIL-125(M) was determined to be 1492 $m^2\ g^{-1}$, with a pore volume of 0.66 $cm^3\ g^{-1}$, compared with 1469 $m^2\ g^{-1}$ and 0.65 $cm^3\ g^{-1}$, respectively, for NH_2-MIL-125 (Fig. 2b and c). The smaller particle sizes indicated for these samples could mean that microwave synthesis might provide more control of particle size, but increased defect density or less structural integrity may also come with some downsides. In this regard, there is often a balance to strike between speed and material quality.

Ultrasonication generates and disintegrates bubbles within the solvent, creating localized high temperatures and pressures that lead to rapid heating and cooling. This environment promotes fine crystallization while intense shear forces excite molecules, accelerating precursor dispersion, bond formation, and breakage. Han *et al.* found that the Ti-based NH_2-MIL-125 prepared using an ultrasonication-assisted solvothermal approach displayed an even distribution in sizes of the nanoparticle, approximately 300 nm.[82] Additionally, a regular and defect-free MOF membrane was successfully created on a porous TiO_2 disk using a combined microwave/ultrasonic/solvothermal process.[83] Attempts to synthesize NH_2-MIL-125 (Ti) crystals on the support using microwave (MW) or ultrasonication (US) alone failed, highlighting the need for a seeding step for heterogeneous nucleation. MW irradiation was more effective in initiating nucleation than the US, and subsequent US treatment densified the crystal population using pre-formed crystals as secondary nucleation sites. The resulting NH_2-MIL125(Ti) membrane showed densely packed, uniform crystals without impurities, confirmed by SEM, XRD, N_2 adsorption–desorption isotherms, and EDS analysis. The membrane exhibited high surface area, pore volume, and strong adhesion to the TiO_2 support. Its heterogeneous catalytic activity was evaluated for the Knoevenagel condensation reaction, suggesting its potential as a recyclable catalyst. The combined MW and US approach effectively produced a high-quality NH_2-MIL-125(Ti) membrane with enhanced catalytic performance. The success of hybrid approaches thus raises a key question: synthesis complexity *vs.* quality of materials. Combining multiple techniques might lead to some improved properties; however, this would also increase the complexity of synthesis.

Our investigation revealed that tetra butyl titanate and titanium isopropoxide are the primary titanium sources for synthesizing NH_2-MIL-125(Ti), paired with 2-amino terephthalic acid as a consistent raw material. Adjusting the proportions of these sources yields varied morphologies without a discernible pattern. Solvents like DMF and CH_3OH are commonly used, typically in a 9 : 1 volume ratio, which often produces tetragonal nanosheets, nano disc cakes, and decahedral prisms. Reactions are generally conducted at 150 °C for 16–72 hours, with 24 hours being the most common. Morphologies—from disc cakes to irregular nanosheets and octahedrons—are influenced by reaction time, pH changes, and the titanium source ratio to 2-amino terephthalic acid, while reactor size has minimal impact. Surfactants and organic reagents, such as CTAB and ascorbic acid, are often added to achieve precise morphology control. Direct synthesis of NH_2-MIL-125(Ti) through hydrothermal or solvothermal methods suffers from a lack of optimization of solvents and reactant concentrations for crystallinity and morphology. Other methods, such as microwave and ultrasonic synthesis, improve crystallization, shorten reaction times, and control particle sizes. Future efforts should target consistency and scalability. While microwave and ultrasound methods press forward, however, issues around reproducibility and large-scale implementation remain. Most work has focused on the crystallinity and surface area of NH_2-MIL-125(Ti), whereas less attention has been paid to stability under real-world conditions. Long-term stability, especially in catalytic and industrial applications, needs to be the focus of attention. Besides, it is of utmost importance to examine green solvents for the synthesis of NH_2-MIL125(Ti) since the current solvothermal routes mostly work with toxic solvents, and new sustainable alternatives should be investigated to see their impact on both synthesis efficiency and material properties.

6. Significance of $-NH_2$ functionalization

The incorporation of amine groups (NH_2) into MOFs has come forth as an effective strategy to improve both their stability and their response to visible light. The existence of amine groups alters the electronic structure by generating additional energy levels within the framework, leading to a decrease in the overall band gap of the material. These changes facilitate charge transfer through alternative pathways and broaden the MOF's absorption spectrum into the visible and near-infrared regions, thereby enhancing its photophysical properties.[84] The amine group, rich in electrons due to the lone pair on the nitrogen atom, can elevate the Fermi level of material, shifting the CB position and thereby lowering the energy barrier for charge transfer. This effect enhances the photogenerated charge carrier separation. Additionally, the $-NH_2$ group facilitates charge transference from the organic linker to metal-oxo clusters, promoting their excitation.[85] Due to the Lewis acidity of amines, they also contribute to an increased generation of free electrons by effectively injecting them into the conduction band of semiconductors. The lone pair of the amine group takes part in extended conjugation within the MOF assembly, which lowers the rate of recombination of charge carriers.[86] Amine groups can also be charge carriers as they trap photogenerated electrons, which can either delay recombination or act as active sites for reactions with adsorbed species. In addition, amine groups modify the electronic properties of the ligand, enhancing its ability to interact with the metal center. This affects the electronic transitions, with optical absorption being transitioned from the UV region to the visible region. The lowering of the excitation energy arises from improved π-conjugation as well as from the electron-donating effect by the amine groups.[87] Amine-functionalization could also induce the formation of localized electronic states responsible for visible-light absorption. These states can modify the material's optical properties, thereby facilitating visible-light-driven photocatalysis by enabling the absorption of lower-energy photons.

To enhance the MOF stability and reliability, the metal center is coordinated with the $-NH_2$ group of organic ligands, forming robust metal–NH_2 bonds. These bonds provide additional structural stability, protecting the MOF from changes during photocatalytic reactions. The amine groups also act as a protective measure against pH fluctuations

induced by reactive species generated during photocatalysis. Furthermore, amine groups help prevent oxidative degradation of the MOF by scavenging reactive oxygen species (ROS), such as hydroxyl radicals ($^{\bullet}OH$) and singlet oxygen ($^1O_2$), thereby diminishing their concentration. When ROS are present, the $-NH_2$ groups experience oxidation, donating electrons to protect the MOF's ligands from oxidation and preserving the material's architectural integrity.[88] Water is frequently taken as a reactant in photocatalysis, although some MOFs may exhibit sensitivity to moisture. Under photocatalytic circumstances, $-NH_2$ functionalization can enhance the aqueous stability of MOFs by incorporating either hydrophobic or hydrophilic properties based on the specific type of $-NH_2$ groups incorporated.[89–91] The upgraded photocatalytic performance is a result of several factors, including enhanced visible light uptake, efficient excitons' separation and transfer, selective interactions with reactant species, the formation of reactive sites, and increased chemical stability. Collectively, these factors contribute to the significant and beneficial impact of MOFs with NH_2-functionalization on photocatalysis.

7. Advantages of NH_2-MIL-125 as photocatalyst

NH_2-MIL-125(Ti) is a titanium-based metal–organic framework (MOF) featuring amine-functionalized organic linkers. This structure offers significant potential in photocatalysis, attributed to its multiple key advantages, as displayed in Scheme 2.

7.1. Improved visible light uptake

The $-NH_2$ functionalization in NH_2-MIL-125(Ti) extends light absorption into the visible range, enabling efficient photocatalysis under natural sunlight. This material displays heightened molar absorptivity owing to the $-NH_2$ group and the organic linker, effectually exploiting the incident light energy. The synergistic interaction between the Ti center and the NH_2-functionalized ligand further enhances light absorption.[92]

7.2. Efficient exciton separation

In NH_2-MIL-125(Ti), the incorporation of $-NH_2$ groups into the organic linkers enhances photocatalytic efficiency by promoting charge separation and suppressing e^-–h^+ recombination. Acting as electron donors, $-NH_2$ groups create localized electronic states, adjust the band structure to reduce the band gap, and enable greater visible light uptake. The well-ordered crystal structure, with robust association of Ti nodes and NH_2-functionalized ligands, ensures efficient electron transport and effective charge transfer to catalytic sites.[93]

7.3. Modifiable pores and structural framework

The tunable pore structure and structural framework of NH_2-MIL-125(Ti) offer significant advantages for photocatalysis, including improved reactant diffusion, faster reaction kinetics,

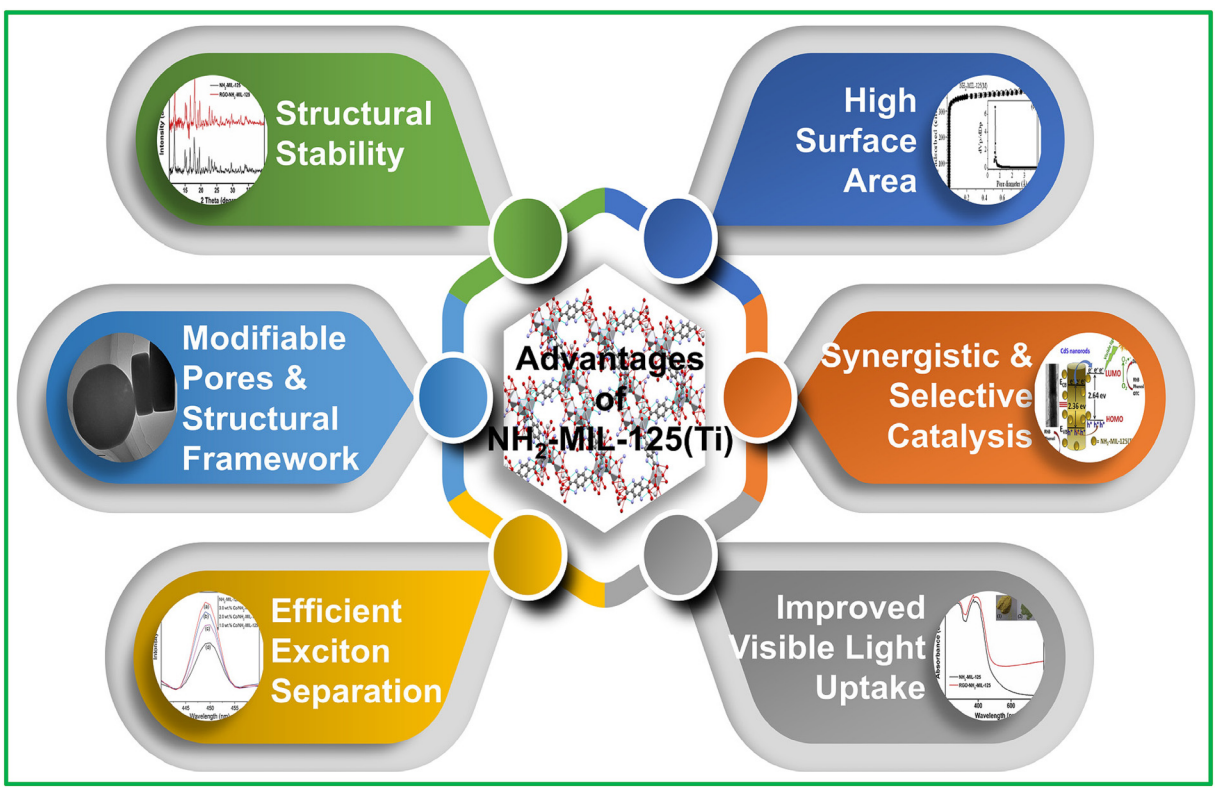

Scheme 2 Advantages of NH_2-MIL-125(Ti)-based photocatalysts.

and enhanced efficiency. The optimized surface area supports selective molecular adsorption and increases active site availability, promoting better light absorption. The tailored pores enable spatial separation of photoinduced e^- and h^+, boosting charge carrier efficacy. Additionally, the controlled pore architecture manages reaction intermediates effectively, reducing side reactions and improving selectivity. These features make NH_2-MIL-125(Ti) adaptable for numerous photocatalytic applications, ranging from environmental remediation to energy harvesting and chemical synthesis, delivering high efficiency and versatility.[94]

7.4. Structural stability

NH_2-MIL-125(Ti) exhibits remarkable thermal and chemical robustness, confirming its structural integrity and effectiveness across a range of reaction conditions. This robustness supports long-term photocatalytic activity without significant degradation, making it highly reliable for prolonged use. Its durability in harsh chemical conditions, encompassing both acidic and alkaline environments, broadens its applicability and ensures sustained functionality in demanding settings. The stable structure protects active catalytic sites, reducing the likelihood of metal ion or linker leaching, thereby preserving the reaction medium's purity and maintaining high photocatalytic efficiency. These characteristics enhance its durability, reliability, and cost-effectiveness, making it a viable option for diverse environmental and industrial processes.[95]

7.5. High surface area

NH_2-MIL-125(Ti) has a significantly large surface area, enhancing photocatalytic efficiency by facilitating the formation of active sites, improving reactant adsorption, optimizing light harvesting, and facilitating exciton pair employment. Its porous structure supports efficient reactant diffusion and adsorption, while surface functionalization further expands its scalability for practical uses. These features synergistically boost reaction rates and overall performance, positioning it as a potential material for addressing energy and environmental challenges.[96,97]

7.6. Selective catalysis

NH_2-MIL-125(Ti) stands out as a highly adaptable photocatalyst, leveraging its amine-functionalized groups and tunable pore structure for enhanced performance. The $-NH_2$ groups and tailored pores enable selective interactions with reactant molecules, allowing adsorption based on size, shape, and functional groups. This selectivity increases the localized abundance of reactants at active sites, accelerating reaction rates and boosting catalytic efficiency. The amine groups also create specific reaction sites that promote precise engagements with target molecules, improving the output and selectivity of target products. The modifiable pore configuration provides a controlled microenvironment, allowing fine-tuning of reaction conditions for optimized performance. This structure supports the selective reduction or oxidation of compounds based on reaction conditions and target molecules, enhancing its versatility. Applications include CO_2 conversion into value-added chemicals and the selective oxidation of organic contaminants, demonstrating the material's potential for energy harvesting and environmental mitigation.[98,99]

7.7. Synergistic effects

The interaction between the metal node and ligands in NH_2-MIL-125(Ti) creates a synergistic impact that boosts its photocatalytic performance. This synergy broadens the light absorption into the visible range, reduces charge recombination, and accelerates reaction kinetics by stabilizing intermediates and lowering activation energy. It also promotes the generation of reactive oxygen species, aiding in the efficient decomposition of organic pollutants. The durable metal–ligand framework ensures stability and long-term usability, making it ideal for industrial and environmental applications. Moreover, the material's design can be customized by modifying the metal center or ligands to suit various needs, including environmental cleanup, renewable energy generation, and chemical production.[100,101]

NH_2-MIL-125(Ti) offers notable benefits in photocatalysis, including enhanced visible light uptake, efficient exciton separation, extensive surface area, selective adsorption, and robust framework stability. These attributes make it suitable for diverse applications, for instance, water splitting, pollutant degradation, CO_2 reduction, and organic transformations. However, challenges like complex synthesis, potential degradation, restricted stability in aqueous conditions, resource demands, by-product management, and scalability must be taken into account to unlock its full strength in practical uses.

8. Photocatalysis in NH_2-MIL-125

Ligand-to-metal charge transfer (LMCT) is the most general method for achieving exciton pair separation in MOFs. The LMCT pathway typically has a low rate of e^- transfer and a high tendency of recombination of charge carriers, which can be upgraded by fine-tuning linker–metal cluster interaction or altering the charge transportation way to enhance photocatalytic performance. The first ever Ti-MOF to exhibit substantial photoresponsiveness was the classic MIL-125, along with its NH_2-functionalized analog, NH_2-MIL-125. Being the first Ti-carboxylate-based MOF, the finding of MIL-125 undoubtedly triggered the current surge in Ti-MOF research, spurring the advancement of newfangled Ti-MOF structures and applications across numerous fields. Notably, MIL-125(Ti) exhibits a fascinating color transformation from white to purple-gray-blue under UV radiation in the presence of alcohol (Fig. 2d).[47] This photochromic behavior indicates photocatalytic activity; however, MIL-125(Ti) can undergo excitation only by UV radiation. In order to expand the light absorption to the visible range, Li *et al.* utilized NH_2-BDC in place of H_2BDC in MIL-125(Ti), resulting in the NH_2-functionalized NH_2-MIL-125(Ti).[50] The thoughtful introduction of amine functionalization in NH_2-MIL-125(Ti) introduced extended

light harvesting in the visible range along with enhancement in CO_2 adsorption ability (Fig. 2e and f). With triethanolamine as a sacrificial agent, the MOF CO_2 can be reduced to formate in visible light (Fig. 2g). ESR study showed that the ATA ligand performed as a light probe, harvesting light and becoming excited, following the e-transportation to the titanium-oxo clusters to generate Ti^{3+} for CO_2 reduction (Fig. 2h). This effective display of photocatalytic CO_2 reduction using NH_2-MIL-125(Ti) marked the very first instance of a visible-light-induced CO_2 reduction reaction utilizing MOFs, opening new perceptions for developing photocatalysts valuable for CO_2 reduction.

The LMCT mechanism in NH_2-MIL-125(Ti) was further confirmed by García *et al.* through their study of the transient states generated upon photoexcitation.[102] The article provides strong evidence for photoinduced charge separation in NH_2-MIL-125. Laser flash photolysis of dry powder and aqueous suspensions showed a transient spectrum with broad absorption (380–800 nm), indicating charge separation upon excitation. The transient signal, with long lifetimes, decreased in the presence of oxygen, suggesting quenching of photogenerated species. Blue-colored radical ions of the electron acceptor (methyl viologen) and donor (*N*,*N*,*N*′,*N*′-tetramethyl-*p*-phenylenediamine) confirmed NH_2-MIL-125's ability to drive reduction and oxidation reactions. Comparison with TiO_2 (P25) showed similar photochemical behavior, reinforcing NH_2-MIL-125's semiconductor nature. Despite challenges such as slow electron transfer and high exciton recombination *via* the LMCT pathway, incorporating functional groups like amines broadens the light absorption spectrum into the visible range and enhances charge separation. NH_2-MIL-125(Ti) is thus appropriate for photocatalytic implementations in energy generation, contaminant degradation, and organic synthesis. Even though NH_2-MIL-125(Ti) is quite promising, fundamental issues, such as charge transport and recombination, hamper its photocatalytic efficiency. These cannot be solely overcome by functional group modification, but rather it requires further mechanistic insights combined with the development of novel strategies that could improve electron transport as well as integration of MOFs with other materials to improve catalytic properties.

9. Improvement strategies for NH_2-MIL-125-based materials

Photocatalysis typically includes three primary phases: (i) light absorption to produce a charge-separated state, (ii) separation and relocation of these exciton pairs, and (iii) origination of redox reactions *via* photoinduced excitons.[103] Effective photocatalysis requires a photocatalyst with strong light absorption and rapid exciton pair separation and migration. Flexible frameworks of MOFs permit modifications in structures that compel the addition of titanium ions for the creation of photoactive sites, followed by elongation of π-conjugated linkers to improve charge separation and transport. In titanium-based MOFs, enhancing photocatalytic performance involves crystal engineering of metal nodes, ligands, and voids. Strategies like post-synthetic modification, linker functionalization, and metal node doping are used to improve optoelectrical properties and exciton pair separation (Fig. 3a).[104]

9.1. Linker modification

Several reports have shown that substituents such as $-NH_2$, $-NO_2$, –OH, and –SH on MOF ligands significantly influence the E_g of the MOFs.[108–110] Specifically, $-NH_2$ functionalization is an efficient technique to shift the optical absorption capacity of MOFs toward the visible-light region.[47,111] Given that most of the sunlight energy is in the Vis-NIR range, piloting the photochemical activity towards the visible range is essential, which calls for E_g alteration of the concerned photocatalysts. MIL-125(Ti) has an optical E_g value of approximately 3.6 eV with an absorption maximum of 345 nm, suggesting its photoactivity under UV irradiation. For Ti-based MOF construction, amino-modified, photosensitizer-functionalized ligands, electron-rich-conjugated, and with extended light-harvesting range are time and again chosen.[47] NH_2-MIL-125 was the first example, where introducing an NH_2-group into the ATA linker matrix produced an additional absorption maximum at 550 nm (visible light region), decreasing the E_g value to 2.6 eV, giving the MOFs noteworthy photocatalytic activity for CO_2 reduction.[50] This functionalization is practically appealing because it provides the photocatalysts with extended functional wavelengths—giving photocatalysts access to a broader range of sunlight, which is important in large-scale application scenarios.

To elucidate the exact influence of $-NH_2$ on the optical characteristics of MOFs, Walsh *et al.* conducted a joint computational and experimental analysis (Fig. 3b).[105] They studied MIL-125(Ti) analogs with varied amounts of $-NH_2$ sites per unit cell (approximately 1, 6, and 12 BDC-NH_2 linkers) and found that the samples exhibited the same E_g value of nearly 2.6 eV, with the molar extinction coefficient rising proportionately with the ATA content, indicating that a solo $-NH_2$ group is accountable for the decreased E_g in the mono-aminated MIL-125(Ti). Electronic environment experiments indicated that adding $-NH_2$ to MIL-125(Ti) elevates the VB by 1.2 eV, leaving the CB unaffected. Adding another $-NH_2$ group to the ligand further marked a decreased E_g value. Assessment of the substituents with varied e^- donating abilities, such as $-CH_3$, –OH, and –Cl, revealed the fact that strong e^- donating substituents notably reduced the E_g, which justifies the most significant redshift exhibited by di-aminated BDC-$(NH_2)_2$ linker. This study depicts the function of $-NH_2$ in the optical attributes of MOFs and guides the design of MOFs with excellent light-harvesting properties. Van Der Veen and co-workers' recent studies demonstrated that besides enhanced light absorption, $-NH_2$ in NH_2-MIL-125(Ti) also performs as a hole stabilizer, prolonging the photoexcited state's life period and allowing effective utilization of photogenerated charges for photocatalytic reactions.[112] Hendon and his team used experimental and computational methods to explore the influence of the

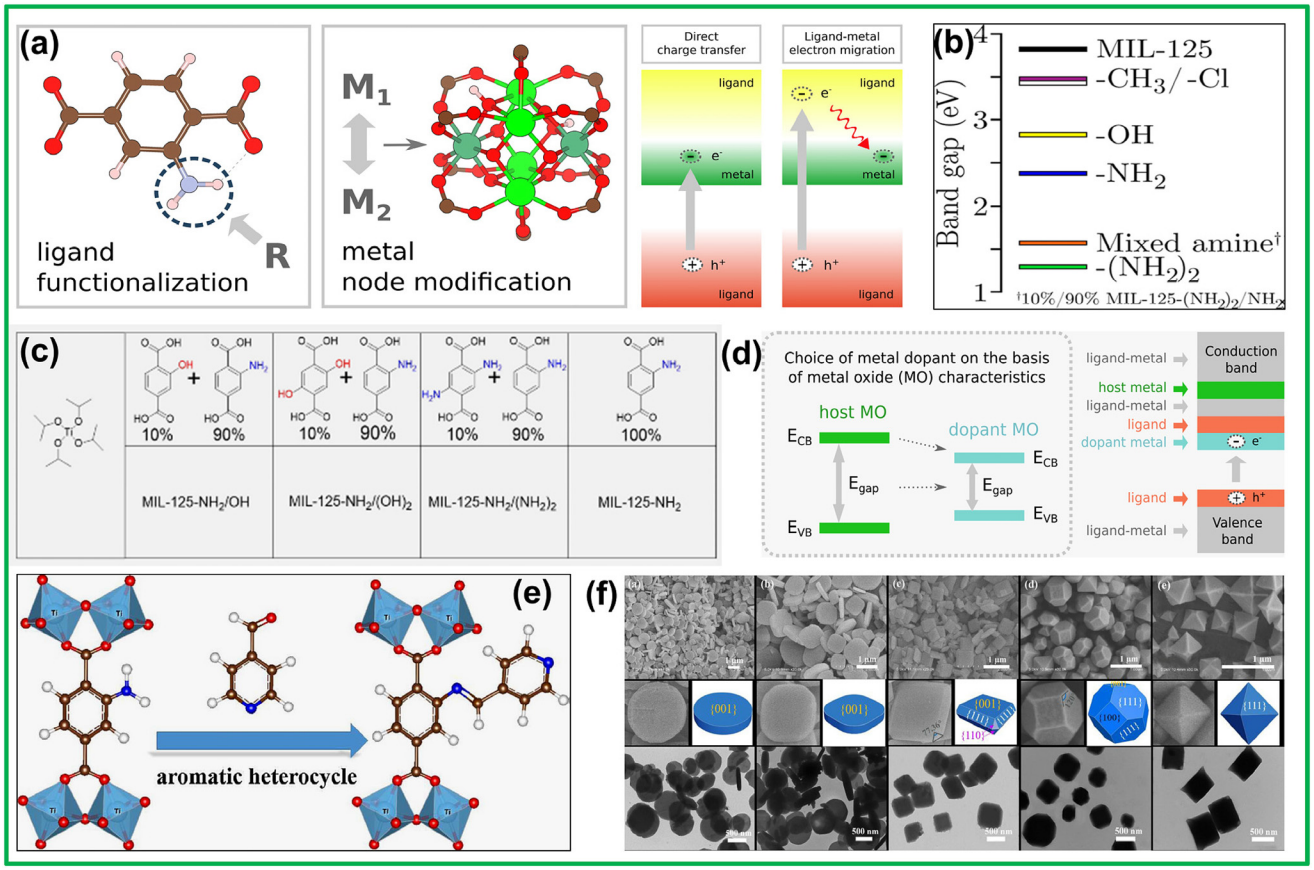

Fig. 3 (a) Strategies for compositional tuning of MOF photoactivity by ligand functionalization or metal node modification. Excited state pathways to achieve a metal node reduction in a MOF. Reprinted with permission from ref. 104. Copyright 2019 American Chemical Society. (b) HSE06-predicted band gaps of MIL-125 (black) and its analogs containing functionalized BDC linkers. Reprinted with permission from ref. 105. Copyright 2013 American Chemical Society. (c) Tabular representation of NH_2-MIL-125/OH, NH_2-MIL-125/$(OH)_2$, NH_2-MIL-125/$(NH_2)_2$, and NH_2-MIL-125, made of titanium isopropoxide and either a 1 : 9 ligand ratio or only a NH_2-BDC ligand. Reprinted with permission from ref. 106. Copyright 2021 American Chemical Society. (d) Modification of band gap, CB alignment, and creation of localized electron traps using metal doping of a MOF. Reprinted with permission from ref. 104. Copyright 2019 American Chemical Society. (e) Post-synthetic strategy of grafting NH_2-MIL-125(Ti) with aromatic heterocycles. Reprinted with permission from ref. 51. Copyright 2017 Elsevier B.V. (f) SEM, enlarged SEM, TEM images, and the corresponding 3D geometry models of as-synthesized NH_2-MIL-125(Ti) obtained under different concentrations of CTAB. Reprinted with permission from ref. 107. Copyright 2019 The Royal Society of Chemistry.

functional modification of ligands on the E_g in depth.[105] They found that bringing in a di-aminated ligand further lowered the E_g compared with NH_2-MIL-125. The synthesis of mixed-amine MIL-125, which had 10% and 90% BDC-NH_2 ATA ligands, achieved an experimental E_g value of 1.3 eV that showcased a significant shift towards the red/IR region. The $-NH_2$ group does enhance electron density and light absorption, but it also makes the material more susceptible to thermal and photoinduced instability owing to the oxidatively unstable nature of amines, especially under prolonged exposure to UV and visible light. These issues are not fully treated within the current literature. In particular, the practically important aspects of real-world applications, such as long-range stability and scalability, need to be explored in greater depth, especially concerning amine-functionalized MOFs.

He *et al.* observed that introducing defects into the ligand structure *via* a one-step heating-stirring method reduced the E_g from 2.70 to 2.60 eV and created both microporous and mesoporous structures, which exposed more metal active sites. The inclusion of defects in the original MOF matrix expanded visible light harvesting and promoted the full utilization of solar energy.[113] Defects may often create localized electronic states that, if not carefully controlled, can become trap states, increasing charge carrier recombination or giving rise to unwanted side reactions. This is an ever-recurring problem with many photocatalytic materials, putting into question the controllability of defect density. Overengineering defects may enhance charge separation in photocatalysis but may instead lower structural integrity or photochemical stability at the same time.

Similarly, Mohammadnezhad *et al.* explored the optical characteristics of NH_2-MIL-125 MOF by incorporating three variants of functionalized BDC ligands – $(NH_2)_2$-BDC, $(OH)_2$-BDC, and OH-BDC – into the framework at relatively low con-

centrations (Fig. 3c).[106] Incorporating multiple ligands with varying functionalization into the MOF matrix is an alluring tactic to enhance the efficiency of the photocatalyst.[47] The method yields a potential photocatalyst owing to the π-conjugation formed by individual chromophore-functionalized units coupled loosely.[105,114] With chromophoric $-NH_2$ and/or –OH groups as the visible light-harvesting sites, it promotes an e^- from the VB maxima to the CB minima. This transition in NH_2-MIL-125 takes place from the π-orbital of the ligands to the oxygen's 2p orbital along with the titanium's split 3d orbital. Amid the process, exciton pairs are created, with h^+ confined to $-NH_2$ and e^- at relative liberty to transit from the linker to the metal cluster, stabilizing the photoexcited charge carriers that allow e^- migration to the MOF's exterior. The –OH and $-NH_2$ functional groups, chosen for their e^--donating capability, were located on the ATA linker because of the presence of free electron pairs that do not take part in coordination, which enhances LMCT increasing both the overall reaction rate as well as the e^- density on the ligand.[115] Increasing electron density enhances electron delocalization upon radiation, boosting photocatalytic efficiency. The chromophoric $-NH_2$ and –OH groups make the catalyst active in the visible spectrum, giving the material orange or yellow hues and improving light absorption. NH_2-MIL-125/$(OH)_2$ shows a redshift with stronger absorption, partly due to p–π conjugation between the –OH groups and the ATA linker's benzene ring. While NH_2-MIL-125 and NH_2-MIL-125/OH have comparable E_g values of approximately 2.6 eV, NH_2-MIL-125/$(OH)_2$ has a lower E_g of 2.2 eV, enhancing visible light uptake. Although NH_2-MIL-125/$(NH_2)_2$ exhibits the most significant redshift (E_g = 1.6 eV), its absorption intensity is weaker than NH_2-MIL-125/$(OH)_2$. PL spectra at 420 nm show similar emission peaks near 450 nm for all samples. However, NH_2-MIL-125/$(OH)_2$ exhibits a redshift to ~510 nm, highlighting the energy gap shift toward the visible spectrum with $(OH)_2$-BDC inclusion.

Logan *et al.* created a series of NH_2-MIL-125 analogs by switching the NH_2-groups with alkyl groups of varying chain lengths and connectivity.[116] The incorporation of these functional groups led to a reduction in the E_g value, decreasing from 2.46 eV to 2.29 eV for MIL-125-NHMe and for MIL-125-NHCyp, respectively. MIL-125-NHCyp, featuring a small E_g, an extended excited state lifetime of 68.8 ns, and a high AQY of 1.80%, exhibited significantly enhanced photoactivity compared with the original MOF. These findings indicate that the optoelectronic properties of NH_2-MIL-125 MOF-based materials can be effectively modulated through the strategic functionalization of the linking units. In conclusion, while the strategies listed above may show great promise, we believe there is a need for this field to broaden its scope from the mere demonstration of enhanced photocatalytic activity in a controlled laboratory to tackle practical dilemmas. Future works must also address multi-strategy optimization that adopts functions like functionalization, defect engineering, alkyl substitution, *etc.*, giving rise to more holistic approaches that assume real-world conditions.

9.2. Metal node modification

The modification of metal nodes in MOFs is one of the most powerful strategies for enhancing photocatalytic efficiency. The inherent advantage of MOFs, including NH_2-MIL-125, lies in their ability to host coordinatively unsaturated metal sites (CUSs). MOFs often feature metal nodes initially coordinated with solvent molecules such as DMF or H_2O. By applying heat or using vacuum activation, these solvent molecules can be eliminated, leading to the formation of CUSs. These sites enable MOFs to engage in Lewis acid catalytic reactions.[117] These CUSs, however, are masked or deactivated by organic ligands coordinating with metal centers. This, in turn, limits the chances of successful charge transfer and catalytic performance.[118] Enhancing the photocatalytic efficacy of MILs necessitates modifying the metal nodes to yield more efficient catalytic sites.

Zhang *et al.* illustrated that partly substituting Ti with Ru in NH_2-MIL-125 leads to increased exposure of titanium-oxo clusters, thereby improving its catalytic properties.[119] Replacing metal nodes partially, or by metal doping, within the SBUs represents a potential but comparatively underexplored approach to tailoring MOF characteristics. This method enables the adjustment of both the relative and absolute energy positions of metal nodes within a MOF's band structure. When choosing a metal for doping, it's essential to consider its electron affinity, which acts as a critical condition in defining the position of its states. Since metal nodes within MOFs can be conceptualized as fixed metal–oxide clusters, the reducibility measures of metal oxides can guide the selection of suitable dopants. Intended for MOFs, criteria such as a suitably small E_g value and superior e^- affinity, determined *via* the absolute position of the CB edge, are pertinent (Fig. 3d).[104,120,121] These metal nodes in MOFs, which bond with oxygen atoms from the polycarboxylate-ligands to create metal-oxo clusters, frequently act as catalytic active sites in photocatalytic processes. Titanium, having multi-valence states (Ti^{4+}/Ti^{3+}), emerges as a favorable choice for node incorporation in MOF photocatalysts due to its abundance in Earth's crust and non-toxicity. To facilitate efficient charge transfer, a MOF ought to have an optimum E_g value, with energetically favorable positioning of the CB and VB edges for photocatalytic reactions. A feasible approach for achieving this ideal E_g value involves the partial substitution of the metal nodes, producing mixed-metal center MOFs. This synthetic approach allows for fine-tuning the energy positions within the MOF band structure.

Given NH_2-MIL-125, metal doping aims to improve the localization of metal nodes while diminishing the input from ligands. For instance, Syzgantseva *et al.*, through a combination of computational simulations and experimental studies, demonstrated that incorporating V into NH_2-MIL-125 induces a notable redshift in the UV–Vis spectrum, changing its color from yellow to brown. This observation was supported by theoretical computations showing that V incorporation decreases the position of the CB edge.[104] Doping NH_2-MIL-125 with W and Nb lowers its CB edge. Nb enhances metal node

localization, though the DOS still shows contributions from C atoms and Ti to the LUCO state. Nb_2O_5 has a 0.2 eV higher E_g than TiO_2, with modest localization. WO_3, despite its higher electron affinity, shows contributions from both Ti and W at the CB bottom, suggesting electron affinity alone doesn't guarantee localization. W-doping modestly reduces the CB position, aligning with optical E_g reductions in W-doped TiO_2. For effective exciton separation, the dopant must create a more reducible metal oxide, lowering both E_g and the CB edge position. While these modifications enhance light absorption and charge transport, metal doping can occasionally result in unintended effects, like the creation of defective sites or unfavorable bonding configurations. The reducibility of the doped metals, along with the risk of leaching or deactivation over time, may undermine the overall catalytic performance.

Li *et al.* produced a bifunctional photocatalyst, Yb–NH_2-MIL-125(Ti), coordinated with Yb, which plays a pivotal role in photocatalysis. During the reaction, charge carriers generated by light transfer from the organic ligand to the metal center instead of the Ti–O cluster, potentially through a transient Yb (II/III) center. This mechanism enhanced the rate of e-transportation and reduced the recombination of exciton pairs.[122] Compared with the neat material, the light absorption efficiency and absorption region of Yb–NM–X were improved, with a decrease in E_g from 2.51 to 2.37 eV, indicating enhanced light energy utilization with the introduction of Yb species. In their research, Chen *et al.* opted for Ni, recognized for its superior affinity for e^-s, as a dopant to inspect its impact on e-allocation within NH_2-MIL-125. Their findings demonstrated that the inclusion of Ni^{2+} ions enhanced e^- transference and promoted carrier separation by modifying the electronic band structure of the Ti–O clusters in NH_2-MIL-125. Due to Ni's greater electronegativity relative to Ti, its integration around the oxygen atoms of these Ti–O clusters resulted in a significant alteration of their electronic configuration. Ni doping favors the excitons' separation; on the contrary, W and Nb doping do not necessarily favor charge localization, which proves that electron affinity alone cannot render the process of doping successful. The energy alignment between the dopant and host material becomes a significant factor. It should not be only the case of high electron-affinity metals; doping strategies must also tune carefully the electronic structure. Studies show that there were only slight changes attributed to Nb and W doping regarding band gap; hence band gap narrowing does not always improve photocatalytic activity. The relationship between dopant concentration, localization of metal sites, and electronic structure is complex. Future work should be directed toward multi-doped materials, which synergistically integrate dopants but remain stable.

9.3. Encapsulation of active species

The combination of metal nodes and functional ligands in MOFs creates open frameworks with large voids and extensive internal specific surface areas. This structure allows MOFs to house active molecular catalysts individually, preventing agglomeration that could diminish catalytic performance. Gascon *et al.* employed a "ship-in-a-bottle" synthetic approach to encapsulate a Co-dioxime-diimine catalyst inside the void of the photoactive NH_2-MIL-125. This resulted in a sturdy, multi-operational Co@MOF photocatalyst, which was highly effective for photocatalytic hydrogen production in visible regions.[123] ESR studies demonstrated that the incorporation of the Co complex within the NH_2-MIL-125(Ti) cavity facilitated effective charge transference from the excited MOF to the active Co(II) sites, greatly enhancing photocatalytic activity. As a result, a 20-fold increase in the hydrogen production of Co@MOF was observed compared with that of the parent NH_2-MIL-125. Building on this strategy, Jiang *et al.* incorporated a Co(II) molecular catalyst, [CoII(TPA)Cl][Cl], into NH_2-MIL-125.[124] This composite enhanced photocatalytic hydrogen production efficacy by facilitating photogenerated charge transference from the MOF to the Co(II) complex. The incorporation of photon absorption, charge dissociation, electron movement, and catalytic activity within the guest@MOF multifunctional framework highlights the significant potential of MOFs as podiums for crafting versatile photocatalysts. This process has shown significant improvements in charge transfer and prevents catalyst leakage, a common occurrence in conventional methods. The drawback lies especially in the unexplored complexity of charge transfer mechanisms that exist among all such systems. Although the studies mentioned previously show the possible transfer of charges from the MOF to the enclosed catalyst, there would still exist some bottlenecks which could primarily include kinetic limitations and electron transport between the MOF matrix and the active species. It could, therefore, add more understanding to studies on charge dynamics within encapsulated systems.

Enhancing the reactivity of catalytic active centers is an additional approach for boosting photocatalytic activity, aiming to increase overall photochemical productivity. Noble-metal NPs such as Pt or Ru are highly efficient multifunctional catalysts widely recognized for their effectiveness in various critical reactions. Encapsulating nanoparticles like Pt, Pd, Au, or Ru inside the voids of NH_2-MIL-125 has been documented and utilized to carry out photocatalytic processes.[56,125] In these structures, the separation of photoinduced exciton pairs is efficiently achieved, with e^-s migrating to the surfaces of the noble metal NPs rather than to the Ti-containing secondary building units. This electron transfer facilitates reduction reactions. The photocatalytic efficiency of coordinatively unsaturated Pt or Ru atoms far surpasses that of intrinsic Ti^{3+} sites in titanium-MOFs, resulting in enhanced overall photocatalytic performance. Additionally, incorporating other functional materials such as MoS_2, hetero-poly acids, QDs, and carbon nano species with Ti-MOFs presents promising opportunities for further investigation. Encapsulating active species in MOFs is challenging due to issues like catalyst aggregation and uneven distribution. The "ship-in-a-bottle" approach improves photocatalytic activity but struggles with homogeneity and efficient charge transfer. Incorporating noble metal nanoparticles enhances activity through better charge separation and electron transport, but optimizing their uniform distri-

bution and interaction with the MOF matrix is essential. Exploring the loading of other functional materials and studying charge transfer mechanisms will be key to developing more effective and stable photocatalysts.

9.4. Post-synthetic modification

Post-synthetic modification (PSM) is a crucial technique for the functionalization of MOFs, allowing for the introduction of specialized functionalities *via* a "tag".[102,126] In 2013, Gascon and colleagues conducted a study illustrating that the alteration of NH_2-MIL-125(Ti) with dye-like moieties enhances its efficacy for visible light employment. By employing the $-NH_2$ groups in the ligands as markers, dye-like moieties were introduced into the MOF, resulting in the formation of methyl red-MIL-125(Ti) (MR-MIL-125(Ti)).[126] In comparison with the original MOF, MR-MIL-125 displayed a noticeable red shifting, exhibiting an absorption edge extending to nearly 700 nm, which could be owing to the expanded conjugation of the ligand's aromatic system. The enhanced light-harvesting capability of MR-MIL-125(Ti) contributed to its greater performance in the photocatalytic oxidation of benzyl alcohol to benzaldehyde upon exposure to visible light, outperforming the neat MOF.

Garcia and colleagues showed that photogenerated charge carrier separation occurs in NH_2-MIL-125 when methyl viologen is used as the e^- acceptor and *N*,*N*,*N*,*N*-tetramethyl-*p*-phenylenediamine is used as the e^- donor.[102] Their findings confirmed that upon irradiation, NH_2-MIL-125(Ti) can concurrently facilitate the redox processes, which are dependent on the redox potential of the probe molecule involved. Such an approach notes a limit: while redox couples like methyl viologen serve a good purpose in characterizing charge dynamics, their electron donor and acceptor will depend on the context and cannot be generalized. Future studies should reflect how photocatalytic efficiencies vary between environments with respect to different electron donor and acceptor combinations of differing redox potential.

Wu and team created an innovative and simple post-grafting method, utilizing a Schiff base chemical interaction amongst the aldehyde and $-NH_2$ groups in MOF to develop aromatic heterocycle-grafted MOF photocatalysts (Fig. 3e).[51] The enhanced conjugation in these MOFs demonstrated reduced E_gs and superior catalytic performance. After modification with aromatic heterocycles, NH_2-MIL-125(Ti) exhibited a red shifting in its absorption wavelength. This modification introduced a Schiff base structure formed between the aldehydes and NH_2^- groups and on the organic linkers, creating a superconjugation effect with the aromatic benzene ring in the MOF and the aromatic heterocycles. This superconjugation enhances charge excitation and transition during photocatalytic reactions. The post-synthetic incorporation of aromatic heterocycles extended the π-delocalized system, enhancing the separation and transference of photoinduced exciton pairs while preserving the original framework. This led to a marked advancement in visible region absorption efficiency. PSM provides several benefits, such as the incorporation of diverse functional groups, independence from the solvothermal process, easy isolation of modified MOFs, and feasible reaction conditions. Nevertheless, how the changes result in the long-term stability of the MOF for photocatalysis has to be evaluated. The Schiff base structure might degrade under reaction conditions, and improved conjugation may lead to side reactions or changes in the distribution of products. Critical assessment of such PSM concepts has to take place, focusing both on immediate catalytic enhancement and long-term stability in practical applications.

Facet engineering on MILs is another approach for revealing more active metal centers. While this technique is frequently used to improve the surface characteristics of conventional nano photocatalysts, its employment towards soft crystal MOFs is seldom documented.[127–129] Based on recent research, Guo *et al.* performed the facet engineering of nano-structured NH_2-MIL-125(Ti) by adjusting the amount of the structure-directing surfactant, CTAB (Fig. 3f).[107] This adjustment increased the occurrence of metal clusters on the material's planes, thereby boosting its photoactivity. Specifically, NH_2-MIL-125(Ti) with the active facet (110) exhibited a significantly better quantum yield. It achieved a three-fold better photocatalytic H_2 production rate than that observed with the sample dominated by the (111) facet. Functionalization can be done through various techniques, but maintaining the structural integrity of MOF during modification is important. Unlike traditional nano photocatalysts, which are well known for facet engineering, MOFs create difficulty in their delicate crystal structures and their modifiability. Therefore, the basic challenge lies in the functional enhancements, ensuring that the modifications do not affect the material's stability in practical applications and efficiency.

10. Photocatalytic application

In recent decades, thanks to its renewable nature, photocatalysis has gained significant attention for applications like H_2 generation *via* water splitting, CO_2 reduction, organic pollutant degradation, and H_2O_2 production. Photocatalytic reactions occur in three steps (Fig. 4a).[130] (1) Photons with energy exceeding the semiconductor's E_g excite electrons from the VB to the CB, forming e^- and h^+ pairs. (2) These pairs separate and migrate to the surface. (3) The pairs interact with chemical species on the surface, though some may recombine instead of reacting. Ti-centered MOFs, like MIL-125(Ti), are effective for photocatalysis due to the LMCT mechanism, which facilitates charge transfer from the organic ligand to the metal cluster. MIL-125 can only be excited by UV light, while NH_2-MIL-125, made from 2-amino terephthalate, can absorb visible light, improving solar energy utilization. The NH_2 group enhances charge transfer from oxygen to titanium in the $TiO_5(OH)$ cluster, shifting the absorption edge of NH_2-MIL-125 to 520 nm, a significant red shift from MIL-125's 350 nm. Table 1 lists the different photocatalytic performances of NH_2-MIL-125 (Ti)-based multifunctional materials.

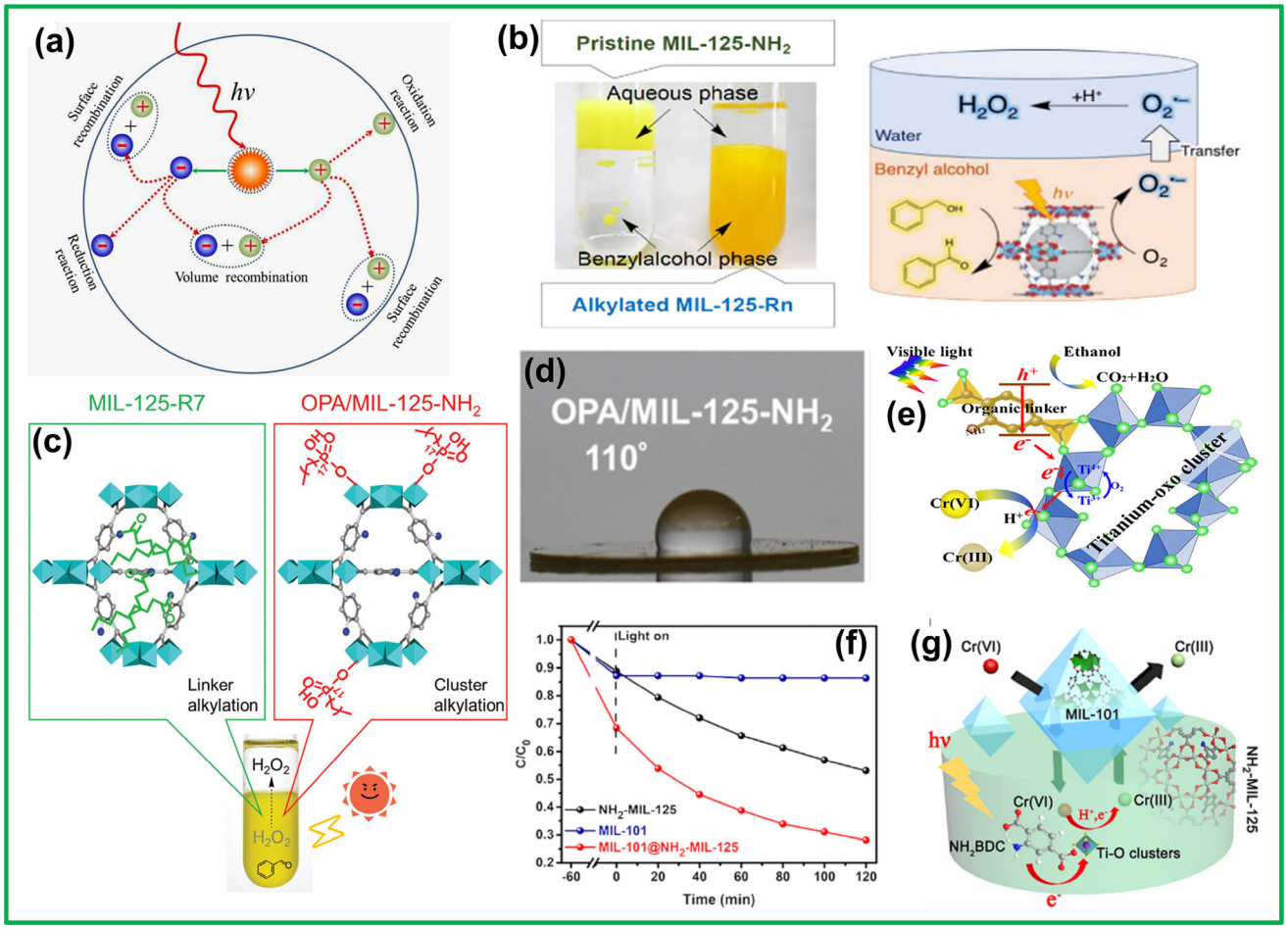

Fig. 4 (a) Photoexcitation and charge decay pathway in photocatalyst. Reprinted with permission from ref. 130. Copyright 2019 Wiley-VCH Verlag GmbH & Co. (b) (left) Digital pictures of two-phase systems composed of aqueous phase and benzyl alcohol phase containing NH_2-MIL-125 (left) and MIL-125-R*n* (right). (right) Photocatalytic H_2O_2 production utilizing the two-phase system. Reprinted with permission from ref. 131. Copyright 2019 Wiley-VCH Verlag GmbH & Co. (c) Structures of linker-alkylated NH_2-MIL-125, MIL-125-R7 (top left), and cluster-alkylated NH_2-MIL-125, OPA/NH_2-MIL-125 (top right). (bottom) The digital picture of the two-phase system composed of a BA/water phase containing OPA/NH_2-MIL-125 in the BA phase. (d) Photographs of water droplets on tablets of OPA/NH_2-MIL-125. Reprinted with permission from ref. 132. Copyright 2019 The Royal Society of Chemistry. (e) Schematic illustration of photocatalytic Cr(VI) reduction over NH_2-MIL-125(Ti) under visible-light irradiation. Reprinted with permission from ref. 133. Copyright 2014 Elsevier B.V. (f) Adsorption and photocatalytic degradation toward Cr(VI) with MIL-101, NH_2-MIL-125, and MIL-101@NH_2-MIL-125. (g) Schematic illustration of the enhanced photocatalytic degradation process towards Cr(VI) with micro/mesoporous MIL-101@NH_2-MIL-125 materials. Reprinted with permission from ref. 134. Copyright 2017 Wiley-VCH Verlag GmbH & Co.

10.1. H_2O_2 generation

Hydrogen peroxide (H_2O_2) is a clean oxidant and reductant extensively needed in industrial chemistry and a potential high-energy fuel for fuel cells.[176] H_2O_2 production typically follows two primary routes: a successive two-step single-e^- reduction ($O_2 \rightarrow O_2^{\bullet-} \rightarrow H_2O_2$) or a one-step two-$e^-$ reduction ($O_2 \rightarrow H_2O_2$). In photocatalytic systems, h^+ in the VB oxidizes H_2O to form O_2 and H^+ (eqn (1)), while electrons (e^-) in the CB reduce adsorbed O_2 to H_2O_2. From a photoelectrochemical standpoint, the direct one-step two-e-reduction path has better efficiency for producing H_2O_2.[177–179]

The mechanism of the two-step single-electron pathway involves the reactions discussed in eqn (1)–(5). Alternatively, the one-step, two-electron pathway involves the direct reaction of O_2 with two H^+ to produce H_2O_2 (eqn (6)). The photocatalytic overall response can be summarized as follows (eqn (7)):

$$2H_2O + 4h^+ \rightarrow O_2 + 4H^+ \quad (1)$$

$$O_2 + e^- \rightarrow O^{2\bullet-} \quad (2)$$

$$O^{2\bullet-} + H^+ \rightarrow HO_2^{\bullet} \quad (3)$$

$$HO_2^{\bullet} + e^- \rightarrow HO_2^- \quad (4)$$

$$HO_2^- + H^+ \rightarrow H_2O_2 \quad (5)$$

$$O_2 + 2H^+ + 2e^- \rightarrow H_2O_2 \quad (6)$$

$$2H_2O + O_2 \xrightarrow{h\nu} 2H_2O_2 \quad \Delta G_0 = 117\ \mathrm{kJ\ mol^{-1}} \quad (7)$$

Table 1 List of NH_2-MIL-125(Ti)-based multifunctional materials towards different photocatalytic applications

Sl. no.	Photocatalytic application	Material	Band gap (eV)	Light source	Photocatalytic activity	Ref.
1	H_2O_2 production	NiO/NH_2-MIL-125	—	500 W Xe lamp (λ > 420 nm)	160 μM, 20 h	135
2		OPA/NH_2-MIL-125	—	500 W Xe lamp (λ > 420 nm)	—	132
3		MIL-125-R*n*	~2.55	—	—	131
4		NH_2-MIL-125-D	2.50	200 W metal halide lamp	62.7 μM, 120 min	136
5	Cr(VI) reduction	NH_2-MIL-125(Ti)	~2.65	500 W Xe lamp (λ > 420 nm)	90% reduction, 120 min	133
6		M/NH_2-MIL-125 (M = Pt and Au)	2.2 and 2.38	300 W Xe lamp	—	137
7		MIL-101@NH_2-MIL-125	2.4	200 W metal halide lamp	88% reduction, 100 min	134
8		PPynt@NH_2-MIL-125	1.52	300 W Xe lamp (λ > 400 nm)	99.02% reduction, 60 min	138
9		NA/NH_2-MIL-125(Ti)	2.3	White light (100 W LED)	85% reduction, 90 min	139
10	CO_2 reduction	NH_2-MIL-125(Ti)	2.65	300 W Xe lamp (λ > 400 nm)	$HCOO^-$ = 8.14 mmol, 10 h	140
11		Pt/NH_2-MIL-125(Ti)	2.2	300 W Xe lamp	HCOOH = 235 μmol g^{-1} h^{-1}	125
12		Co/NH_2-MIL-125(Ti)	2.4	300 W Xe lamp (λ > 400 nm)	HCOOH = 38.4 mmol g^{-1} h^{-1}	141
13		Ni/NH_2-MIL-125(Ti)	2.5	500 W Xe lamp (λ > 420 nm)	—	142
14		Bi_2S_3@NH_2-MIL-125	2.1	300 W Xe lamp (λ > 400 nm)	CO = 12.46 μmol g^{-1} h^{-1}	143
15		ZnS/CQDs/NH_2-MIL-125(Ti)	2.68	300 W Xe lamp with 420 nm cut-off filter	CH_3OH = 501.57 μmol g^{-1}, CH_3CH_2OH = 564.70 μmol g^{-1}	144
16		rGO/NH_2-MIL-125(Ti)	2.43	300 W Xe lamp (λ > 400 nm)	CH_3OH = 47.2 mmol g^{-1} h^{-1}	145
17		Cu_2O/Pt/NH_2-MIL-125(Ti)	2.68	300 W Xe lamp with 400 nm cut-off filter	CH_3OH = 434.46 μmol g^{-1} h^{-1}, CH_3CH_2OH = 718.47 μmol g^{-1} h^{-1}	146
18		TiO_2@NH_2-MIL-125	2.35	—	CO = 159 μmol g^{-1}	147
19	N_2 fixation	CH_3-MIL-125(Ti)	—	300 W xenon lamp with 400 nm cut-off filter	1.39 μmol g^{-1} h^{-1}	148
20		OH-MIL-125(Ti)	—	300 W xenon lamp with 400 nm cut-off filter	5.03 μmol g^{-1} h^{-1}	148
21		NH_2-MIL-125(Ti)	—	300 W xenon lamp with 400 nm cut-off filter	12.25 μmol g^{-1} h^{-1}	148
22		Ce-NH_2-MIL-125	2.66	300 W xenon lamp (light intensity of 200 mW cm^{-2})	39.4 μmol g^{-1} h^{-1}	149
23	H_2 evolution	PtNPs@NH_2-MIL-125(Ti)	—	500 W Xe lamp (λ > 420 nm)	367 μmol g^{-1} h^{-1}	56
24		Pt/NH_2-MIL-125/$(OH)_2$	~2.2	500 W Xe lamp (λ > 420 nm)	707 μmol g^{-1} h^{-1}	106
25		NH_2-MIL-125/OH	—	500 W Xe lamp (λ > 420 nm)	377 μmol g^{-1} h^{-1}	106
26		NH_2-MIL-125/$(NH_2)_2$	~1.6 eV	500 W Xe lamp (λ > 420 nm)	253 μmol g^{-1} h^{-1}	106
27		$CdIn_2S_4$@NH_2-MIL-125	—	300 W xenon lamp (λ > 400 nm)	2550 μmol g^{-1} h^{-1}	150
28		CdS/NH_2-MIL-125(Ti)	—	350 W xenon lamp (λ > 420 nm)	6.62 mmol g^{-1} h^{-1}	151
29		Pd/NH_2-MIL-125(Ti)/$CdIn_2S_4$	2.08	300 W xenon lamp (λ > 420 nm)	4.60 mmol g^{-1} h^{-1}	152
30		$ZnIn_2S_4$@NH_2-MIL-125(Ti)	2.48	300 W xenon lamp (λ > 420 nm)	2204.2 μmol g^{-1} h^{-1}	153
31		NH_2-MIL-125(Ti)@$ZnIn_2S_4$/CdS	1.84	300 W xenon lamp (λ > 400 nm)	2.367 mmol g^{-1} h^{-1}	154
32		NH_2-MIL-125(Ti)/Ti_3C_2 QDs/$ZnIn_2S_4$	2.35	Visible light	2931.9 μmol g^{-1} h^{-1}	155
33		1T-MoS_2/NH_2-MIL-125	—	Xenon lamp ($\lambda \geq$ 420 nm)	1454 μmol g^{-1} h^{-1}	156
34		Ni_2P/NiO@NH_2-MIL-125(Ti)	—	Visible light	1611 μmol g^{-1} h^{-1}	157
35		Co@NH_2-MIL-125(Ti)	2.59	500 W Hg/Xe lamp (λ > 408 nm)	—	123
36		NH_2-MIL-125@TiO_2	—	300 W xenon lamp ($\lambda \geq$ 420 nm)	496 μmol g^{-1} h^{-1}	158
37		NH_2-MIL-125(Ti)/Pt/g-C_3N_4	2.6	300 W Xe lamp with 380 nm UV cutoff filter	3986 μmol g^{-1} h^{-1}	57
38	Drug degradation	Oxygen-enriched vacancy NH_2-MIL-125(Ti)	2.36	300 W Xe lamp	TCH = 80%, 2 h	159
39		Bi_3O_4Br/NH_2-MIL-125(Ti)	2.8	300 W xenon lamp (λ > 400 nm)	TCH = 88.5%, 90 min	160
40		g-C_3N_4/NH_2-MIL-125	2.56	UV LED irradiation (384 nm)	DCF = 100%, 2 hours	161
41		$LaFeO_3$/NH_2-MIL-125	2.4	150 W xenon lamp	CAF = 87% and CBZ = 74%, 1 hour	162
42		NH_2-MIL-125@CoFe PBA	2.59	300 W Xe lamp ($\lambda \geq$ 420 nm)	TCH = 86.9%, 2 hours	163
43		UiO-66/NH_2-MIL-125/g-C_3N_4	2.68	Visible light (300 W xenon lamp, λ > 420 nm)	—	95
44		NH_2-MIL-125@MIL-88B	—	300 W Xe lamp	TCH = 96.26%, 120 minutes	164
45		Ag/NH_2-MIL-125(Ti)/CdS	2.35	Simulated sunlight (350 W Xe lamp)	KP = 94.2%, 180 minutes	165
46		Pt/NH_2-MIL-125(Ti)	2.48	Simulated solar light	—	100
47		Pd/NH_2-MIL-125(Ti)	2.50	Simulated solar light	—	100
48		Ag/NH_2-MIL-125(Ti)	2.70	Simulated solar light	—	100
49	Dye disposal	Au@NH_2-MIL-125(Ti)/CdS	2.28	300 W xenon lamp, $\lambda \geq$ 420 nm	MB = 93.3%, 30 min	166
50		NH_2-MIL-125(Ti)/CdS/Graphene	2.2	300 W xenon lamp (λ > 420 nm)	RhB = 95%, 30 min	167
51		NH_2-MIL-125(Ti) nanodots on CF/MoS_2	—	300 W xenon lamp	AO7 = 67.9%, MB = 94.3%, 120 MIN	168
52		BiOI/$ZnFe_2O_4$/g-C_3N_4	—	LED light	AB92 = 80%, MB = 73.8%, phenol: 66.6%, 120 min	169
53		NH_2-MIL-125@$BiVO_4$	—	300 W xenon lamp (λ > 420 nm)	MG = 93.6%, MB = 97.6%, CV = 97.9%, CR = 58.2%, 3 hours	170
54		Ag_3PO_4@NH_2-MIL-125	2.39	Philips 100 W equivalent daylight lamp	MB = 93.3%, RhB = 95.5%, 60 min	171
55		Ag_3VO_4@NH_2-MIL-125	2.27	UV and visible light	MB = 99.68% (MB), RhB = 102.38%, 60 min	172
56		Ag_2WO_4@NH_2-MIL-125	2.57	UV and visible light	MB = 49.12%, RhB = 38.55%, 60 min	172
57		Ag/AgBr/NH_2-MIL-125(Ti)	2.6	300 W xenon lamp (λ > 420 nm)	MO = 70%, 120 min	173
58		CQDs/P25/NH_2-MIL-125	2.0	300 W xenon lamp with an AM1.5 G optical filter	MB = 90.4%, 150 min	174
59		BNQDs/NH_2-MIL-125(Ti)	2.43	300 W xenon lamp ($\lambda \geq$ 420 nm)	RhB = 100%, 45 min	175

The generation of H_2O_2 from H_2O and O_2 *via* photocatalysis is an energetically demanding reaction characterized by a standard ΔG_0 of 117 kJ mol^{-1}.

NH_2-MIL-125 was produced and subsequently modified with NiO to create NiO/NH_2-MIL-125 *via* the method outlined by Isaka *et al.*[135] The UV-DRS spectrum shows high-energy absorption due to $\pi \rightarrow \pi^*$ transitions of the organic ligands and a visible region absorption from LMCT involving NH_2-groups on the ligands, confirming that both NH_2-MIL-125 and NiO/NH_2-MIL-125 are responsive to visible light for photoactive reactions. Photocatalytic H_2O_2 generation, using NH_2-MIL-125 in oxygen-saturated acetonitrile with TEOA as an electron donor under visible light, showed no H_2O_2 without light or TEOA. The H_2O_2 production rate improved significantly with NiO/NH_2-MIL-125 or Pt/NH_2-MIL-125 compared with NH_2-MIL-125 alone. Oxidation of TEOA produced aldehyde and its hydrated form. Stoichiometric analysis of H_2O_2 and electron donor association was complicated by multiple alcohol moieties in TEOA, so photocatalytic H_2O_2 production was carried out by oxygen reduction and oxidation of benzyl alcohol. NH_2-MIL-125 resulted in H_2O_2 being only 5.7% of the benzaldehyde generated after 8 hours, while NiO/NH_2-MIL-125 increased this yield to 93%. NiO/NH_2-MIL-125 also showed half the H_2O_2 decomposition rate of NH_2-MIL-125 at high H_2O_2 concentrations, suggesting repression of NiO's two-electron reduction as the cause for the enhanced selectivity. EPR experiments with DMPO detected $O_2^{\bullet-}$ species, confirming their formation under visible light with NH_2-MIL-125 but with a reduced rate for NiO/NH_2-MIL-125. These results show that NiO accelerates the conversion of O_2 to H_2O_2. The higher H_2O_2 selectivity in NiO/NH_2-MIL-125 is attributed to the faster decomposition of $O_2^{\bullet-}$, while under visible light, photogenerated electrons reduce Ti(IV) to Ti(III), forming $Ti_8O_8(OH)_4^{\bullet-}$, which reduces O_2 to superoxide that forms H_2O_2 *via* disproportionation, further enhanced by NiO. Although NiO/NH_2-MIL-125 efficiently catalyzed H_2O_2 production in a single-phase system, its performance declined during recycling tests due to the instability of NH_2-MIL-125, a typical issue with Ti-based MOFs that emphasizes the requirement for robust materials or surface modifications that can prevent the degradation of the framework without a reduction in photocatalytic efficiency. Furthermore, using a single-phase system for both H_2O_2 production and catalyst mixing complicates H_2O_2 collection and leads to its catalytic decomposition, requiring an additional separation process to isolate H_2O_2 from the MOFs.

To address the mixing issues of H_2O_2 and MOFs, a two-phase system of benzyl alcohol (BA) and H_2O was considered for photocatalytic H_2O_2 production (Fig. 4b).[131] This system separates MOFs in the BA phase and H_2O_2 in the aqueous phase *via* NH_2-MIL-125's hydrophobicity. PSM added alkyl chains to the MOF, creating MIL-125-R*n* (n = 4 and 7). Alkylation caused a blue shift in UV–vis DRS absorbance but maintained visible region absorption. NH_2-MIL-125 dispersed into the water phase, with H_2O_2 generation only in the aqueous phase. MIL-125-R*n* (n = 4 and 7) dispersed into the BA phase, with H_2O_2 formation in the aqueous phase. MIL-125-R*n* showed significantly higher H_2O_2 production than NH_2-MIL-125, while benzyl alcohol oxidation rates were similar, indicating selective H_2O_2 production increased activity. In a single-phase system, H_2O_2 decomposes into OH^- and $^{\bullet}OH$, suppressing its production, but this issue is avoided in the bi-phase system.[132] Seawater further enhances H_2O_2 production by stabilizing $O_2^{\bullet-}$ through Na^+ complexation. Under visible light, MIL-125-R*n* generates electrons that reduce Ti(IV) to Ti(III) *via* LCCT, forming $Ti_8O_8(OH)_4^{\bullet-}$, which reduces O_2 to superoxide, then forms H_2O_2 through disproportionation, accelerated by H^+ or Na^+. MIL-125-R7's H_2O_2 production is four times greater than NH_2-MIL-125 but still limited, likely due to a reduced surface area (560.7 m^2 g^{-1} *vs.* 1498 m^2 g^{-1} for NH_2-MIL-125), resulting from alkylation (Fig. 4c). Inclusion of alkyl chains in MOFs can, however, result in trade-offs between their hydrophobicity and surface area, thus reducing the available sites for the adsorption of reagents and for catalytic activity. This reveals a significant lacuna in balancing hydrophobic and surface area parameters for realizing high photocatalytic efficiencies while limiting decomposition rates. To counteract the reduction in SSA of the parent MOF due to the alkylation of the linker, an additional hydrophobic MOF, OPA/NH_2-MIL-125, was developed by alkylating the Ti cluster with octadecyl phosphonic acid (OPA). In MIL-125-R7, the alkyl chains filled its pores, while in OPA/NH_2-MIL-125, OPA modified the $Ti_8O_8(OH)_4$ cluster only on the exterior part, preserving most pores. This selective modification maintained higher photocatalytic activity for H_2O_2 production, attributed to the rapid reactant's diffusion and product generation. The specific surface area of OPA/NH_2-MIL-125 was measured at 1242 m^2 g^{-1}, showing that the majority of the SA was preserved after metal cluster alkylation, with the authentic pore diameter and volume remaining intact. OPA/NH_2-MIL-125's water contact angle, 110°, indicates its hydrophobic nature (Fig. 4d). In a benzyl alcohol/H_2O bi-phasic system, the OPA/NH_2-MIL-125 selectively dispersed in the benzyl alcohol phase. At the same time, H_2O_2 generation took place in the water phase with visible-light radiation. H_2O_2 generation with OPA/NH_2-MIL-125 was threefold greater in comparison with MIL-125-R7 after three hours of irradiation. Additionally, the photocatalytic activity of OPA/NH_2-MIL-125 in the benzaldehyde phase was 1.7 times more in comparison with MIL-125-R7 as they diffused swiftly through unblocked pores. These findings prove that cluster-alkylated OPA/NH_2-MIL-125 has better efficiency for photocatalytic H_2O_2 generation.

Zhang *et al.* reported the formation of NH_2-MIL-125(Ti) and NH_2-UiO-66(Ti) isomers *via* simple hydrothermal and post-synthesis exchange (PSE) methods.[136] Upon high-temperature treatment, defective NH_2-MIL-125(Ti) (NH_2-MIL-125-D) was formed, featuring a relatively short Ti–O bond length advantageous for charge transportation, thus improving photocatalytic performance compared with NH_2-UiO-66(Ti). NH_2-MIL-125-D has extra active sites owing to the loss of ligands, creating defective titanium sites that enhanced the reduction of adsorbed O_2 to H_2O_2 and increased yield. The N_2-adsorption isotherms showed higher adsorption for NH_2-MIL-125(Ti) than

NH_2-UiO-66(Ti), attributed to topological properties, allowing more significant oxygen adsorption. In contrast, NH_2-MIL-125-D showed lower N_2 uptake with hysteresis around 0.4–0.8 P/P_0, indicating mesopore formation due to high-temperature-induced ligand loss. Photocatalytic H_2O_2 production in water with catalysts (15 mg in 50 ml) under visible light showed slightly enhanced activity for NH_2-MIL-125(Ti) over NH_2-UiO-66(Ti), while NH_2-MIL-125-D significantly enhanced H_2O_2 production, achieving 62.7 mM H_2O_2 after 120 min. The increased performance of OPA/NH_2-MIL-125 can be ascribed to the presence of additional active sites created by defect-rich titanium resulting from ligand shortage in the framework. These defects facilitated the adsorption of oxygen and its rapid reduction to H_2O_2. However, there are critical issues in maintaining structural integrity during repeated use and in the effective separation of H_2O_2 from the catalyst to avoid decomposition. Furthermore, improvements in H_2O_2 collection techniques and the development of a biphasic system with hydrophobic treatments spatially separate the catalyst and H_2O_2, thus enhancing the efficiency and selectivity.

10.2. Cr(VI) reduction

The Cr(VI) photoreduction typically involves photogenerated electrons (e^-) in the conduction band (CB) of a semiconductor, with the CB edge needing a more negative potential than the Cr(VI)/Cr(III) redox potential. Direct reduction to Cr(0) is not possible due to the more negative Cr(III)/Cr(0) potential. e^- can reduce Cr(VI) either directly or *via* intermediates like Cr(V) and Cr(IV), following two main pathways: a one-step, three-electron transfer to Cr(III) (eqn (8)) or a stepwise, single-electron transfer (eqn (9)).[180–182] Acidic conditions are favored, and hole scavengers are added to prevent reoxidation of Cr(III) by ROS, improving e^- separation and reaction efficiency. Without scavengers, the reaction is slower in pure water due to recombination, leading to a four-electron transfer process (eqn (10)).[183,184]

$$Cr_2O_7^{2-} + 14H^+ + 6e^- \rightarrow 2Cr^{3+} + 7H_2O \quad (8)$$

$$Cr(VI) + e^- \rightarrow Cr(IV) + e^- \rightarrow Cr(III) \quad (9)$$

$$Cr(III) + ROS \rightarrow Cr(VI) \quad (10)$$

Wang and colleagues conducted research on the Cr(VI) photoreduction under visible light with NH_2-MIL-125(Ti), which was synthesized using an adapted solvothermal method in comparison with MIL-125(Ti).[133] MIL-125(Ti) is a well-crystallized white powder with particle sizes around 2 nm, while NH_2-MIL-125(Ti) is a yellow powder with particles ranging from 400 to 600 nm. XRD analysis of NH_2-MIL-125(Ti) showed no peaks related to bulk TiO_2 anatase or rutile phases, indicating the disappearance of large titanium oxide aggregates. UV–vis DRS spectroscopy revealed that MIL-125 absorbs light up to 350 nm, while NH_2-MIL-125 extends absorption to about 520 nm due to the 2-amino terephthalate ligand, enhancing its visible light absorption. Photocatalytic optimization studies showed that at pH 2.1, adding the hole scavenger ethanol increased the photocatalytic Cr(VI) reduction efficiency of NH_2-MIL-125(Ti) from 76% to 91%. In contrast, citric acid and EDTA reduced the efficiency to 72% and 66%, respectively. Ethanol, absorbed into NH_2-MIL-125(Ti), aids its mineralization and enhances Cr(VI) reduction by capturing photogenerated holes (eqn (11)–(13)), improving electron utilization. Conversely, citric acid and EDTA, through hydrogen bonding with NH_2-MIL-125(Ti), promote electrostatic adsorption of Cr(VI) but limit electron transfer at Ti sites, reducing the Cr(VI) reduction efficiency.

$$NH_2\text{-MIL-125(Ti)} + h\nu \rightarrow NH_2\text{-MIL-125(Ti)}(h^+ + e^-) \quad (11)$$

$$CH_3CH_2OH + h^+ \rightarrow CH_3CH_2OH^+ \rightarrow CO_2 + H_2O + \text{others} \quad (12)$$

$$14H^+ + Cr_2O_7^{2-} + 6e^- \rightarrow 2Cr^{3+} + 7H_2O \quad (13)$$

The Cr(VI) reduction efficiency by NH_2-MIL-125 lessened significantly as the pH increased from 4.07 to 8.17. Under acidic conditions, the photocatalytic reaction follows eqn (13), where the abundance of H^+ ions enables the reduction of Cr(VI). Conversely, in basic environments, eqn (14) predominates as CrO_4^{2-} becomes the dominant species. The zeta potential values of both MIL-125 and NH_2-MIL-125 become increasingly negative along with rising pH levels. NH_2-MIL-125(Ti) exhibits a positive zeta potential below pH 4.6, which enhances the adsorption of anionic Cr(VI) and consequently improves photoreduction efficiency. At higher pH values, the catalyst surface becomes negatively charged, repelling the anionic Cr(VI) entity and promoting the cationic Cr(III) adsorption entity. Moreover, at pH > 6, there is precipitation of Cr(III) as $Cr(OH)_3$, which can mask active sites on NH_2-MIL-125.

$$CrO_4^{2-} + 4H_2O + 3e^- \rightarrow Cr(OH)_3 + 5OH^- \quad (14)$$

XPS analysis confirmed the valence states of chromium bound to the MOF. Peaks observed at 577.3 eV and 580.7 eV for Cr $2p_{3/2}$ orbitals indicate the presence of Cr(III), suggesting the reduction of Cr(VI) to Cr(III). Additionally, a peak at 586.7 eV corresponds to Cr(VI) absorbed onto the titanium MOF, attributed to the material's large specific surface area, pore assembly, and electrostatic interactions. This was further supported by a shift in the N 1s peak in Cr/NH_2-MIL-125(Ti). The projected mechanism (Fig. 4e) comprises the enhancement of visible light harvesting by H_2ATA in NH_2-MIL-125. Photoexcited H_2ATA transfers photoinduced e^-s to the Ti–O clusters, producing Ti^{3+}. These Ti^{3+} ions re-oxidize to Ti^{4+} upon exposure to air. The charge transfer between Ti^{3+} and Ti^{4+} in the Ti–O clusters was clarified by Horiuchi *et al.* using ESR and UV–Vis spectra.[56] Ethanol, which was adsorbed onto the NH_2-MIL-125, functions as a hole scavenger, decomposing into CO_2 and H_2O, thereby creating a basic environment that promotes the Cr(VI) reduction. NH_2-MIL-125 also demonstrated good reusability, with only an 8% reduction in photoactivity after five consecutive cycles of washing with HNO_3, deionized water, and drying. Furthermore, ethanol enhanced Cr(VI) reduction efficiency from 76% to 91%, while the exact mecha-

nism of stabilizing the separation of electron and hole remains to be studied. Decoding the pH dependency in Cr(VI) reduction is also important, as its higher efficiency under acidic conditions reduces catalyst reusability, owing to Cr(III) precipitation. Thus, pH-stabilized photocatalysts or dual-function photocatalysts could be investigated to maintain high activity over a wider pH range, thereby minimizing Cr(III) precipitation.

Modification of MIL-125 and NH_2-MIL-125 with highly dispersed platinum nanoparticles (3–9 nm) resulted in improved Cr(VI) photoreduction, as the Pt nanoparticles accelerated electron transfer and delayed electron–hole recombination.[137] In 2017, Kitagawa *et al.* developed a MOF-on-MOF hybrid heterostructure using the internal extended growth method (IEGM).[134] Typically, epitaxial growth requires MOFs with similar crystallographic parameters. However, IEGM overcomes lattice mismatching limitations, enabling the synthesis of MIL-101(Cr) over NH_2-MIL-125(Ti). This process involves microwave treatment of pre-made MIL-101(Cr) and NH_2-MIL-125(Ti) precursors with PVP as a structure-directing entity, resulting in MIL-101(Cr) nanoparticles homogeneously distributed on NH_2-MIL-125 nano tablets. The synthesized micro–mesoporous MOF-on-MOF system, MIL-101@NH_2-MIL-125, demonstrated a substantially higher Cr(VI) adsorption capacity (3.16 mg g^{-1}) in comparison with NH_2-MIL-125(Ti) and MIL-101(Cr). After being exposed under visible light for two h, MIL-101@NH_2-MIL-125 accomplished a 72% reduction in Cr(VI), whereas NH_2-MIL-125(Ti) achieved a reduction of 47%, and MIL-101(Cr) exhibited negligible reduction (Fig. 4f and g). This improved photocatalytic performance is credited to the harmonious interface among NH_2-MIL-125 and MIL-101(Cr), with the mesopores in MIL-101(Cr) significantly enhancing Cr(VI) adsorption.

Defect engineering in photocatalysts is a promising approach aimed at enhancing the number of active sites and promoting effective photogenerated exciton pair separation.[185–187] In 2021, researchers developed a defective NH_2-MIL-125(Ti) with linker vacancies over controlled thermal treatment, which involved decomposing the carboxylic acid group of 2-amino terephthalic acid.[188] Through prolonged thermal treatment, the decomposition of the NH_2-MIL-125 ligand progressed inward from the surface, leading to an increased presence of linker-vacancy defects. This modification significantly impacted the material's framework structure, light-harvesting properties, and energy band structure. Moderate levels of linker-vacancy defects have been found to enhance the photoinduced charge carrier separation significantly. This enhancement resulted in a Cr(VI) photoreduction that was 9.2 times higher compared with the neat MOFs. However, high concentrations of linker-vacancy defects are known to deteriorate the crystal structure and impede efficient charge separation. There should be a balance between too much and too little defect content, as too many will destabilize the framework, whereas too few will not effectively improve photocatalytic activity. This balance is sensitive and needs further study.

Conductive polymers such as polyaniline and polypyrrole have garnered considerable interest owing to their versatile applications, including their ability to reversibly switch between oxidation and reduced states, which is advantageous for reducing toxic metal ions such as hexavalent chromium.[189] Choe *et al.* established a core–shell heterostructure called polypyrrole nanotube@NH_2-MIL-125 (PPynt@NH_2-MIL-125) by growing NH_2-MIL-125 *in situ* on polypyrrole nanotubes.[138] The PPynt@NH_2-MIL-125 heterostructure exhibited outstanding outcomes in Cr(VI) photoreduction under visible light conditions. Incorporating 5 wt% of PPynt resulted in a superior elimination efficiency, approximately 70% improvement compared with pure NH_2-MIL-125. Moreover, these nanocomposites demonstrated excellent robustness and cycling stability. The study puts the critical role played by MOFs in the spotlight in enhancing the photocatalytic performance of NH_2-MIL-125 for Cr(VI) photoreduction, specifically by facilitating the effective charge carrier separation under visible light in the PPynt@NH_2-MIL-125 nanocomposite.

In 2023, Wang *et al.* fabricated a NA/NH_2-MIL-125(Ti) homojunction by partially post-synthesis modifying the Ti-MOF with 1-naphthylamine (–NA, a chromophoric group).[139] Unlike the earlier reported MR/NH_2-MIL-125(Ti), the conjugated N=N bond and the naphthalene ring offered advanced photoactivity. Photoreduction of Cr(VI) using white light showed NA/NH_2-MIL-125 had the highest activity among tested MOFs, with dark control experiments confirming the necessity of photoexcitation. Physical mixture experiments suggested a tightly bound complex, supporting its superior performance. Pseudo-first-order kinetics analysis revealed NA/NH_2-MIL-125 had a rate constant 1.5 times greater than NH_2-MIL-125. The NA-group was designed *via* mixing 1-naphthylamine with diazonium salt, with an optimal $NaNO_2$: amino group ratio of 0.1 : 1. Lower pH favored Cr(VI) reduction, and EDTA-2Na performed like a hole scavenger and influenced reaction efficiency. NA/NH_2-MIL-125 exhibited wide-spectrum responsiveness, with peak performance under purple light (410–420 nm). Incorporating the –NA chromophore notably improved light absorption, charge separation, and the formation of active species. The homojunction with optimal ratio demonstrated the highest photocurrent, and the synthesized samples showed excellent reusability over multiple operation cycles.

Tin disulfide (SnS_2) is a favorable semiconductor owing to its appropriate E_g in the visible region, strong light absorption efficiency, abundance, and resistance to photocorrosion, unlike CdS semiconductors.[151,190–192] Sun *et al.* demonstrated that SnS_2 nanosheets loaded onto NH_2-MIL-125 form a new Z-scheme heterostructure that effectively reduces Cr(VI) in visible light.[193] The photocatalytic efficiency of NTS_2 for Cr(VI) reduction is influenced by pH, with acidic conditions enhancing reduction efficiency due to increased Cr(VI) adsorption and electron capture. In contrast, alkaline conditions lead to $Cr(OH)_3$ precipitation, covering active sites and reducing activity. Metal ion leaching, such as Sn from NTS_2, increases with pH due to sodium stannate formation in alkaline environ-

ments. However, Cr(VI) reduction is of utmost effectiveness in strongly acidic media, minimizing Sn ion leaching. NTS_2 exhibited excellent recyclability, maintaining a high elimination rate of 90.28% after four cycles, with XRD patterns indicating structural stability. The Z-scheme heterojunction facilitated electron transfer from SnS_2 to NH_2-MIL-125, enhancing electron–hole pair separation. Photon absorption by NT and SnS_2 generated electron–hole pairs, followed by electron transfer and Cr(VI) reduction to Cr(III). However, challenges include inefficiency observed at higher pH levels due to electrostatic repulsion and the precipitation of $Cr(OH)_3$, which masks the active sites. Much remains to be discovered about intermediate species, such as Cr(V) and Cr(IV), which are generated during the stepwise reduction of Cr(VI). The combined application of *in situ* real-time tracking and computational modeling could provide valuable insights into designing photocatalysts that selectively reduce Cr(VI) with the fewest possible side reactions. Optimizing conditions, such as using scavengers and maintaining acidity, alongside exploring hybrid structures, defect engineering, and core–shell heterostructures, can enhance electron transfer, charge separation, and stability.

10.3. CO_2 reduction

The challenge of converting carbon dioxide (CO_2) into valuable chemicals is both formidable and essential for advancing sustainable energy and addressing climate change. CO_2's inherent stability, combined with significant thermodynamic and kinetic barriers, makes its transformation particularly difficult. Having a Gibbs free energy change (ΔG°) of −400 kJ mol^{-1}, CO_2 requires substantial energy input and effective catalysis to undergo efficient conversion [C2]. It has a linear molecular structure characterized by two carbon–oxygen double bonds. This inherent stability poses significant challenges to its transformation into useful chemicals without the assistance of a catalyst and the input of energy.[194] Both thermodynamic and kinetic constraints, combined with a substantial energy gap between the LUMO and HOMO of 13.7 eV, besides a superior electron affinity of −0.6 ± 0.2 eV, contribute to the inert nature of CO_2.[195] Photocatalytic CO_2 reduction pathways vary based on the reductant, with carbon-free reductants (H_2O and H_2) generally forming C1 products and carbon-rich entities (CH_4 and CH_3OH) potentially forming C2 and C3 products. Common CO_2 photoreduction products include CO, HCOOH, HCHO, CH_3OH, CH_4, and C_2H_5OH.[196–199] Scheme 1 illustrates the required reducing electrons, oxidizing holes, and protons (H^+) for forming these main products (Fig. 5a).[200]

A promising approach for CO_2 reduction involves creating materials that work under visible light. Photoactive titanium-based MOFs, like NH_2-MIL-125, are effective. Li *et al.*[50] showed that NH_2-MIL-125, as a semiconductor, converts CO_2 to formate using triethanolamine (sacrificial agent). Amino groups in the framework created an LMCT band that absorbed visible light, generating a long-lived exciton pair. Electrons moved to Ti^{4+} ions, reducing them to Ti^{3+}, which acted as active centers for CO_2 reduction, while TEOA served both as an e^- donor and Lewis base. The team also studied NH_2-MIL-125 in combination with noble metals like Pt and Au in a saturated environment of CO_2.[125] Noble metal NPs embedded in the MOF acted as electron traps, enhancing redox reactions and, thus, overpotential reduction. Over 8 hours, Pt/NH_2-MIL-125 showed a 21% increase in CO_2 reduction compared with unmodified NH2-MIL-125, while Au/NH_2-MIL-125 had a 16% decreased performance with a reduction yield of 9.06 μmol. The stronger Pt–O bond stabilized Pt, facilitating Ti^{3+} formation, whereas the weaker Au–O bond led Au to prefer NH_2 sites, preventing this effect. Selecting the right MOF–metal pair is crucial for boosting photocatalysis. Such difference displays how sensitive the photocatalytic system is to the metal–support interactions, thereby emphasizing the importance of the appropriate choice of metal nanoparticles.

Non-noble metal doping offers distinct advantages over noble metal doping in NH_2-MIL-125 for photocatalytic CO_2 reduction owing to the abundance and cost-effectiveness of non-noble metals, making large-scale production more economically viable. In 2017, Fu *et al.* introduced Co-doped NH_2-MIL-125 photocatalysts for visible-light-assisted CO_2 reduction.[141] The embodiment of Co nanoparticles (NPs) into the MOF framework enabled these particles to act as efficient electron traps, capturing electrons from the excited ligands. Furthermore, replacing triethanolamine with benzylic alcohols as electron donors significantly enhanced the reduction process. Co/NH_2-MIL-125(Ti) demonstrated dual catalytic activity: it facilitated the reduction of CO_2 to formic acid (HCOOH) while selectively oxidizing benzylic alcohols to their corresponding aldehydes. This dual functionality enhances the economic and environmental viability of the process. To address the challenge of regulating electron transfer within metal-oxo clusters of MOFs *via* heteroatom doping, Gao *et al.* selected Ni for its high electron affinity. They investigated the impact of Ni on electron distribution in NH_2-MIL-125 by preparing NH_2-MIL-125-Nix/Ti materials with precise Ni concentrations through *in situ* doping.[142] Nickel, being more electronegative than Ti, alters the electronic arrangement of Ti–O clusters in NH_2-MIL-125. PDOS calculations (Fig. 5b) showed a reduced organic ligand contribution in Ni^{2+}-doped NH_2-MIL-125's HOMO and LUMO, with increased Ni 3d and Ti 3d contributions. Ni^{2+} created states between HOMO and LUMO, facilitating electron transfer and enhancing charge separation. Doping with Ni^{2+} significantly enhanced CO_2 to CH_4 conversion. The addition of Ni^{2+} dopants significantly enhanced the photocatalytic performance, resulting in a three-fold increase in CO yield with 0.5% Ni^{2+} doping and a six-fold increase with 1% Ni^{2+} doping in NH_2-MIL-125 compared with the undoped counterpart. NH_2-MIL-125-Ni1%/Ti showed 98.6% CO selectivity due to enhanced charge carrier separation and conductivity. EPR spectra indicated increased exciton separation, more photoinduced holes, and Ti^{3+} signals, which enhanced electron production and charge separation, boosting photoelectric conversion efficiency and photocatalytic performance.

ZnS is an effective, low-cost semiconductor photocatalyst with a wide E_g.[203] However, reverse electron flow and recombination can hinder its performance.[204,205] Combining ZnS and NH_2-

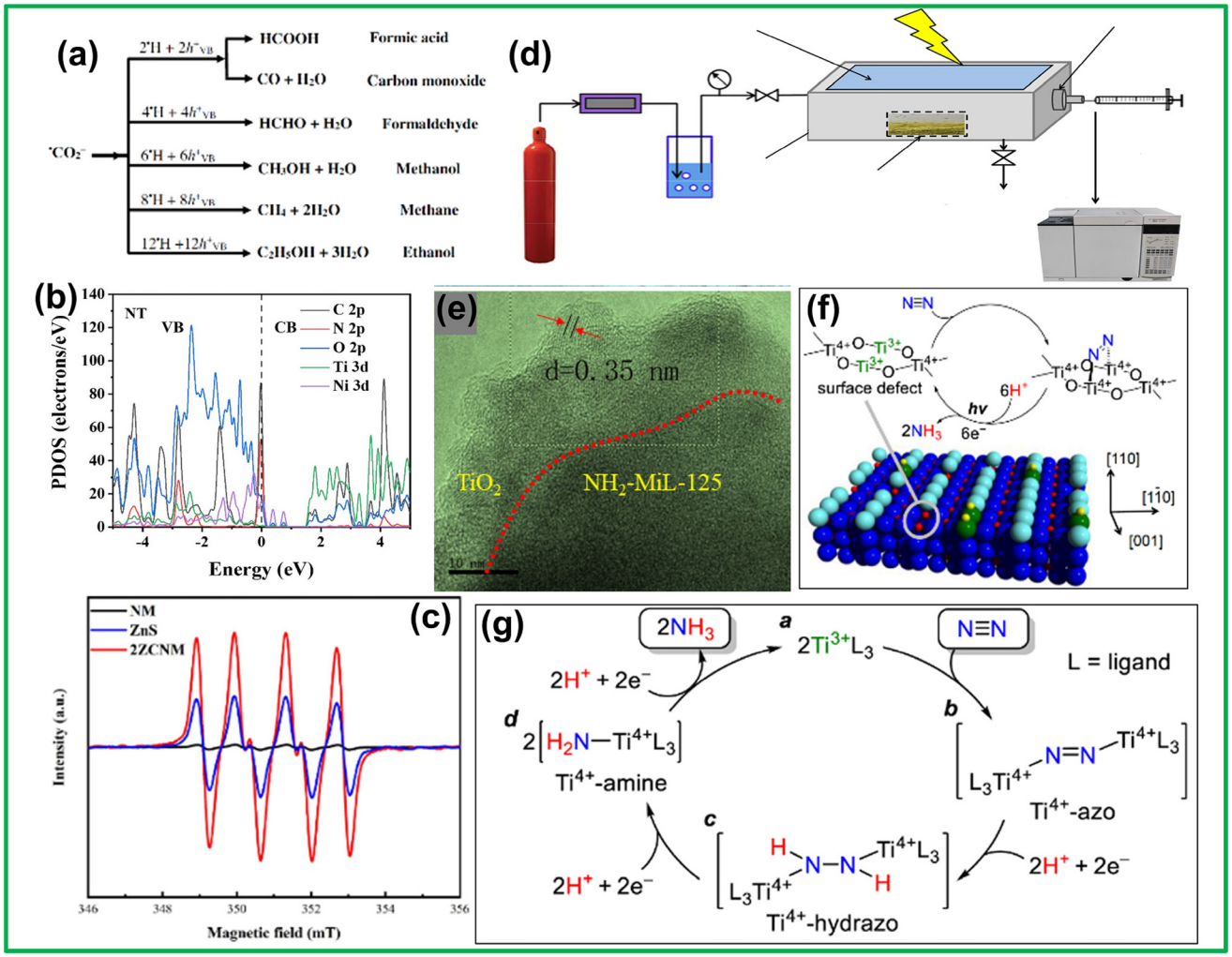

Fig. 5 (a) The total pathways for production of the main products of photocatalysis of CO_2. Reprinted with permission from ref. 200. Copyright 2016 Elsevier Ltd. (b) PDOS for Ni^{2+}-doped Ti-MOF indicated as NT. Reprinted with permission from ref. 142. Copyright 2020 Elsevier B.V. (c) ESR spectra by adding DMPO to capture $^{\bullet}O_2^-$ with NM, ZnS, and 2ZCNM. Reprinted with permission from ref. 144. Copyright 2023 Elsevier B.V. (d) A schematic illustration of the photoreactor set-up for photocatalytic CO_2 reduction in a gas phase system. Reprinted with permission from ref. 201. Copyright 2021 Elsevier Ltd. (e) HR-TEM image of CNMT-40. Reprinted with permission from ref. 147. Copyright 2023 Elsevier B.V. (f) Proposed photocatalytic cycle for N_2 fixation on the rutile TiO_2 (110) surface. (g) Catalytic cycle for N_2 fixation by Ti^{3+}-containing complexes. Reprinted with permission from ref. 202. Copyright 2017 American Chemical Society.

MIL-125 in a heterojunction addresses these issues and improves performance.[206] Mediating agents can further boost photocatalytic activity and carrier separation.[207,208] In 2024, Zhou *et al.* used carbon quantum dots (CQDs) derived from waste biomass sludge as mediators to link ZnS and NH_2-MIL-125 towards CO_2 photoreduction.[144] This Z-scheme approach treats waste muck and enhances charge transfer, offering two-fold benefits.[209,210] The 2ZCNM composite catalyst showed significant photocatalytic performance enhancements for CO_2 reduction, yielding 501.57 μmol g^{-1} of CH_3OH and 564.70 μmol g^{-1} of CH_3CH_2OH in 3 hours. The improvement was due to the synergistic effects of CQDs and ZnS, which altered the pore structure and introduced mesoporous features, enhancing H_2O and CO_2 adsorption. While ZnS boosted photocatalytic activity, excess loading blocked active sites, causing electron–hole recombination. The formation of CH_3OH and CH_3CH_2OH was exclusively from CO_2, confirming process selectivity and efficiency. The 2ZCNM composite showed minimal activity loss after five cycles, highlighting its stability as a CO_2 reduction photocatalyst. ESR spectroscopy (Fig. 5c) confirmed the Z-scheme of 2ZCNM, enhancing carrier separation and $O_2^{\bullet-}$ radical generation. NM and ZnS created exciton pairs with visible light, while CQDs facilitated electron transfer from NM's LUMO to ZnS's CB. Electrons in ZnS's CB reacted with CO_2 to form CH_3OH and CH_3CH_2OH, and NM's HOMO generated hydroxyl radicals ($^{\bullet}OH$), improving charge separation and CO_2 reduction performance. While harnessing CQDs has shown promise in improving carrier separation and enhancing the stability of photocatalysts, optimizing the balance between material loading and undue recombination still presents challenges.

Publications on graphene-assisted MOF composites for visible light photocatalysis are limited. However, reduced graphene oxide (rGO) has exceptional properties such as high thermal conductivity,[211] chemical robustness,[212] large surface area,[213] mechanical strength,[214] charge carrier mobility,[215] and optical transparency,[216,217] making it ideal for composites with NH_2-MIL-125. Olowoyo *et al.* investigated the photoreduction efficacy of pristine MOF and RGO-NH_2-MIL-125 composites for CO_2 reduction in a CH_3CN + H_2O medium with TEOA as a sacrificial reagent in 2020.[145] They found that RGO-NH_2-MIL-125 showed only marginal increases in methane and ethylene production compared with NH_2-MIL-125 but significantly enhanced methanol selectivity in both liquid and gas phases. This performance was due to RGO-NH_2-MIL-125's greater visible light absorption and narrower E_g, leading to more efficient solar spectrum use. RGO also improved charge transport and separation, boosting product formation. Computational studies confirmed charge localization and CO_2–TEOA interactions with the MOF, supporting RGO-NH_2-MIL-125's potential as a potent CO_2 reduction photocatalyst under visible light exposure. The alignment of CB and VB plays a pivotal part in facilitating charge carrier transfer within heterostructures. The band positions of g-C_3N_4 and NH_2-MIL-125 MOF are well matched, creating a Z-scheme heterojunction. rGO is an electron mediator crucial for suppressing charge recombination in this configuration. In 2021, Muhammad Tahir and colleagues used thermal and hydrothermal synthesis to prepare an RGO-mediated g-C_3N_4/NH_2-MIL-125 nanocomposite (Fig. 5d).[201] This composite embedded Ti-MOF on the g-C_3N_4-RGO matrix, achieving better dispersion and enhancing charge transference. TEM images showed favorable heterojunction interactions. The neat MOF exhibited H_3 hysteresis loops, while the composite showed type H4 hysteresis due to the MOF's high surface area. Pore size distribution increased after combining MOF with g-C_3N_4, with higher pore volumes at ~50 nm. NH_2-MIL-125 had intense visible-range absorption, improving solar energy use. The g-C_3N_4-RGO matrix showed improved light absorption with 20 wt% MOF loading. The g-C_3N_4-RGO-MOF (20%) composite achieved maximum efficiency with CO generation of 383.79 μmol per g, thanks to RGO's enhancement of charge carrier separation and transfer, and NH_2-group functionalization in MOF increasing activity in the visible light region and also CO_2 adsorption. The amino group promoted CO_2 interactions, and oxygen in ligands and Ti-metal complexes increased water adsorption. At various CO_2 pressures (0.2, 0.4, and 0.8 bar), the ternary composite showed increased CO (25.08 μmol g^{-1}) and CH_4 (597.63 μmol g^{-1}) production rates, with higher pressure enhancing CO_2 concentration and availability. The indirect Z-scheme heterojunction and RGO's role as an electron mediator reduced recombination rates, boosting productivity and quantum yields.

TiO_2, known for its nontoxicity, availability, and light stability, is widely used as a semiconductor. Huang *et al.* advanced photocatalytic CO_2 and CH_4 conversion using NH_2-MIL-125 with TiO_2 quantum dots.[147] The NH_2-MIL-125@TiO_2-40 catalyst showed superior CO_2 conversion efficiency, achieving a CO yield of 159 μmol g^{-1}, surpassing previous reports and indicating potential for practical CO_2 utilization. A heterojunction structure was found at the NH_2-MIL-125 and 0D TiO_2 interface in CNMT-40, while SNMT-15 exhibited excessive TiO_2 crystallization, potentially affecting the MOF structure (Fig. 5e). The red-shift in CNMT-40's absorption spectrum suggests an E_g modification due to Ti–C–N bond formation and electronic structure changes, enhancing visible light absorption. TiO_2 integration significantly improved the photocurrent density of the MOF, indicating better exciton pair separation. CNMT-40 executed superior photocurrent intensity and stable performance during tests, highlighting its superior e^- and h^+ transportation and separation compared with other catalysts. The hybrid material NMT, prepared *via* a wet chemical method, outperformed 2D TiO_2 and NM. CNMT-40 maintained a 93.7% photocatalytic CO_2 conversion efficiency after six cycles, demonstrating decent stability. Its better performance in converting CO_2 and CH_4 was due to an efficient and stable heterojunction that improved electron and hole transport rates, inhibited charge recombination, and enhanced catalyst stability. Amorphous titanium dioxide (Am-TiO_2) offers benefits like milder synthesis conditions and a larger surface area.[218] Though it has a wide band gap and high recombination rates, limiting visible light harvest and thus the photocatalytic performance, Am-TiO_2 can be an efficient co-catalyst. Hu *et al.* fabricated Am-TiO_2/NH_2-MIL-125 *via* a one-pot water bath method.[219] Am-TiO_2 acted as an electron acceptor, enhancing photocarrier separation. XRD patterns showed effective integration with NM, and Raman spectroscopy confirmed the amorphous nature of Am-TiO_2, showing minimal vibration modes compared with anatase TiO_2. NM and NM/TiO_2 composites produced significant CH_4 from CO_2 reduction, while Am-TiO_2 showed minimal activity. XRD patterns and FTIR/TGA analysis indicated no significant changes in structure or properties post-reaction, showing robustness. The 0.25 ATN composite had a stronger visible light response due to defects in amorphous TiO_2, resulting in more electron–hole pairs. Generally, a smaller contact angle indicates better hydrophilicity of the catalyst.[220] Contact angle tests revealed higher hydrophilicity for 0.25 ATN, enhancing photoactivity. Pre-irradiation bands indicated CO_2 adsorption capability, while post-irradiation decreases in Ti^{3+}–OH and Ti^{4+}–OH peaks suggested CO_2 reaction to form bicarbonate species. The mechanism involves electron photoexcitation from NM to Am-TiO_2, with efficient exciton separation boosting the performance of NM/Am-TiO_2 composites in CO_2 reduction.

The facet-dependent photocatalytic behavior of MOFs, particularly NH_2-MIL-125(Ti), remains largely unexplored. In one study, Cheng *et al.* synthesized NH_2-MIL-125(Ti) with controlled {001} and {111} facet ratios *via* a one-step solvothermal method, enabling precise tuning of active facet exposure. By adjusting the solvent ratio of DMF and MeOH and varying titanium sources, they modulated the facet ratios effectively. With increased {111} facet exposure, a red shift in the absorption spectrum was observed, while NM001 displayed the narrowest

absorption. Using TEOA as a sacrificial agent, NM111 exhibited significantly higher photocatalytic performance for CO and CH_4 production, with yields of 8.25 and 1.01 μmol g^{-1} h^{-1}—9 and 5 times higher than NM001, respectively. This enhancement was attributed to the larger surface area and higher Ti content in the {111} facets, which facilitated Ti^{4+}/Ti^{3+} interconversion and unveiled more active sites for CO_2 reduction.[221] Building on prior research, the group demonstrated that loading Ag NPs onto the {111} facets of NH_2-MIL-125(Ti) *via in situ* photodeposition significantly enhanced photocatalytic activity and CH_4 selectivity for CO_2 reduction. The Ag-loaded catalysts exhibited more negative HOMO levels, boosting product yields. The Ag NPs improved CO_2 adsorption by serving as additional adsorption sites, with a small Q_{st} value indicating weak CO_2–catalyst interactions that facilitated CO_2 migration to active sites. Additionally, the SPR effect of Ag NPs enhanced light absorption, charge separation, and transfer. These synergistic effects broadened light absorption, increased CO_2 adsorption, and suppressed charge recombination, offering new insights into facet engineering for optimizing CH_4 selectivity in CO_2 reduction.[222] Guo *et al.* developed an ultrasound-assisted method to synthesize NH_2-MIL-125 nanosheets with predominantly exposed {110} facets, which contained a higher concentration of active metal clusters than {001} and {111} facets. Ultrasound waves created strong shear forces that promoted the formation of thin sheet structures. This ultrathin morphology increased active sites, enhanced charge carrier transfer, and suppressed electron–hole recombination. DFT simulations revealed that in the 2D {110} facet, conduction band states were distributed across the entire outer layer, allowing more Ti atoms to participate in the catalytic reaction, thereby boosting photocatalytic performance.[223]

In a recent study, Cheng *et al.* synthesized MIL-125-NH_2(Ti) MOFs with controlled facet exposure ({001}, {110}, {111}) and mixed-facet heterojunctions ({001}/{110}, {001}/{111}, {110}/{111}) *via* a solvothermal method to explore facet-dependent photocatalytic CO_2 reduction. The {110}/{111} heterojunction (T23) exhibited the highest CO and CH_4 yields, at 15.49 and 5.46 μmol g^{-1} h^{-1} which were 10- and 18-fold higher than the {001} facet (T1). This enhancement was due to improved charge separation and transfer facilitated by the heterojunction. DFT calculations showed that the {111} facet had the lowest Gibbs free energy barrier for *COOH formation, aiding efficient CO_2-to-CH_4 conversion.[224] In a follow-up study, Cheng *et al.* examined high-index {112} facets of NH_2-MIL-125(Ti), which significantly boosted photocatalytic activity. CO and CH_4 yields increased by 33- and 31-fold, respectively, compared with the {001}/{111} facets. The distinct surface chemistry of the {112} facets provided a larger surface area, higher CO_2 adsorption, and stronger CO_2 interactions, resulting in greater adsorption enthalpy and efficient CO_2 activation. Additionally, more exposed Ti-oxo clusters facilitated the Ti^{4+}/Ti^{3+} transition, enhancing electron transfer and reducing charge recombination. This study highlights the potential of high-index facet engineering as a powerful strategy for optimizing MOF-based photocatalysts, offering a promising approach for designing next-generation MOFs with tailored facets for efficient CO_2 photoreduction.[225]

In conclusion, noble metals enhance charge carrier separation but are expensive. Non-noble metals are cost-effective but require precision. Hybrid and graphene-based composites improve interactions and charge transport but face challenges in uniform dispersion and stability. New strategies include using conductive polymers and Z-scheme heterojunctions. Future research should focus on optimizing material combinations, doping, facet engineering, and stability for efficient and scalable CO_2 reduction.

10.4. N_2 fixation

Ammonia (NH_3) serves as a critical precursor in fertilizer manufacturing, and industrial N_2 fixation traditionally depends on the Haber–Bosch process, which necessitates high temperature and pressure for transforming N_2 and H_2 into NH_3. Photocatalytic nitrogen fixation occurs through two main processes: nitrogen reduction reaction (NRR) and nitrogen oxidation reaction (NOR). When exposed to sunlight, the photogenerated holes in VB facilitate the oxidation of H_2O into H^+ and O_2 (eqn (15)). Additionally, NH_3 is synthesized from N_2 reduction by hot electrons under sunlight (eqn (16)), enabling NH_3 production from H_2O and N_2 under optimal conditions with solar light as the primary source of energy (eqn (17)).[226]

$$2H_2O + 4h^+ \rightarrow O_2 + 4H^+ \quad (15)$$

$$N_2 + 6H^+ + 6e^- \rightarrow 2NH_3 \quad (16)$$

$$2N_2 + 6H_2O \rightarrow 4NH_3 + 3O_2 \quad (17)$$

During photocatalytic N_2 oxidation, photogenerated holes (h^+) react with N_2 and H_2O to produce NO (eqn (18)), while photoexcited electrons reduce O_2 to H_2O (eqn (19)). The generated NO is subsequently oxidized to nitrates, resulting in the evolution of O_2 and H_2O (eqn (20)). Under ambient conditions, nitric acid is produced using sunlight as the primary energy source by synthesizing it from water, O_2, and N_2 (eqn (21)).

$$N_2 + 2H_2O + 4h^+ \rightarrow 2NO + 4H^+ \quad (18)$$

$$O_2 + 4H^+ + 4e^- \rightarrow 2H_2O \quad (19)$$

$$4NO + 3O_2 + 2H_2O \rightarrow 4HNO_3 \quad (20)$$

$$\text{Overall}: \ 2N_2 + 5O_2 + 2H_2O \rightarrow 4HNO_3 \quad (21)$$

The two pathways for photocatalytic N_2 fixation are referred to as the associative alternating route (Path 1) and the associative distal route (Path 2).[227]

Artificial N_2 fixation under milder conditions remains a significant challenge to date. TiO_2 containing oxygen vacancies can function as a photocatalyst for N_2 fixation, leveraging the presence of Ti(III); however, its activity is restricted to the UV region only (Fig. 5f and g).[202] In contrast, the titanium-based NH_2-MIL-125, featuring a titanium-oxo cluster and acting as a visible light photosensitizer, is emerging as a promising candi-

date for achieving artificial N_2 fixation under visible light conditions. Li *et al.* introduced a novel range of titanium-based MOFs designed for N_2 fixation under visible light exposure, marking a significant advancement.[148] They synthesized three types of visible light-responsive titanium-MOFs—CH_3-MIL-125, NH_2-MIL-125, and OH-MIL-125—via either one-pot synthetic method or solvent-assisted linker exchange approaches. When compared with neat MIL-125(Ti), these MOFs modified with different ligands exhibited enhanced light-absorption capabilities, ranked as CH_3-MIL-125(Ti) < OH-MIL-125(Ti) < NH_2-MIL-125(Ti). Consequently, their photocatalytic performance also followed the same order for producing ammonia. Control experimentations employing isotope labeling confirmed N_2 and water as the sources of the generated ammonia. Mechanistic insights revealed that the organic ligands, responsive to visible light, acted as efficient photosensitizers, while the reduced Ti(III) species served as the active catalytic sites. Although research about these materials is very promising, there is still a critical gap in the literature regarding the mechanistic pathways of N_2 reduction in these systems. The precise role that organic ligands play in Ti-based MOFs acting as photosensitizers is being studied, but their presence seems to be critical for achieving better electron transfer and, thus, better catalytic efficiency.

Atomic or ion doping can modify M–O clusters, thereby altering the electronic and microenvironment around these catalytic sites crucial for photocatalytic reactions.[228] Hou *et al.* employed a one-step solvothermal method to produce a range of Ce-doped NH_2-MIL-125, aiming to investigate their efficacy in photocatalytic N_2 fixation.[149] The incorporation of Ce extends the absorption edge into the visible region and introduces additional reaction sites, thereby enhancing the charge transfer and facilitating dual electron O_2 reduction reactions. Upon light excitation, the Ce^{4+}/Ce^{3+} redox pair adjusts e-states adjacent to the Fermi level, engaging additional active e^-s in N_2 fixation.[229] Ce doping also increases the Ti^{3+} content, which serves as an active site and facilitates N_2 chemisorption by donating electrons. Additionally, Ce boosts LMCT efficiency, improving the separation of photogenerated carriers. Under full-spectrum radiation, NH_2-MIL-125 achieves an NH_3 generation rate of 10.6 μmol g^{-1} h^{-1}. Incorporating 2% Ce into the MOF matrix significantly enhances its N_2 fixation performance, achieving an NH_3 synthesis rate of approximately 39.4 μmol g^{-1} h^{-1}, which is 3.7-fold better than the undoped MOF. This improvement underscores the synergistic effect between Ti^{4+}/Ti^{3+} and Ce^{4+}/Ce^{3+} ions, which boosts the proficiency of the photocatalytic nitrogen fixation reaction. While doping improves the catalytic efficiency, the relative success of doping depends on finely tuning the dopant concentration to avoid loss of structural integrity or unwanted secondary reactions in real-world situations. The main challenge in nitrogen fixation is achieving high catalytic efficiency under mild conditions by optimizing heterojunctions for improved exciton separation and light absorption. Ensuring stability and reusability during operation is vital, particularly when adding dopants to enhance activity and maintain structural integrity. Mechanistic studies of electronic interactions are crucial for designing more potent catalysts.

10.5. H_2 evolution

Photocatalytic H_2 production *via* water splitting represents a potential solution to the global energy crisis.[52,230,231] The process of photocatalytic H_2 evolution involves three main stages: (i) photons with energy exceeding the semiconductor's E_g excite e^-s from the VB to the CB, simultaneously generating h^+s in the VB; (ii) the exciton pairs generated get separated and migrate to the exterior of the material; (iii) surface adsorbed H^+ is reduced by the e^-s in the CB to form H_2, while holes in the VB oxidize H_2O to produce O_2. For efficient H_2 production, the following redox reactions must occur:[232]

$$\text{Oxidation}: \ 2H_2O \rightarrow O_2 + 4H^+ + 4e^- \quad E_0 = 1.23 \text{ eV} \quad (22)$$

$$\text{Reduction}: \ 2H^+ + 2e^- \rightarrow H_2 \quad E_0 = 0.00 \text{ eV} \quad (23)$$

$$\text{Overall}: \ 2H_2O \rightarrow O_2 + 2H_2 \quad E_0 = 1.23 \text{ eV} \quad (24)$$

For HER to occur, the CB potential must be lower than 0 V under the NHE. Additionally, the VB potential must be higher than 1.23 V for the water oxidation reaction to proceed.

Since Matsuoka *et al.*'s pioneering work in 2012 using NH_2-MIL-125 as a photocatalyst for H_2 generation, numerous titanium-based MOFs have been developed for this reaction. Pt metal particles are commonly used as efficient cocatalysts. Pt NPs photodeposited on the MOF enhanced its activity, yielding a visible region active photocatalyst PtNPs@NH_2-MIL-125(Ti) with a hydrogen generation activity of 367 μmol g^{-1} h^{-1}, using e^- donor triethanolamine (Fig. 6a).[56] Mechanistic studies have revealed that upon excitation, photogenerated electrons on NH_2-BDC transfer initially to the metal-oxo cluster and subsequently to platinum NPs towards H_2 production. UV light illumination has been shown to significantly enhance activity, reaching 1170 μmol g^{-1} h^{-1}, primarily because of the direct excitement of titanium-oxo clusters. Additionally, Matsuoka *et al.* explained the improved photoactivity of PtNPs@NH_2-MIL-125 by optimizing the platinum deposition. They determined that a platinum loading of 1.5 wt% achieved the maximum activity of 517 μmol g^{-1} h^{-1}. Besides the outstanding performance of the PtNPs@NH_2-MIL-125(Ti) system, a major drawback seen in this system is the structural instability and Pt NP leaching during long-term reactions.

In response to this challenge, C. Stylianou and team explored the photocatalytic H_2 evolution of Pt/NH_2-MIL-125 composite materials functionalized with three distinct ligands: $(NH_2)_2$-BDC, OH-BDC, and $(OH)_2$-BDC.[106] Without Pt NPs, hydrogen generation rates ranged between 39 and 80 μmol h^{-1} g^{-1}. Adding Pt NPs improved performance, with optimal loading of about 2.5 wt%. Pt/NH_2-MIL-125/$(OH)_2$ exhibited the highest activity at 707 μmol h^{-1} g^{-1}, followed by NH_2-MIL-125 at 619 μmol h^{-1} g^{-1}, while NH_2-MIL-125/OH and NH_2-MIL-125/$(NH_2)_2$ had lower rates (377 and 253 μmol h^{-1} g^{-1}, respectively). Despite NH_2-MIL-125/$(NH_2)_2$'s reduced E_g suggesting enhanced visible-light absorption, its photo-

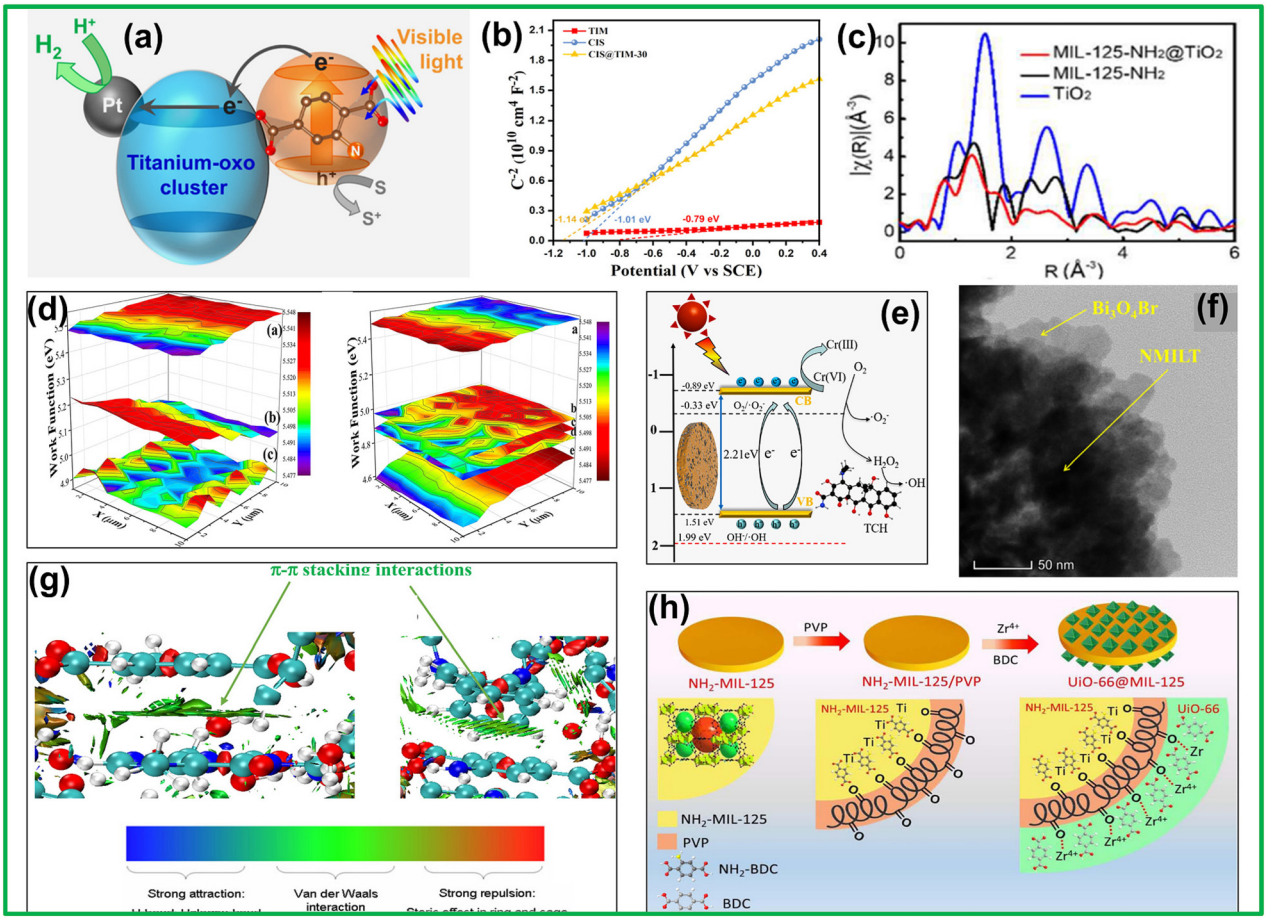

Fig. 6 (a) A schematic illustration of photocatalytic hydrogen production reaction over Pt-supported Ti-MOF-NH_2 based on the LCCT mechanism. Reprinted with permission from ref. 56. Copyright 2012 American Chemical Society. (b) Mott–Schottky curve of pure CIS, TIM, and CIS@TIM-30. Reprinted with permission from ref. 150. Copyright 2022 Elsevier Ltd. (c) EXAFS spectra at Ti K-edge. Reprinted with permission from ref. 158. Copyright 2018 American Chemical Society. (d) The work functions of ZIS, TiM, and CdS (left), respectively, and ZIS, TiM/CdS, ZIS/CdS, TiM@ZIS, and TiM@ZIS/CdS (right), respectively. Reprinted with permission from ref. 154. Copyright 2019 Elsevier B.V. (e) Diagram showing an example of the photocatalytic mechanism of NMTi-OVs-300. Reprinted with permission from ref. 159. Copyright 2023 Elsevier B.V. (f) TEM image for BOB/NMILT composite. Reprinted with permission from ref. 160. Copyright 2022 Elsevier B.V. (g) 3D Plot of noncovalent interactions (π–π stacking) using an NCI analysis technique for MIL-125 NH_2 interaction with caffeine (left) and carbamazepine (right). Reprinted with permission from ref. 162. Copyright 2022 Elsevier B.V. (h) Schematic representation for the systematic growth of MOF-on-MOF heterostructure. Reprinted with permission from ref. 95. Copyright 2022 Elsevier B.V.

catalytic performance was inferior. Computed wavefunctions revealed that NH_2-MIL-125/$(OH)_2$ had greater charge carrier mobility due to the spatial distribution of electron density within Ti-octahedra and NH_2-BDC ligands, leading to longer lifetimes of photogenerated charge carriers. This enhanced charge separation and migration improved photocatalytic efficiency. NH_2-MIL-125/$(OH)_2$ displayed the highest conductivity (5.79×10^{-6} S m^{-1}), attributed to increased electron density, enhancing redox potential and electron spatial distribution. The effects of ring activation of –OH groups were found to be greater than those of amines, enhancing p–π conjugation and electron conductivity, thereby improving photocatalytic efficiency. Such studies relate ligand activation to charge mobility but may require further research to optimize the interaction between the electronic properties of the ligand and the metal-oxo clusters to achieve greater efficiency. Charge mobility was increased with NH_2-MIL-125/$(OH)_2$, but performance remained constrained by recombination in the bulk material, thus demonstrating the need for synergistic ligand engineering with prevention of bulk-recombination strategies.

Zhang *et al.* fabricated CdS/NH_2-MIL-125 Z-scheme heterojunction *via* a solvothermal process.[151] FESEM images showed CdS nanoparticles adhering to NH_2-MIL-125 nanoplates, with fewer nanoparticles as Ti-MOF concentration increased, promoting better contact interfaces for charge carrier migration. TEM confirmed strong interfacial contact between CdS NPs and MOF nanoplates. The absorption edge at 517 nm corresponds to CdS's band gap, while bands at 280 nm and 370 nm are due to metal oxo clusters and amine ligands. CM-X samples absorbed less visible light with more Ti-MOF loading. Photocurrent intensity improved with NH_2-MIL-125(Ti), except for CM-50, likely due to the "shielding effect". CM-10 showed

the highest charge separation and migration efficiency, with the strongest photocurrent signal and an H_2 production rate of 6.62 mmol $h^{-1}g^{-1}$, about 3.5-fold more than CdS alone. ESR experiments under simulated sunlight showed characteristic $O_2^{\bullet-}$ radical signals, indicating a Z-scheme heterojunction with efficient electron transfer. Pure NH_2-MIL-125(Ti) and CdS showed weaker signals, and $^{\bullet}OH$ radical experiments supported the Z-scheme hypothesis, with stronger signals for Ti-MOF and CM-10 compared with pristine Ti-MOF. The absence of $^{\bullet}OH$ radicals in Type-II heterojunctions supported the Z-scheme heterojunction hypothesis.

Ternary metal sulfides like $CdIn_2S_4$ (CIS) are notable for their narrow band gaps and strong visible light absorption.[233,234] NH_2-MIL-125 is effective for H_2 production due to its porous nature and H_2 adsorption,[154] but its stability and efficiency are compromised by moisture and high recombination rates.[235,236] To address this issue, Zhou *et al.* created a $CdIn_2S_4$@NH_2-MIL-125 core–shell structure *via* hydrothermal methods for H_2 generation.[150] This heterojunction enhanced carrier separation and migration, improving photocatalytic performance by matching band gaps and extending carrier life. Increased $CdIn_2S_4$ content raised peak intensity, confirming incorporation, while NH_2-MIL-125's absence in diffraction peaks indicated its encapsulation. Evaluated under visible light with Na_2S/Na_2SO_3 as a sacrificial agent, CIS showed a steady hydrogen production increase, reaching 2650 μmol g^{-1} in 3 hours due to efficient carrier separation at the CIS–TIM heterojunction. Higher CIS loading didn't always improve performance, likely due to excess CIS masking active sites. CIS@TIM-30 exhibited the highest performance, producing 7650 μmol g^{-1} hydrogen in 3 hours, over three times that of pure CIS. Mott–Schottky (M–S) curves (Fig. 6b) confirmed the n-type behavior of both CIS and TIM, with CIS@TIM-30 showing enhanced charge separation efficiency. The lower arc radius in the EIS study and lower PL intensity of CIS@TIM-30 indicated improved charge separation and accelerated electron transfer at the CIS–TIM heterojunction. Efficient electron transfer from TIM to CIS enables hydrogen evolution through H^+ reduction in water. With optimized carrier dynamics and a robust heterojunction interface, CIS@TIM-30 demonstrates superior photocatalytic performance. Tianding Hu and colleagues, using a hydrothermal method, developed a novel ternary photocatalyst, NH_2-MIL-125(Ti)/$CdIn_2S_4$/Pd, where Pd was incorporated into NH_2-MIL-125(Ti).[152] The optimized Pd/NH_2-MIL-125(Ti)/$CdIn_2S_4$ material displayed a remarkable photocatalytic H_2 evolution activity of 4.60 mmol $g^{-1}h^{-1}$. This rate was 31 times greater compared with neat CIS and 16 times more than the parent MOF. The boosted activity resulted from efficient energy band alignment between CIS and Ti-MOF, facilitating electron transfer under visible light. Pd nanoparticles create active sites for H_2 production, reducing electron–hole recombination. This enhances light absorption, improves mass transfer, and offers more active sites, significantly improving catalytic performance.

Liu and team synthesized a series of $ZnIn_2S_4$@NH_2-MIL-125 heterostructures with varying MOF contents using a straightforward solvothermal approach.[153] The nanosheets of $ZnIn_2S_4$ were well dispersed on the MOF matrix, and the composite photocatalysts demonstrated superior photocatalytic action compared with their individual components under visible-light conditions for H_2 generation. The incorporation of NH_2-MIL-125 MOF significantly enhanced the SSA and pore volume of the composite, particularly at higher MOF content, resulting in a higher number of active sites for increased adsorption of the substrate. The ideal MOF content was approximately 40 wt%, resulting in a photoinduced hydrogen production rate of 2204.2 μmol $h^{-1}g^{-1}$ and an AQE of 4.3% at 420 nm. This performance was 6.5 times better than that of neat ZIS. The superior photocatalytic performance can be credited to the favorable band alignment and the close interfacial contact interface between ZIS and the MOF, which enabled photogenerated charge carriers' efficient transfer and separation. Considering these factors, ZIS and CdS were used to create an ordered tandem heterojunction, with CdS as a co-catalyst on the titanium MOF core and ZIS shell, enhancing charge carrier separation.[154] Fig. 6d illustrates the work function maps identifying samples labeled as ZIS, TiM, and CdS for (a), (b), and (c), respectively. The work functions of (a), (b), and (c) measured approximately 5.53, 5.15, and 4.93 eV, respectively. This indicates the hierarchy of electron transfer abilities in TiM@ZIS/CdS heterostructure as follows: ZIS > TiM > CdS. Therefore, electrons were observed to transfer from TiM to ZIS and from CdS to ZIS, validating the electron enrichment strategy. This configuration resulted in a significantly enhanced photocatalytic hydrogen production rate, reaching 2.367 mmol $g^{-1}h^{-1}$. This innovative core@shell hierarchical tandem heterojunction provides valuable insights for developing high-functioning heterojunctions with enhanced multi-channel charge transference capabilities.

In Z-scheme photocatalysts, close semiconductor contact is vital for effective charge separation, with mediators like MXenes improving this by forming Schottky barriers and reducing noble metal shielding.[237–240] Liu *et al.* synthesized a Z-scheme photocatalyst (NH_2-MIL-125, Ti_3C_2 MXene QDs, and $ZnIn_2S_4$) for visible-light-induced H_2 production, achieving a high rate of 2931.9 μmol g^{-1} h^{-1}.[155] Although not all Ti_3C_2 MXene QDs bridge both semiconductors, some facilitate charge transfer in a Z-scheme pathway. Superoxide trapping and redox potential tests suggest a Z-scheme mechanism, where electrons transfer from Ti-MOF's CB to $ZnIn_2S_4$'s VB *via* Ti_3C_2 MXene QDs.

1T-MoS_2, an economically viable and abundantly available metal sulfide, is recognized as a promising co-catalyst.[241] Nguyen *et al.* established a photocatalyst nanocomposite by integrating 1T-MoS_2 into NH_2-MIL-125, showing superior rates of photocatalytic hydrogen production compared with Pt/NH_2-MIL-125, Co-oxime@NH_2-MIL-125, and Ni_2P/NH_2-MIL-125. The higher output of 1T-MoS_2 was ascribed to its plentiful reaction sites present on both the edges and the basal planes, which contrasts with 2H-MoS_2, which predominantly features active sites only on its edges.[156,242]

Ti-MOF composites assisted by non-noble metals have shown effectiveness in photocatalytic water splitting and hydrogen evolution. Nasalevich *et al.* pioneered a cobaloxime-derived Ti-MOF photocatalyst that established a more noteworthy 20-fold rise in H_2 evolution rise than NH_2-MIL-125.[123] The catalyst exhibited excellent stability, maintaining a constant turnover frequency even after 65 hours of light irradiation, and retained its efficiency through multiple cycles of experiment. The photocatalytic activity of Co@NH_2-MIL-125 was found to be less than the LUMO of the neat MOF. In this system, photoinduced h^+s located at the organic ligand interact with a sacrificial e^- donor, while electrons are promptly transferred to cobalt species, reducing Co(III) to Co(II) and thereby enhancing overall photocatalytic activity due to the existence of high-spin Co(II) species. Recently, Cu^{2+}/Cu^+ was introduced into the linkers to form mixed-valence redox sites, leading to a substantial increase in charge density by 7000 and lifetime by 27 times, respectively. This modification led to a remarkable improvement in the hydrogen production rate of the Cu-modified NH_2-MIL-125(Ti) to 490 mmol g^{-1} h^{-1}, which represents an increase of 27 times compared with parent MOF and 10 times than Pt-NH_2-MIL-125(Ti).[243] In 2016, Meyer and colleagues integrated the Ni(II) catalyst [Ni(dmobpy)(2-mpy)$_2$] into NH_2-MIL-125, leading to the development of Ni@NH_2-MIL-125(Ti), marking the first among MIL-based photocatalyst to incorporate Nickel(II) particles.[244] Under light irradiation, the composite system demonstrated hydrogen yields that were 1800-fold higher than bare MOF and ten times higher than the Ni catalyst molecular catalyst. Moreover, the prepared nanocomposite exhibited a 10-fold increase in catalytic activity and sustained performance for 3000 minutes. This increase was attributed to mixed-valence redox sites, which enhanced the charge density and carrier lifetime. The main challenge related to non-noble metal co-catalysts is stability, with efficient charge transfer persisting over time. Their electronic properties must be tuned towards the photocatalytic process, with long-term stability, for them to compete with platinum.

A variety of co-catalysts based on transition metals (Ni_2P, NiO, Co_3O_4, CoP, CuO, Fe_2O_3) were united with the Ti-MOF, leading to enhanced visible light-induced photocatalytic H_2 production. Remarkably, NiO/NH_2-MIL-125(Ti) and Ni_2P/NH_2-MIL-125 demonstrated notable H_2 generation rates of 1084 and 1230 μmol g^{-1} h^{-1}, respectively.[157] PL study indicated that all the co-catalysts can suppress the emission of neat MOF, with the efficiency of charge separation ranked as Ni_2P > CoP ≈ Co_3O_4 > Fe_2O_3 > CuO > NiO. This order was in agreement with the photocatalytic H_2 evolution results, except for NiO/NH_2-MIL-125. Cyclic voltammetry measurements addressed this discrepancy, showing that NiO had a current density around three times higher than Ni_2P at −0.9 V *versus* Ag/AgCl, indicating higher intrinsic activity of NiO that partly compensates for its lower electron capture ability.

Zhang *et al.* developed a post-solvothermal method for removing organic ligands from MOFs, providing a simple, fast process at ~350 °C compared with conventional pyrolysis.[158] This method created NH_2-MIL-125 NPs coated with TiO_2 nanosheets, forming a core–shell type NH_2-MIL-125@TiO_2 structure. This structure combined active TiO_2 nanosheets, MOF photosensitizers, linker deficiency, oxygen vacancies, and a mesoporous architecture, enhancing H_2 production under visible light exposure. The process reduced the BET surface area from 1169 m^2 g^{-1} to 780 m^2 g^{-1} due to linker etching. EXAFS spectra showed deviations from individual NH_2-MIL-125 and TiO_2, indicating changes in metal site coordination, with peak shifts and reductions suggesting linker defects and oxygen vacancies advantageous for catalytic processes, enhancing active sites and facilitating the efficiency of mass/charge transfer (Fig. 6c). Varying temperatures and solvents affected the core–shell structure formation: propanol yielded core–shell particles, while methanol resulted in multiporous structures. The NH_2-MIL-125@TiO_2 composite boosted photocatalytic hydrogen production by enhancing titanium-oxo cluster exposure, light harvesting, and active sites, outperforming the parent MOF. It also showed durability across three runs, maintaining its crystallinity and morphology due to the protective TiO_2 layer.

The introduction of suitable co-catalysts can further enhance the photocatalytic output of MOF/g-C_3N_4 hybrids. In 2015, Su *et al.*[57] conveyed the successful preparation of NH_2-MIL-125/Pt/g-C_3N_4 hybrids, demonstrating a notable three-fold enhancement in photocatalytic hydrogen production compared with Pt/g-C_3N_4 alone. This approach highlights the synergistic benefits of integrating an appropriate co-catalyst with robust light-absorption capacity, leveraging both interface effects and localized SPR to augment the productivity of light energy conversion for H_2 generation.[245,246] These co-catalysts incorporate metal nanoparticles that efficiently absorb light, thereby enhancing visible-light absorption, generating more exciton pairs, and facilitating energy transfer to the semiconductor's CB. Additionally, synergistic effects in various photocatalytic applications have been demonstrated by combining two different metal nanoparticles (NPs).[247] Xu *et al.* expanded on this concept by anchoring CN nanosheets with NH_2-MIL-125 and subsequently loading Ni/Pd co-catalysts onto the NH_2-MIL-125/CN surface to create an NH_2-MIL-125(Ti)/CN/NiPd nanostructure.[248] Ni/Pd co-catalysts, as photosensitizers, enhanced light absorption and photocatalytic productivity of CN and MOF. The close interface between MOF and CN enabled direct charge transference and efficient charge carrier separation. Consequently, the resulting composites demonstrated a significantly elevated hydrogen production rate of 8.7 mmol $h^{-1}g^{-1}$, 322 times greater than NH_2-MIL-125(Ti)/CN alone. Upon discussion, it is realized that while the noble metal loading onto the MOF can enhance hydrogen production, issues like structural collapse and metal leaching persist. Key issues involve improving catalyst stability, charge carrier separation, and reduction of dependence on precious metal co-catalysts. A comprehensive approach combining material design, catalytic optimization, and stability will be necessary to address these challenges.

10.6. Drug degradation

The photocatalytic degradation of pharmaceuticals involves three primary steps: photon absorption, excitation, and reaction.[53] The photocatalyst absorbs photons, generating exciton pairs that move to the surface to react with adsorbed substances. Photogenerated holes can directly break down drug molecules (eqn (26)). Two degradation pathways exist: a reductive pathway, where electrons react with O_2 to form superoxide radicals ($O_2^{\bullet-}$) if the CB potential is more negative compared with $O_2/O_2^{\bullet-}$ redox potential (−0.13 eV *vs.* RHE) (eqn (27)), and an oxidative pathway, where holes generate hydroxyl radicals ($^{\bullet}OH$) from H_2O/OH^-, depending on pH (eqn (28)). Recombination of hydrogen ions with electrons generates heat, reducing efficiency (eqn (29)). The photocatalyst's redox potential must exceed $^{\bullet}OH/OH^-$ (+1.99 eV *vs.* RHE).[249,250] Reactive radicals ($^{\bullet}OH$ and $O_2^{\bullet-}$) efficiently mineralize drugs and intermediates into water and CO_2 under prolonged UV exposure (eqn (30)).[251,252] Both pathways synergistically prevent electron accumulation in the CB and reduce electron–hole recombination compared with direct interaction pathways.

$$\text{Photocatalyst} + h\nu \rightarrow \text{photocatalyst} + h^+ + e^- \quad (25)$$

$$h^+ + \text{drug} \rightarrow H_2O + CO_2 + \text{degradation products} \quad (26)$$

$$O_2 + e^- \rightarrow O_2^{\bullet-} \quad (27)$$

$$H_2O/OH^- + h^+ \rightarrow {}^{\bullet}OH + H^+ \quad (28)$$

$$H^+ + e^- \rightarrow \text{energy} \quad (29)$$

$$\text{Drugs} + {}^{\bullet}OH \text{ or } O_2^{\bullet-} \rightarrow CO_2 + H_2O + \text{degradation product} \quad (30)$$

Introducing defect sites enhances charge separation, stability, and performance by preserving the crystal structure and increasing active sites. Vacant O-sites trap electrons, speeding up exciton pair generation and separation, boosting charge carrier generation, and improving reactant adsorption and activation. This alters photoelectric properties, enhancing photocatalytic activity. Li *et al.* developed NH_2-MIL-125 MOF enriched with vacant O-sites to eliminate tetracycline hydrochloride and hexavalent chromium with simulated sunlight.[159] They introduced oxygen vacancies through heat treatment and examined how varying the treatment duration affected the SSA, band configuration, vacant sites' concentration, mesoporous structure, and the efficiency of exciton pair migration and parting in the oxygen-enriched NMTi-OVs-X photocatalyst. Increased heat-treatment time led to the gradual decomposition of the MIL linker and penetration from the exterior to the interior, enhancing oxygen vacancy amount. The presence of optimally vacant oxygen in NMTi-OVs-X improved the photogenerated charge carrier separation, enhancing the catalytic performance. These vacancies, activated by O_2 to form reactive species (such as $^{\bullet}O_2$, $^{\bullet}OH$, and H_2O_2), improved pollutant degradation efficiency. The oxygen-enriched Ti-MOF achieved 100% photocatalytic elimination efficiency of Cr(VI) and TCH degradation in 2 hours under simulated sunlight with minimal heat treatment at 300 °C for 300 minutes (Fig. 6e). This demonstrates the potential of single-MOF strategies for environmental remediation applications.

To improve the activity of pristine MOFs and address their limitations, hybridizing semiconducting MOFs with another semiconductor to create heterostructures is considered an effective strategy. This approach is thought to combine the advantages of both materials – e.g., enhanced charge carrier separation, improved adsorption properties, and synergistic catalytic effects – for higher photocatalytic efficiency. Hu *et al.* fabricated a microspherical Bi_3O_4Br/NH_2-MIL-125(Ti) (BOB/NMILT) composite photocatalyst, where Bi_3O_4Br nanosheets were firmly wrapped over the NMILT surface using a hydrothermal method (Fig. 6f).[160] The optimal BOB/NMILT-5 exhibited significant photocatalytic activity, achieving 88.5% tetracycline (TC) degradation in 90 minutes under simulated solar light, 6.5 and 3-fold superior to parent MOF and Bi_3O_4Br, respectively. This enhancement was primarily ascribed to the Z-scheme heterojunction construction, which effectively minimized exciton charge recombination, and the major role played by radicals such as h^+ and $^{\bullet}O_2$ in the TC degradation pathway. The building of hybrid materials based on MOF and binary semiconductor systems with layered nanostructures has significantly improved. Muelas-Ramos studied the photocatalytic removal of diclofenac using hybrid materials fabricated from g-C_3N_4 and NH_2-MIL-125, varying the loading amounts (MOF : C_3N_4 ratios of 25 : 75, 50 : 50, and 75 : 25).[161] Analysis of morphological features revealed plate-like particles and fiber-like forms from the MOF and g-C_3N_4. The E_g of the hybrid materials was similar to the parent MOF, indicating that the optoelectrical properties depend on both components. The synergistic effect of the MOF/g-C_3N_4 (50 : 50) hybrid resulted in excellent photocatalytic activity, achieving complete diclofenac degradation in 2 hours under LED irradiation. Optimizing the interface between the two materials is one of the major hurdles in this approach. Even though the concept of heterojunction is theoretically attractive, the interface quality is of great importance for efficient charge transfer and overall photocatalyst efficiency.

MOFs and their heterostructure composites with perovskites have been utilized in photocatalysis, with NH_2-MIL-125 MOFs serving as a stable, highly photoactive matrix for incorporating $LaFeO_3$. Younes *et al.* studied the composite's efficacy for photocatalyzing carbamazepine and caffeine degradation.[162] The adsorption mechanism at the interface among pollutants and NH_2-MIL-125, $LaFeO_3$ involves metal–π, π–π stacking, and H-bonding relationships (Fig. 6g). The optimal $LaFeO_3/NH_2$-MIL-125 composite exhibited excellent degradation efficiencies (carbamazepine 74%, caffeine 87%) due to efficient heterojunctions facilitating charge separation. MOF-on-MOF heterostructures, formed by growing one MOF on another, showed outstanding photocatalytic performance in aqueous media thanks to their structural stability, enhanced interfacial contact, large specific surface area, and increased porosity, advancing pollutant degradation. Sepehrmansourie

et al. fabricated NH_2-MIL-125@UiO-66, a Z-scheme heterojunction, by epitaxially growing UiO-66 on the surface of MOF using a solvothermal technique, creating MOF-on-MOF heterostructure (Fig. 6h).[95] The hybrid was then decorated with g-C_3N_4 nanosheets to design a dual Z-scheme heterojunction, UiO-66/NH_2-MIL-125/g-C_3N_4 photocatalyst for visible light-induced OFL degradation. Constructing MOF-on-MOFs with different physicochemical structures is challenging due to the PVP and Zr^{4+} ions' polar interactions in UiO-66, enhancing UiO-66's affinity for NH_2-MIL-125. Kitagawa *et al.* found PVP's zeta potential to be −0.27 mV and UiO-66's to be +44.0 mV, indicating greater affinity between UiO-66 and PVP/NH_2-MIL-125. Consequently, UiO-66 nuclei accumulated over NH_2-MIL-125 crystals, forming micelles, followed by internal growth *via* solvothermal conditions. Epitaxial growth of UiO-66 over NH_2-MIL-125's edge was attributed to the {110} NH_2-MIL-125/{001} UiO-66 lattice similarity, as confirmed by TEM and EDX spectrum data. Decorating g-C_3N_4 nanosheets on the exterior surface of the MOF-on-MOF matrix preserved both MOFs' structural and morphological aspects but reduced NH_2-MIL-125 crystal size (200–250 nm) while increasing UiO-66 crystal size (230–300 nm). The double Z-scheme heterojunction significantly improved photocatalytic performance for OFL degradation under visible light. Photocatalytic mechanism studies, scavenging tests, and EPR techniques established the formation of $^{\bullet}OH$ and $O_2^{\bullet-}$ radicals, crucial for OFL photodegradation. This study provides an updated, straightforward approach for MOF-on-MOF architecture and dual Z-scheme heterojunction materials, advancing environment and energy-related applications. MOF-on-MOF heterojunctions improve interfacial charge transfer efficiency, enhancing photocatalytic performance while preserving the porous structure for superior adsorption. Constructing such a heterojunction allows the two MOFs to maintain their porous nature, thus boosting adsorption capabilities. For example, Gao *et al.* developed a Z-scheme heterojunction of NH_2-MIL-125@MIL-88B by solvothermal growing of MIL-88B on a MOF matrix.[164] This heterojunction leveraged the advantages of both MOFs, providing atomic-level charge transport channels, promoting directional charge transfer, and significantly improving tetracycline degradation using visible light, achieving a 96.26% degradation rate within 120 minutes. Different from conventional MOF and non-MOF hybrids, the groundbreaking MOF-on-MOF strategy in S-scheme heterojunctions combines the benefits of double semiconducting units of MOF into a single unit through a close interface connected by well-defined chemical bonds, enhancing photocatalytic properties. Yuan *et al.* created a NH_2-MIL-125@CoFe Prussian blue analog (PBA) heterojunction that operates on an S-scheme mechanism.[163] This MOF-on-MOF composite structure has a sandwich-like structure, having hollow CoFe PBA nano cages precisely brought together on the upper and lower surfaces of Ti-MOF. Theoretical and experimental discoveries confirmed the establishment of an internal electric field through interfacial Ti–O–Co bonds within the heterojunction. This internal field acted as a driving force and an atomic transport pathway, facilitating S-scheme charge transfer and improving redox performance. The hollow sandwich-like structures with exposed incremental active sites contributed significantly to the improved photocatalytic activity for TCH degradation.

Beyond heterostructure design, incorporating noble metals (*e.g.*, Au, Ag, Pt) into MOFs is highly effective in enhancing semiconductor photocatalyst performance. Noble metal/MOF hybrids benefit from (i) the surface plasmonic resonance (SPR) effect of noble metal nanoparticles, broadening optical responses in the visible range, and (ii) the establishment of Schottky junctions with other semiconductors, controlling photoinduced electron flow and facilitating exciton pair separation. In this context, Zheng *et al.* fabricated Ag/NH_2-MIL-125(Ti)/CdS photocatalysts, demonstrating high catalytic activity for photodegrading ketoprofen (KP) under simulated sunlight (94.2% after 180 min).[165] The hybrid material exhibited enhanced visible light harvesting and robustness compared with the neat MOF or CdS alone. This improvement in photocatalytic performance was largely attributed to the Z-scheme heterojunction activity and efficient hot e^- conduction facilitated by Ag nanoparticles. The material achieved a remarkable 94.2% degradation of potassium persulfate (KP) after 180 minutes under simulated sunlight conditions. Following this, Muelas-Ramos reported the solvothermal preparation method for depositing NH_2-MIL-125 with Pd, Pt, and Ag nanoparticles, aiming to maintain visible light photocatalytic behavior.[100] The incorporation of noble metals did not induce structural changes; however, it did alter the surface properties, which varied depending on the specific noble metal used. XPS characterization indicated the reduced state of the metal nanoparticles (1.8 to 3.8 nm) in the hybrid (M/NH_2-MIL-125, where M = Pd, Ag, Pt), enhancing visible range activity as a result of the SPR effect of the noble metal NPs. The presence of these nanoparticles in the MOF minimized charge recombination, verified by photoluminescence techniques. Pt/NH_2-MIL-125 exhibited the maximum photocatalytic activity, achieving maximum acetaminophen (ACE) conversion in less than 3 hours under simulated solar irradiation. Yet, effective synthesis of the MOF-based composite has to be done to avoid aggregation of noble metal nanoparticles, which would decrease its efficiency. Another important direction that requires more attention is selective photocatalytic degradation. Generally, photocatalysts degrade a variety of contaminants, but being selective toward a specific drug or pharmaceutical would be helpful in cases where certain contaminants need to be removed from the water.

10.7. Dye disposal

The disposal of dyes from industrial wastewater into natural water bodies poses serious environmental and health risks. Current removal methods often fail to fully degrade dyes and generate excess waste. Among the conventional water treatment methods, photocatalysis offers a promising solution for efficiently degrading toxic organic pollutants in wastewater while minimizing waste. The detailed photocatalytic

mechanism can be elucidated through the following reactions.[253–255]

$$H_2O + h\nu \rightarrow HO^{\bullet} + H^{\bullet} \quad (31)$$

$$HO^{\bullet} + O_2 \rightarrow HO_2^{\bullet} \quad (32)$$

$$O_2 + e^- \rightarrow O_2^{\bullet -} \quad (33)$$

$$O_2^{\bullet -} + H^+ \rightarrow HO_2^{\bullet} \quad (34)$$

$$HO_2^{\bullet} + H^+ \rightarrow H_2O_2 \quad (35)$$

$$H_2O_2 \xrightarrow{h\nu} 2HO^{\bullet} \quad (36)$$

Ultimately, the dye undergoes a reaction with a hydroxyl radical ($HO^{\bullet}$), leading to the formation of intermediate and final products:

$$HO^{\bullet} + \text{dye} \rightarrow \text{Intermediates} \rightarrow CO_2 + H_2O$$

MOF/CdS composites are effective in photocatalysis but suffer from instability and rapid charge recombination, while noble metals enhance charge transfer through SPR effects in heterogeneous architectures.[256] Wang *et al.* innovatively produced a ternary nanocomposite photocatalyst with extended visible range responsivity and heightened absorption efficiency by sequentially loading Au and CdS onto NH_2-MIL-125 using a dual-step approach.[166] The CdS-core and Au-shell structure not only stabilized CdS but also utilized the SPR effect of Au to facilitate efficient carrier separation, leveraging the compatible energy band alignments. Experimental zeta potential analyses verified the presence of electrostatic interactions, confirming the successful fabrication process (Fig. 7a). Compared with pristine CdS, the ternary 5Au@40NMT/CdS system exhibited superior degradation efficiency of 93.3%- and nine-times faster degradation kinetics than CdS within just 30 minutes. This enhancement stemmed from the expansive SSA of the MOF, which facilitated the dispersion of CdS and Au nanoparticles, thus encouraging efficient carrier separation. The visible light harvesting ability of CdS and enhanced transference of carriers can be achieved by the incorporation of Au NPs. ESR analysis identified superoxide radicals as the primary entity accountable for the elimination of MB dye.

Graphene is an exceptional 2D material showcasing high thermal stability and charge carrier mobility with remarkable SSA, making it an ideal support for photocatalysts. Nivetha *et al.* presented an NH_2-MIL-125(Ti)/CdS/Graphene ternary composite that exhibited effective catalytic activity for exciton pair separation, low overpotential, and better activity in comparison with parent MOF.[167] The light-responsive behavior was studied, where NH_2-MIL-125(Ti) and CdS/Graphene both showed n-type semiconductor behavior. NH_2-MIL-125(Ti)/CdS/Graphene (5 wt%) demonstrated superior charge separation efficiency. The TGA analysis results showcased significant weight loss due to solvent removal and MOF decomposition, followed by the production of amorphous TiO_2 residue (Fig. 7b). The NH_2-the ternary composite (5 wt%) exhibited enhanced thermal stability due to the presence of graphene. NH_2-MIL-125(Ti) and NH_2-MIL-125(Ti)/CdS/Graphene (20 wt%) composites had surface areas of 1156 $m^2\ g^{-1}$ and 544.78 $m^2\ g^{-1}$, respectively. The lower surface area of NH_2-MIL-125(Ti)/CdS/Graphene (20 wt%) than the parent MOF is because of the internal cavities occupied by the CdS/Graphene surface.

MoS_2, with its layered structure, promotes carrier separation, enhancing the adsorption of e^- and photoactivity, especially when narrow bandgap MoS_2 (1.9 eV) forms heterojunctions with other semiconductor catalysts.[257–259] Zhang *et al.* reported a ternary composite of MoS_2 nanosheets, ultra-small titanium-based MOF nanodots (<10 nm), and CF matrix as a competent and recyclable photocatalyst.[168] ROS have restricted diffusion distances (20 nm),[260] making ultra-small nanodots more effective in generating ROS under visible light for pollutant photodegradation. The ternary composite exhibited both type I and IV isotherms related to microporous and mesoporous nature, enhancing adsorption capacity and catalytic efficiency. Under the visible light illumination, the ternary composite cloth efficiently eliminated 81.1% of LVFX drug and 94.3% of MB dye, attributed to the ultra-small NH_2-MIL-125 nanodots being decorated onto the CF/MoS_2 matrix (Fig. 7c). The CF/MoS_2/NH_2-MIL-125(Ti) nanocomposite showed a higher surface area of 290.1 $m^2\ g^{-1}$, supplying active sites for pollutant binding. Large MoS_2 nanosheets enhanced nanodot growth and created mesopores for better pollutant removal through synergistic effects and effective ROS formation. The nanocomposite cloth (4 × 4 cm^2) remained stable and effective after four recycling cycles (Fig. 7d). This study addressed the potential of nanostructuring with layered materials to significantly improve photocatalytic performance, an approach that has great prospects in recyclable photocatalysts that can be readily used without losing efficiency.

Various bismuth-based metal oxide photocatalysts have been developed to enhance photocatalytic efficiency, demonstrating exceptional performance due to their high efficiency and improved charge transfer capabilities.[261,262] Bismuth oxyhalides (BiOX, X = Cl, Br, I) present good photoactivity due to their $[Bi_2O_2]^{2+}$ layered structure flanked by the halogen atom, which generates an electrostatic region that inhibits exciton pair recombination.[263,264] In 2016, Zhu *et al.* synthesized a hybrid photocatalyst by compounding two-dimensional BiOBr with the MOF to form BiOBr/NH_2-MIL-125 aimed at RhB degradation.[169] The suitable band gap value and the so-formed heterojunction facilitated electron transfer from BiOBr to Ti^{4+}, enhancing the degradation activity of the composite compared with the individual components.

Direct doping of Ag semiconductors is a straightforward procedure to adjust MILs' band structures. For instance, coating NH_2-MIL-125 with silver phosphate nanoparticles to form a well-suited heterogeneous interface of Ag_3PO_4@MIL reduced the E_g from 2.51 eV to 2.39 eV, leading to a 39-fold enhancement in photoactivity for MB degradation compared with TiO_2.[171] Similarly, doping NH_2-MIL-125 with Ag_3VO_4 and Ag_2WO_4 showed that Ag_3VO_4, with an E_g reduction from 2.65 eV to 2.27 eV, is more effective for optimizing NH_2-MIL-125's

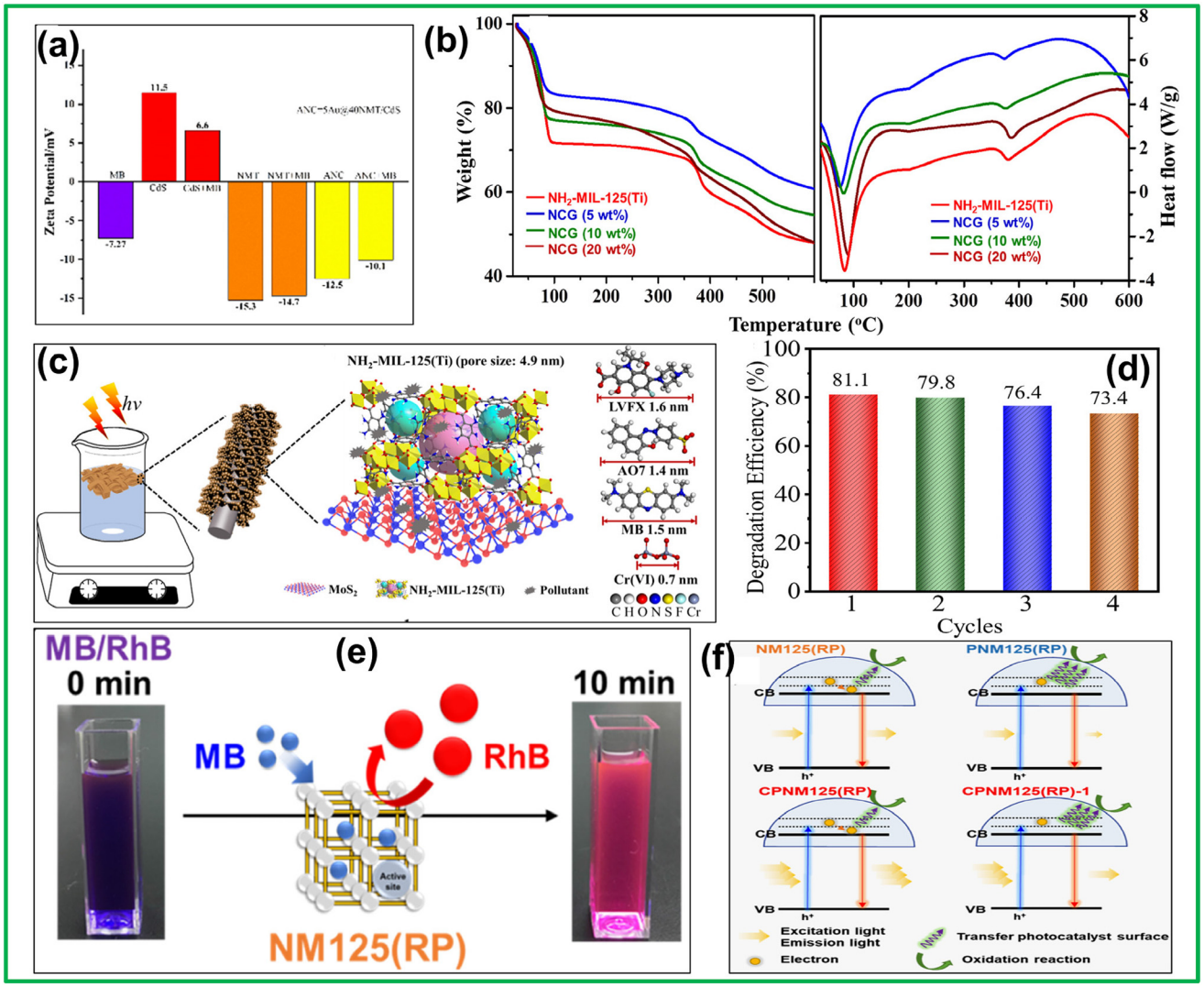

Fig. 7 (a) Zeta potential of MB, CdS, CdS + MB, NMT, NMT + MB, 5Au@40NMT/CdS and 5Au@40NMT/CdS + MB. Reprinted with permission from ref. 166. Copyright 2022 Elsevier B.V. (b) TGA of (left) NH_2-MIL-125(Ti) (right) NH_2-MIL-125(Ti)–CdS/Graphene (20 wt%). Reprinted with permission from ref. 167. Copyright 2021 Elsevier Inc. (c) Photocatalytic reaction device and adsorption process of CF/MoS_2/NH_2-MIL-125(Ti) cloth. (d) Cycle run test in degrading LVFX. Reprinted with permission from ref. 168. Copyright 2021 Elsevier Inc. (e) A schematic representation of NM125(RP)'s selective adsorption capability toward the mixed MB/RhB solution and (f) the proposed mechanism based on the PL results over different samples. Reprinted with permission from ref. 174. Copyright 2023 Elsevier B.V.

band structure.[172] In 2015 Abdelhameed and colleagues improved the Ti-MOF's photocatalytic efficiency and chemical permanency by integrating it with Cr(III) and Ag NPs. Initially, the NH_2-groups in the MOF underwent a treatment with acetylacetone.[171] When exposed to visible light, both Cr-MIL-125-AC and Ag-MIL-125-AC were able to nearly fully degrade methylene blue (MB). Cr(III) served as an h^+ acceptor, while Ag NPs functioned as an e^- acceptor, thereby enhancing the exciton separation and prolonging their period of recombination. Ag-MIL-125-AC showcased effective and constant photocatalytic performance in degrading MB, maintaining a steady photodegradation rate constant through five consecutive reaction cycles. Ag/AgBr nanoparticles generate charge carriers under visible light owing to AgBr's narrow E_g of 2.6 eV and Ag NPs' SPR effect.[265] Typically, AgBr forms by adsorbing Ag^+ ions or Br sources onto semiconductors and adding the complementary ion, often resulting in large, aggregated AgBr particles.[266–268] In 2019, Han *et al.* devised a novel method to produce AgBr NPs and fabricate Ag/AgBr/NH_2-MIL-125 nanocomposites.[173] Initially, they used amino terephthalic acid and 2,5-dibromo terephthalic acid as linkers to form Br_2-NH_2-MIL-125. Subsequently, AgBr was prepared *via* an *in situ* method by reacting the –Br groups in Br_2-NH_2-MIL-125 with $AgNO_3$ in ethanol. Finally, Ag/AgBr/NH_2-MIL-125 was fabricated using a photoreduction method, resulting in small, uniformly sized Ag/AgBr nanoparticles (about 4 nm) as a result of the even dispersal of Br in Br_2-NH_2-MIL-125. The prepared hetero composites demonstrated significantly improved light-

harvesting ability and higher photocatalytic efficiency for the removal of MO compared with Br_2-NH_2-MIL-125. The photocatalytic rate constant of the nanocomposite was roughly 5.1-fold greater than Br_2-NH_2-MIL-125. This enhanced activity was due to the SPR effect of the Ag NPs and the creation of heterojunctions between the components. This research presented a novel method for developing Ag/AgX/MOF (X = Cl, Br) photocatalysts, which holds promise for environmental purification and energy utilization.[269]

Quantum dots (QDs), which are less than 10 nm in size, represent a cutting-edge category of 0D nanomaterials. In 2019, Wang *et al.* devised an upfront way to embed CQDs onto the MOF substrate *via* a solvent-deposition method.[270] The NH_2-MIL-125, characterized by its high SSA, served as an optimal matrix for the dispersion of CQDs. These anchored CQDs maximized the utilization of visible light and reduced the rate of exciton species recombination within the MOF structure. When exposed to a broad spectrum of light, CQDs/NH_2-MIL-125 demonstrated superior photocatalytic activity for the degradation of RhB compared with pristine NH_2-MIL-125, with the optimal performance observed at 1% CQD content. This superior photocatalytic activity was attributed to the effective photogenerated e^-/h^+ pair separations and enhanced light energy utilization. In 2023, Huang and colleagues incorporated CQDs into P25/NH_2-MIL-125 *via* a simplistic reflux technique, forming a ternary composite that significantly boosted photocatalytic performance by promoting longer charge carrier lifetime and promoting up-conversion luminescence.[174] This enhancement allowed for the alteration of near-IR light to visible light, thus advancing the light implementation efficacy. Post-synthesis treatment at 120 °C elevated the stability of the samples in aqueous environments. The UV–vis study revealed a notable red shifting owing to the presence of CQDs, effectively narrowing the E_g. Unlike P25 alone, the CQDs were dispersed across the surface and integrated into the NH_2-MIL-125's pore structure, resulting in weakened XRD patterns and altered porous structures. CQDs efficiently transformed longer-wavelength light with $\lambda >$ 500 nm into shorter-wavelength light with $\lambda <$ 500 nm, thus generating more photoinduced electrons in both P25 and Ti-MOF. Due to their excellent conductivity, CQDs facilitated the effective exciton pair separation, thereby enhancing the overall photocatalytic efficacy (Fig. 7e and f). Boron nitride quantum dots (BNQDs) efficiently separate electron–hole pairs due to their electrostatic affinity for photoinduced positive charges, aided by oxygen-containing groups that carry negative charges.[271,272] In 2023, a range of BNQDs incorporated into NH_2-MIL-125 (NMTB-*x*) nanocomposites from 0D–3D structures were synthesized through co-precipitation for photocatalytic RhB degradation.[175] NH_2-MIL-125 and NMTB-0.7 exhibited SSA of around 1096.82 and 1265.62 $m^2\ g^{-1}$, respectively, offering increased active sites for the catalytic reaction. The study focused on the visible light photocatalytic activity of NMTB-*x* composites for degrading RhB and TC. Free radical scavenging tests reveal that $O_2^{\bullet-}$ significantly impacted photocatalytic performance, followed by hydroxyl radicals $^{\bullet}OH$ and h^+. The improved degradation was due to effective heterojunctions, efficient h^+ quenching by BNQDs, and reduced carrier recombination.

10.8. Organic transformation reactions

Photocatalytic transformations of organic compounds are valued for their high selectivity, yield, and ability to avoid thermal side reactions, all under mild conditions without toxic reagents. Recent advancements have shown significant progress in MOF-catalyzed organic transformations under visible light. Examples include the photocatalytic oxidation of alcohols,[273] the photocatalytic α-alkylation of aldehydes,[274] and aza-Henry reactions.[275] NH_2-MIL-125, Ti-based MOF, has emerged as a versatile heterogeneous catalyst in a number of these transformation reactions. Table 2 lists the organic transformation reaction performances of different NH_2-MIL-125(Ti)-based multifunctional materials.

Zhao and colleagues synthesized NH_2-MIL-125/TiO_2, which displayed outstanding efficiency in the selective oxidation of cyclohexane.[276] This achievement was attributed to its excellent light-harvesting capabilities and abundant catalytic sites. This study investigated not only the rate of reaction and possible yield outcomes but also real-world applications in selective oxidation. Cyclohexane oxidation is an important industrial process, but traditional methods often include high temperature and excessive waste generation. Photocatalytic oxidation may offer a cleaner and more sustainable alternative. In a separate study, Gao *et al.* developed an innovative CdS/NH_2-MIL-125@TiO_2 composite by coating NH_2-MIL-125 with a super thin layer of TiO_2 and embedding CdS within the structure.[277] This TiO_2 layer served to shield the photocatalysts from nitrate and nitrite corrosion and poisoning by photocatalytically removing NO, thus enhancing the composite's durability and stability. The remarkable optochemical characteristics of the nanocomposite resulted from dual excitation pathways, strong interfacial connectivity, and the well-aligned band potentials of NH_2-MIL-125 and CdS quantum dots. Photoexcited e^-s were captured by O_2, forming superoxide radicals, which subsequently oxidized NO into HNO_2 and HNO_3 (Fig. 8a). Each component of the catalyst played a distinct role: the high surface area of the MOF enhanced reactant adsorption, CdS QDs enabled visible light responsiveness, and TiO_2 prevented e^-/h^+ recombination by acting as a buffer.

Li *et al.* investigated the photocatalytic efficiency towards aerobic oxidation of amines, converting them to imines in an O_2 environment (as an oxidant).[281] Their findings revealed that benzylamine credibly transformed into *N*-benzylidene benzylamine with the MOF catalyst, achieving a 73% conversion rate and 86% selectivity in CH_3CN after 12 hours of light exposure. The structural integrity of the parent MOF was maintained, and its transformation efficacy remained fairly similar even after three cycles, demonstrating its durability and reusability. Amines with e-donating groups exhibited increased conversion rates (75–92%) and improved selectivity (90–93%) concerning benzylamine. The mechanism for photocatalytic aerobic oxidation involved e^- movement following the LMCT

Table 2 List of NH_2-MIL-125(Ti)-based multifunctional materials towards different organic transformation reactions

Sl. no.	Photocatalytic application	Material	Band gap (eV)	Reaction type	Substrate	Product	Photocatalytic efficiency	Light source	Ref.
1	Organic transformation reaction	NH_2-MIL-125(Ti)/TiO_2	2.76	Oxidation	Cyclohexane	Cyclohexanol and cyclohexanone	23% conversion, five h	300 W xenon lamp (λ > 420 nm)	276
2		CdS/NH_2-MIL-125@TiO_2	2.50	Oxidation	NO	HNO_2 and HNO_3	48.4% conversion, 5 min	300 W xenon lamp with UV cut filter (λ > 420 nm)	277
3		MR-MIL-125(Ti)	1.93	Oxidation	Benzyl alcohol	Benzaldehyde	—	150 W xenon lamp with 400 nm cut-on filter	126
4		NH_2-MIL-125@TAPB-PDA-3	2.61	Oxidation	Benzyl alcohol	Benzaldehyde	94.7% conversion, 30 h	300 W xenon lamp (λ > 420 nm)	278
5		Pt/Ti-MOF-NH_2	—	Reduction	Nitrobenzene	Aniline	—	500 W Xe lamp (λ > 420 nm)	279
6		Ni-doped NH_2-MIL-125(Ti)	2.5	Oxidation	*p*-Methyl benzyl alcohol	*p*-Methyl benzaldehyde	43.2% conversion, 10 h	300 W xenon lamp with UV cut-off filter (λ > 420 nm)	280
7		NH_2-MIL-125(Ti)	2.4	Oxidation	Benzylamine	*N*-Benzylidene benzylamine	73% conversion, 12 h	300 W xenon lamp with UV cut-off filter (λ > 420 nm)	281
8		SMIL-NH_2	2.4	Oxidation	Acetophenone oxime	Acetophenone	100% conversion, 10 h	Blue LED lamps (4 × 3 W)	282

process, generating Ti^{3+} centers. These highly reactive Ti^{3+} sites interacted with oxygen to produce superoxide radicals and were subsequently reversely oxidized to Ti^{4+}. Meanwhile, carbon-centered radicals generated *via* photoillumination reacted with superoxide radicals, forming aldehydes. These aldehydes were then nucleophilically attacked by amines, leading to the formation of imines through a dehydration process. The high efficacy of the reaction and the mild conditions under which it runs, therefore avoiding harsh reagents and conditions, underlines the increasing trend towards "green" catalytic processes.

Gascon and colleagues modified NH_2-MIL-125 MOF with a dye-like entity (methyl red), creating MR-MIL-125(Ti).[126] This new material demonstrated enhanced photocatalytic productivity in oxidizing the benzyl alcohol, attributed to its significantly improved light absorption than the original MOF. Likewise, novel NH_2-MIL-125 MOFs modified with aromatic heterocycles were developed through a Schiff base reaction to develop the π-delocalized system.[51] 2-Pyridine carboxaldehyde, 3-pyridine carboxaldehyde, 4-pyridine carboxaldehyde, 3-thiophene carboxaldehyde, and 2-quinoline carboxaldehyde were imbedded onto the MOF without affecting its parent framework. Out of these, THI- and QUI-modified MOFs demonstrated superior photocatalytic performance due to the enhanced conjugated system, which promoted a longer separation period and transference of the exciton pairs.

Zhao *et al.* developed a range of NH_2-MIL-125@TAPB-PDA nanocomposites using an innovative seed growth technique to coat porous and crystalline COF onto the titanium MOF.[278] The COF width was adjustable by varying the concentration of COF raw materials. Notably, NH_2-MIL-125@TAPB-PDA-3, with a 20 nm-thick COF shell, achieved the maximum benzyl alcohol conversion rate of 94.7%, outperforming single NH_2-MIL-125 and COF by 15.5 and 12.5 times, respectively. This significant enhancement in its performance was ascribed to the superior exciton pair transference between the MOF and the COF over covalent bondings. Radical trapping experiments and ESR confirmed the presence of superoxide radical anions and holes, which are crucial for the aerobic oxidation reaction.

The aromatic nitro compounds to amines reduction is crucial due to the value of aromatic amines as intermediates in fine chemical synthesis. Matsuoka and co-workers achieved effective photoreduction of nitrobenzene using Pt/NH_2-MIL-125 under the illumination of visible light.[279] The initial conversion rates of nitrobenzene for Pt/Ti-MOF-NH_2 and Ti-MOF-NH_2 were found to be 3.3 and 2.3 mmol h^{-1}, respectively. The enhanced photoactivity of the composite indicated that the Pt NPs acted as an effective co-catalyst. The e^-s were primarily transported to the actively participating Ti–O cluster and subsequently to the Pt (co-catalyst), reducing the nitrobenzene, while TEOA served as an e^- donor (sacrificial agent), being oxidized over the linker of ATA.

Zhu and colleagues examined the capabilities of Ni-doped Ti-based MOF, NH_2-MIL-125, towards aromatic alcohols selectively oxidized to aldehydes, utilizing O_2 as an oxidizing agent

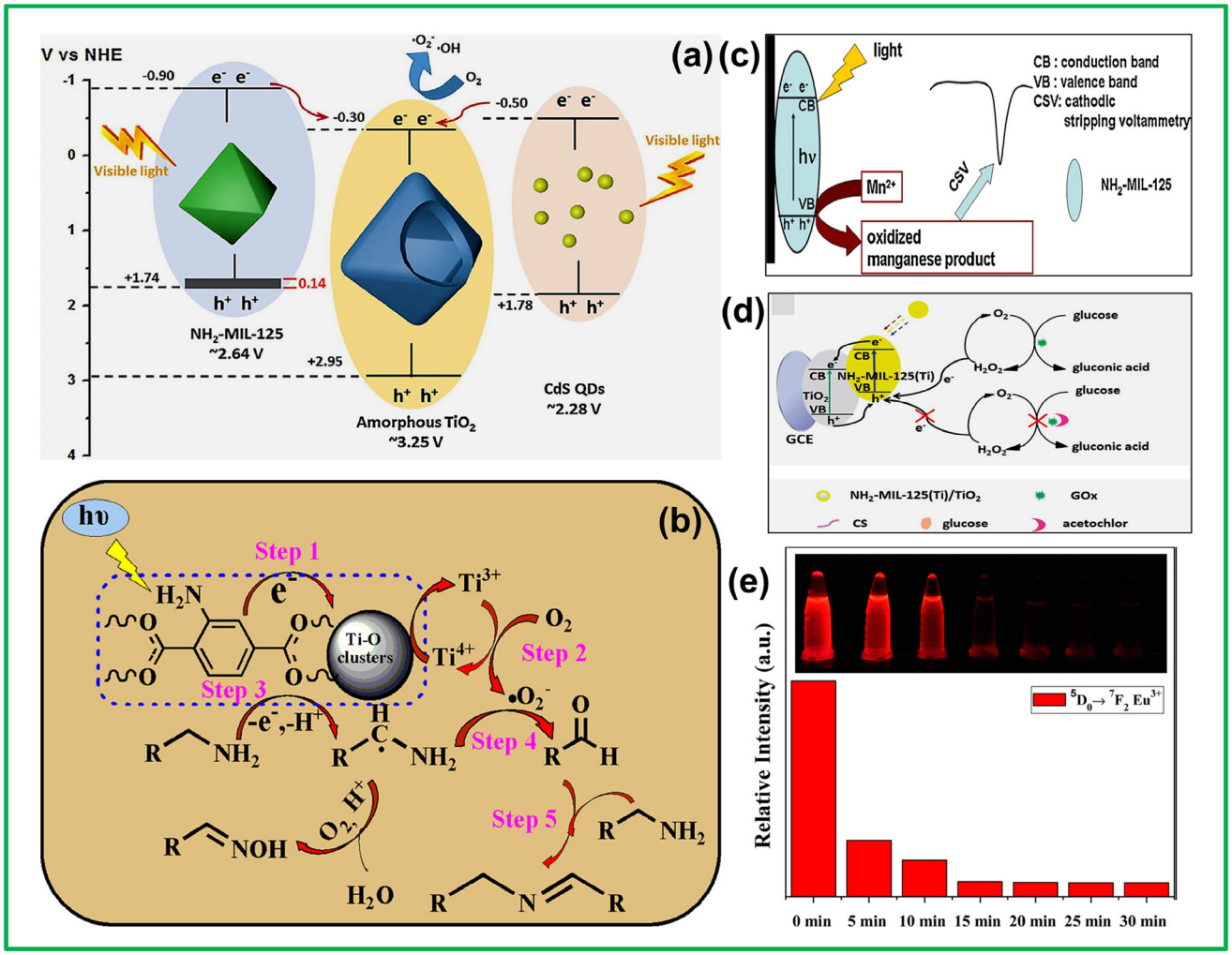

Fig. 8 (a) Possible mechanism of photocatalytic oxidation of NO over CdS/NH_2-MIL-125@TiO_2 catalysts. Reprinted with permission from ref. 277. Copyright 2018 Elsevier B.V. (b) Proposed mechanism of the photocatalytic amines oxidation over NH_2-MIL-125(Ti). Reprinted with permission from ref. 281. Copyright 2014 Elsevier B.V. (c) Schematic illustration for the photooxidation of Mn^{2+} at NH_2-MIL-125(Ti)/CPE and its detection by CSV. Reprinted with permission from ref. 283. Copyright 2014 Elsevier B.V. (d) The electron-transfer mechanism in GO_x/CS/NH_2-MIL-125(Ti)/TiO_2 biosensor. Reprinted with permission from ref. 284. Copyright 2017 The Royal Society of Chemistry. (e) $^5D_0 \rightarrow {}^7F_2$ transition intensity ratios from the emission spectra of MIL-125-AM-Eu introduced into α-phenethyl alcohol after UV radiation for different times. Reprinted with permission from ref. 285. Copyright 2016 American Chemical Society.

and under visible light illumination.[280] Ni-doped NH_2-MIL-125 demonstrated significantly improved photocatalytic behavior compared with NH_2-MIL-125, with *p*-methyl benzyl alcohol conversions of 43.2% and 25.8%, respectively. Ni nanoparticles, averaging 3 nm in diameter, were encapsulated within the pores of the MOF. The increased performance of Ni-doped MOF was credited to its enhanced visible light absorption efficacy, which facilitated the charge transfer efficiency, a result of Ni doping. Furthermore, analyses including N_2 adsorption–desorption, PXRD, and reusability experiments indicated that the structural integrity and photocatalytic performance of the MOF composite remained nearly unchanged after three continuous cycles, demonstrating its stability.

Morsali *et al.* synthesized a surfactant-aided variant of NH_2-MIL-125, named SMIL-NH_2, using the solvothermal technique with Pluronic P123 – a structure-directing entity.[282] They evaluated the performance of photocatalyst SMIL-NH_2 in deoximation reactions. In this efficient photosystem, SMIL-NH_2 facilitated the regeneration of carbonyl complexes from several oximes at twice the rate achieved by NH_2-MIL-125 (Scheme 1). Upon achieving a 100% yield in the photocatalytic deoximation of oximes using SMIL-NH_2, the conversion time for acetophenone oxime to its corresponding ketone was about 10 hours. For acetophenone oxime derivatives with e^- donating methyl and methoxy groups, the reaction times were significantly reduced. Moreover, SMIL-NH_2 exhibited notable structural stability and cycling stability while maintaining its photocatalytic activity intact. However, long-term stability and metal leaching are concerns, especially with doped and metal-deposited composites. Optimizing heterojunction structures is

crucial for efficient electron–hole separation, requiring precise control of coating thickness and interfaces.

10.9. Photocatalytic sensors

Photocatalytic sensors, which integrate irradiation of photon energy with electrochemical detection, have gained considerable interest for their capacity to combine the benefits of optical techniques with those of electrochemical sensors. Ti-based MOFs, renowned for their excellent photocatalytic and redox characteristics, are particularly promising for photoelectrochemical sensors. Table 3 lists the different types of modified NH_2-MIL-125(Ti) multifunctional nanomaterials and their performances towards photocatalytic sensing. In one study, Hu and colleagues enhanced a carbon paste electrode by incorporating NH_2-MIL-125 as the working electrode. By the combination of visible light and CSV methods regarding the oxidized Mn materials, they detected Mn^{2+} quantitatively (Fig. 8c).[283] Upon exposure to light, exciton pairs transferred to the NH_2-MIL-125 surface and reacted with Mn^{2+} species in the mixture solution, facilitating the generation and preconcentration of MnO_2. The detection of this product was achieved using the CSV process, which is responsible for quantifying the oxidation products' stripping peak current. The peak currents exhibited a linear increase with the concentration of Mn^{2+}, demonstrating a strong linear correlation across the range of 1.0×10^{-8} to 1.0×10^{-5} M. This work was particularly remarkable with successful application on real-world samples, including the detection of Mn^{2+} in tea, one of the challenging aspects for most sensing systems that go well in lab conditions alone. The same group also fabricated a photoelectrochemical sensor ground on an NH_2-MIL-125/TiO_2 nanocomposite for determining the herbicide, clethodim. They coated the as-prepared composite on a glassy carbon electrode that served as the working electrode.[286] In this case, during the sensing process, the interaction between photogenerated h^+ on the nanocomposite reacted with water to produce $^{\bullet}OH$ radicals. The herbicide then quickly interacted with these $^{\bullet}OH$ radicals, which improved charge–hole separation efficiency and increased the photocurrent, providing a reliable and sensitive detection method. The photocurrent determined clethodim concentration, displaying a strong linear correlation and a lower detection margin of 10 nmol L^{-1}. This work showcases the significance of nanocomposite materials for optimizing the performances of photocatalytic sensors by enhancing charge transfer efficiencies and sensor response times.

Subsequently, a more intricate yet sensitive photoelectrochemical sensor was created using a GO_x/chitosan/NH_2-MIL-125(Ti)/TiO_2 nanocomposite. This sensor was designed to detect the pesticide acetochlor present in agricultural produce (Fig. 8d).[284] This multi-functional sensor, which integrates the interaction between photogenerated radicals with the pesticide, illustrates the flexibility of photocatalytic sensors in terms of integrating biological elements such as enzymes for further enhancement of selectivity. In this setup, CS was used as a matrix to immobilize GO_x, facilitating the conversion of glucose to H_2O_2. The H_2O_2 acted as an e-donor, scavenging h^+

Table 3 List of NH_2-MIL-125(Ti)-based multifunctional materials towards photocatalytic sensing applications

Sl. no.	Photocatalytic application	Material	Band gap (eV)	Target pollutant/analyte	Light source	Sensor configuration	Detection limit	Stability (cycles)	Ref.
1	Sensors	NH_2-MIL-125	2.25	Mn^{2+}	250 W halogen lamp	Modified CPE	4.0 nmol L^{-1}	>100 cycles	283
2		NH_2-MIL-125/TiO_2	2.25	Clethodim	250 W halogen lamp (λ = 340–850 nm)	Modified GCE	10 nmol L^{-1}	>100 cycles	286
3		NH_2-MIL-125/TiO_2	2.5	Acetochlor	250 W halogen lamp (λ > 400 nm)	GO_x/CS/NH_2-MIL-125(Ti)/TiO_2	0.003 nmol L^{-1}	—	284
4		MIL-125(Ti)-AM-Eu	—	α-Phenethyl alcohol	UV light	Photocatalyst & fluorescence sensor	—	5 cycles	285

in the VB of the nanocomposite, thereby enhancing charge separation efficiency and increasing the photocurrent. However, in the presence of acetochlor, the photocurrent significantly lessened because acetochlor inhibited GO_x enzyme activity. The concentration of acetochlor was quantified by measuring the fraction of inhibition of GO_x activity. This analytical process, which relies on the photocurrent being contrary to the acetochlor concentration, was effectively used to detect acetochlor in fresh produce samples. The vision of this study appears to be compelling because it explains ways photocatalytic materials can be used with bio-recognition elements to tackle particular analytes, an important advancement in developing highly selective sensors. However, it is more likely that enzyme-based sensors will be unstable, especially under varying external environment conditions. Further optimization of the composite and enzyme-immobilization process may reduce this issue.

Yan and colleagues created an Eu-modified NH_2-MIL-125, MIL-125-AM-Eu, as a fluorescence sensor (turn-off) for detecting α-phenethyl alcohol.[285] When exposed to UV light, the sensor exhibited fluorescence from the e^- transition of $^5D_0 \rightarrow {}^7F_2$ 4f in Eu^{3+} attached to MIL-125-AM. The incorporation of lanthanide functionalization introduces a new aspect to photocatalytic sensing. Rare-earth elements like Eu provide improved sensitivity thanks to their distinct electronic properties and their capacity for sharp, well-defined electronic transitions. This fluorescence intensity gradually decreased and was fully snuffed in about 20 minutes (Fig. 8e). α-Phenethyl alcohol became trapped in the MIL-125-AM-Eu channels; as a result, α-phenethyl alcohol oxidized to acetophenone, facilitated by the photoactive Ti(IV). This reaction led to fluorescence quenching due to the formation of carbonyl groups. The consistent luminescent emission intensity, photocatalytic transformation, and Ti to Eu proportion with five reaction cycles demonstrated the material's reusability for detecting α-phenethyl alcohol. The MIL-125-AM-Eu's excellent performance validated its effectiveness as a turn-off fluorescence sensor towards α-phenethyl alcohol. Moreover, researchers have further discovered that MIL-125-AM-Eu can also act as a ratiometric fluorescence sensor for anion recognition and detection. Enhancing sensor sensitivity and selectivity for accurate and reliable analyte detection is a key focus. Challenges include ensuring stability under operational conditions and optimizing charge separation and photocurrent response. Ensuring long-term stability and reusability, expanding detectable substances, and implementing sensors in real-world applications are crucial for advancing the field.

11. Conclusion

Even though Ti-based MOF materials constitute only a compact subset of MOF descendants, significant progression in their structural design and fabrication has been made in recent years. In the case of metal-modified MOFs, like Zr, Cu and Fe-MOFs, Ti-based MOFs offer greater structural and topological divergence in titanium cores owing to their varying nuclearity. However, Ti-MOF structures remain relatively scarce compared with di- and trivalent metal MOFs and Zr-MOFs, primarily because of the increased volatility and hydrophilicity of ionic Ti forerunners. Despite years of research leading to a wealth of Ti-cluster coordination chemistry, the field of Ti-MOFs only saw a breakthrough in recent years with the finding of MIL-125, a significant juncture. However, a higher E_g (3.6 eV) of MIL-125 curbs its activity in the UV region. To address this, NH_2 (organic chromophore) was introduced to extend the light absorption range into the visible light region. The well-defined but tunable structure of NH_2-MIL-125 has attracted intensive research due to its robust architecture and intriguing photoresponsive properties. This makes it a promising material for assembling multifunctional photocatalysts and an ideal platform for mechanistic studies of photocatalytic processes. The review elucidates the critical aspects, such as the nature of the Ti precursor, coordination environment, synthesis procedures, and charge transfer mechanisms, providing a comprehensive understanding of their photocatalytic behavior. Various strategies were also discussed to enhance light-harvesting ability and boost exciton pair split for improved photocatalytic efficacy. These strategies aim to optimize the optical properties, enhance the electron transfer rate, and accelerate surface catalytic reactions in the NH_2-MIL-125 matrix. The broad realm of photocatalytic applications for NH_2-MIL-125 nanomaterials, including hydrogen and oxygen evolution reactions, CO_2 and N_2 reduction, photocatalytic sensors, and organic transformations, highlights their versatility and potential impact.

12. Challenges and future prospects

The aminated MIL-125(Ti) has been exemplified as a photocatalyst for numerous photocatalytic applications. The multinuclear titanium centers, akin to those in TiO_2, endow the MOF with significant photocatalytic potential. Additionally, the titanium-based MOF features outstanding porosity and structural sturdiness, variable valence states of Ti(IV/III), and lower CB concerning Zr-MOFs, which promotes a durable LMCT with photoirradiation, making it an appropriate selection for photocatalytic applications. Despite some eye-catching and notable results in NH_2-MIL-125-related photocatalysis, certain challenges are still faced by the MOF concerning the structure, morphology, and band gap.

i. Ti precursors spontaneously hydrolyze with water, whether present as solvent residue, intentionally added, or generated *in situ* from reactions. This typically results in the development of huge multinuclear SBUs and amorphous TiO_2, partially blocking the cavities of the newly developed MOFs. Enhancing the complex potential of ligands can lead to compact Ti-oxo clusters or surprisingly remote Ti octahedra while suppressing the competitive side formation of TiO_2. There have been reports of only a few systems, mainly invol-

ving common organic ligands, but there remains considerable room for exploring new NH_2-MIL-125-based structures.

ii. Functionalizing MIL-125 analogs has shown promise but is limited. Lowering the E_g below 1.3 eV is difficult due to the large Ti_8-oxo clusters, which form local semiconductive regions and are minimally affected by ligand modifications. Expanding the absorption band may not enhance photocatalytic activity, as low-energy photons insufficient for photoreactions are also absorbed. Additionally, added groups can block MOF apertures and impede mass transport.

iii. Synthesis remains the primary challenge in NH_2-MIL-125 research, primarily due to the greatly unpredictable Ti^{4+} cation polycondensation, leading to unrestricted products. Synthetic parameters, such as solvent composition, time, and reaction temperature, besides the surfactant and modulator addition, significantly affect the end products' design, porosity, and crystalline morphology.

iv. The preparation and usage of NH_2-MIL-125 suffer from difficulties in the handling of large Ti-oxo-carboxylate clusters, while NH_2-MIL-125 has a lower surface area compared with MIL-125 due to partial pore blockage by the free ligand, and both reveal a reversible decrease in crystallinity upon high-pressure treatment.

v. The properties of NH_2-MIL-125 with a mouldable framework are capable of being regulated with the introduction of counterfeiting groups to the linkers or substituting/doping the nodes with the metal ions or the clusters. However, reports of the above-modified MILs are scantily available.

vi. The coordinated NH_2-MIL-125 structure allows the integration of multifunctional modules into an individual framework towards collaborative catalysis, facilitating the construction of diverse MOF-based nano photocatalysts having multiple functions. Yet, the most complex NH_2-MIL-125-based materials show an unclear structure, significantly hindering the study of the relationship concerning structure, property, and performance.

vii. Exploring NH_2-MIL-125-based photocatalysts towards artificial photosynthetic overall processes is a challenging yet significant endeavor, encompassing water splitting, hydrogen peroxide production, artificial carbon dioxide conversion, and nitrogen reduction.

viii. NH_2-MIL-125-based photocatalysts generally exhibit a moderate or low photocatalytic efficiency, necessitating significant improvements for practical applications. The interdisciplinary integration of MOF research and computational techniques – such as machine learning, big data, artificial intelligence, and the Internet of Things – holds the potential to address this challenge.

ix. Presently reported, light harnessing NH_2-MIL-125-based catalysts are budding towards CO_2 reduction and H_2 generation, relying heavily on sacrificial agents that are neither cost nor environment-friendly. Besides, research on NH_2-MIL-125-based photocatalysts remains at the laboratory scale. Catalytic efficiency depends not only on the photocatalyst's properties but also on environmental factors. In real-world conditions, these photocatalysts face challenges such as ion interference, temperature fluctuations, and pH variations (Scheme 3).

The capabilities of NH_2-MIL-125(Ti) are crucial owing to its potential to revolutionize several critical areas, including advanced materials science. Enhancing its photocatalytic efficiency means contributing significantly to renewable energy solutions and pollution control by enabling more effective solar-driven processes. Improvements in gas storage and separation capabilities help to form better energy storage systems and more efficient capture of greenhouse gases, addressing urgent environmental concerns. Furthermore,

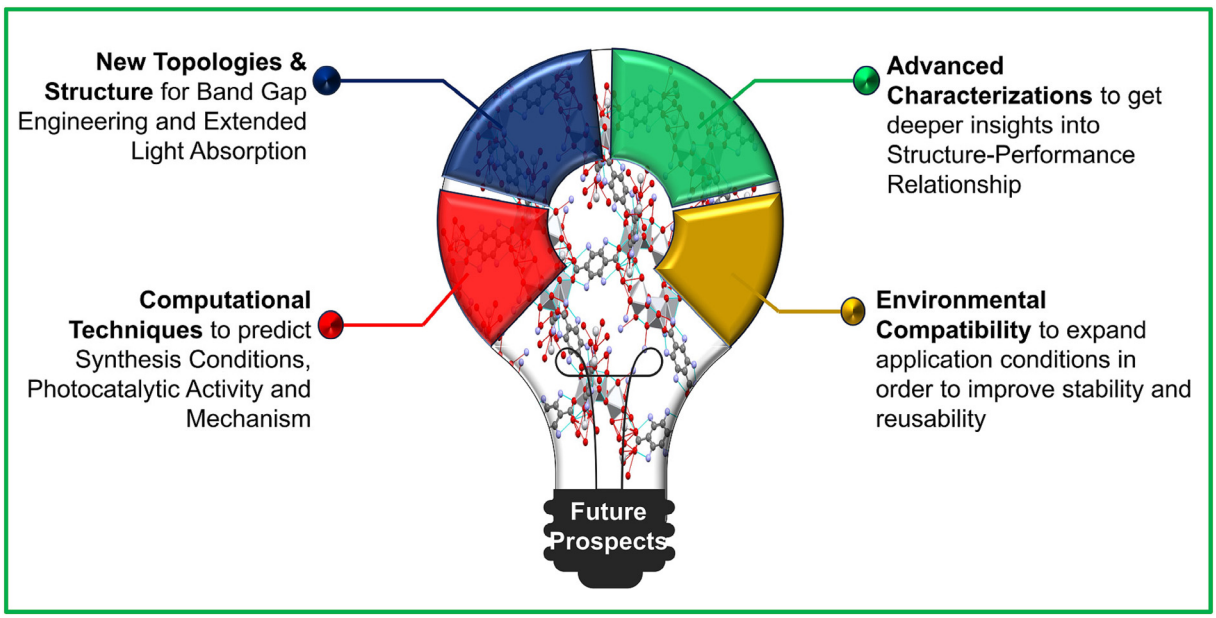

Scheme 3 Future prospects towards the advancements and enhanced photocatalytic performance of the NH_2-MIL-125(Ti)-based nanomaterials.

advancements in sensor technologies using NH_2-MIL-125(Ti) could result in useful and selective devices for detecting pollutants and hazardous substances, promoting public health and safety. Therefore, research in this space is still in its initial phases, providing enough scope for further expansion and optimization of NH_2-MIL-125(Ti), vital for advancing technologies supporting a more sustainable and healthier future. Hence,

i. Despite the challenges, new topology and structure construction is the need of the hour for the bandgap engineering of NH_2-MIL-125-based photocatalysts, to underscore their full potential. The bandgap of the MOF can be engineered by functionalizing ligands and developing new structures.

ii. Currently, the direct solvothermal method is the most customary synthesis procedure for producing this MOF. However, controlling the product structure is hugely empirical and particularly difficult, even though not impossible, while exploring new systems. Further work is needed on optimizing synthesis for better surface area and stability, using different BDC derivatives to modulate photocatalytic properties, and exploring its mechanical stability and structural behaviors under various stimuli to extend the usage of MOFs. Also, it is possible to impromptu assemble SBUs through the coordination of covalent bonds and frameworks in a one-pot reaction. Titanium is particularly well suited for this approach owing to the strength and abundance of Ti-oxo-clusters. The combination of a one-pot reaction strategy with other techniques eventually enables the target-specific synthesis of NH_2-MIL-125 having pre-formed topology and chemical functionality.

iii. Investigation of the morphology and the interface properties of the various components forming a heterojunction with MOF and alteration of its organic ligands/metal nodes *via* thorough research can help in developing multiple NH_2-MIL-125 structures to improve its photocatalytic efficiency, stability, and reusability. Besides, catalytic ability can be further enhanced by incorporating different hugely active species, such as nanoparticles of metal and graphene. Additionally, new NH_2-MIL-125-based composites should be explored, having explicit textural structures, low E_g, and high energy transfer efficiency.

iv. While expanding the applications of NH_2-MIL-125 is crucial, an ultimate goal for this family of materials is the efficient employment of solar energy through its distinct photoactive moieties, spanning the absorption of solar energy into the visible and NIR regions. Also, the E_g engineering of the MOF can be brought about by functionalizing ligands to develop innovative structures.

v. Additionally, using NH_2-MIL-125(Ti)-based photocatalysts for photocatalytic oxidative desulfurization could be a groundbreaking approach for addressing environmental issues.

vi. Advanced computational techniques could efficiently identify optimal synthetic conditions for tuning the morphology or the MOF for specific photoassisted catalytic reactions. For instance, artificial intelligence involving machine learning aims to design models based on previous literature. A standard machine learning model, capable of predicting electronic E_g and photocatalytic activities and guiding the engineering of morphology, could provide new perceptions for the well-reasoned blueprint of NH_2-MIL-125-based photocatalysts with enhanced catalytic performance utilizing solar energy.

vii. To address the issue of the need for sacrificial agents and to eliminate them, a combination of oxidation side reactions, such as oxygen evolution reaction (OER), with reduction reactions is crucial. Additionally, the use of single atoms as co-catalysts can assist the evolution of hydrogen in place of precious metals.

viii. The mechanistic pathway of photocatalytic reactions over NH_2-MIL-125-based photocatalysts remains unclear. Advanced characterization procedures such as *in situ* analysis, flash-photolysis without electrodes, transient absorption techniques, time-dependent microwave conductivity, and isotopic methods, along with DFT (Density Functional Theory) calculations, can be feasibly employed to gain deeper insights into the performance and structure relationship. This understanding is crucial for the well-reasoned design of MOFs (Ti-based) with enhanced photocatalytic efficiency.

ix. Future research must also focus on the interrelation between NH_2-MIL-125-based photocatalysts and their surroundings, expanding the application horizon of the MOF. Additionally, stability and recyclability are pivotal for the practical implementation of these materials. Therefore, further research is required to investigate the causes and prerequisites of the structural disintegration of light-harnessing NH_2-MIL-125-based catalysts.

Although still in its early stage, the rapid developments in the realm of NH_2-MIL-125 as a photocatalyst envision a bright future for the above nanomaterial. We believe that with the help of rationally designing MOFs' structure, we likely look forward to enhanced performance pertaining to photocatalytic solar-to-energy conversion. Through our review, our wish and aim are to inspire researchers to explore novel MOF structures based on NH_2-MIL-125 towards fresh applications carrying conceptual innovativeness in the existing and upcoming intriguing fields.

Author contributions

Priyanka Priyadarshini: conceptualization, writing-original draft, visualization. Anshumika Mishra: writing-original draft, review, and editing. Susanginee Nayak: writing-original draft. Kulamani Parida: conceptualization, visualization, supervision.

Data availability

The submitted review article synthesizes and discusses data that have already been published and publicly available from the sources cited in the manuscript. No new data were generated during the preparation timeframe of this review.

Conflicts of interest

There are no conflicts to declare.

Acknowledgements

The authors express their profound gratitude toward Siksha 'O' Anusandhan (deemed to be University) for giving all the necessary facilities and financial support to carry out this immense research work.

References

1 M. Alvaro, E. Carbonell, B. Ferrer, F. X. Llabrés I Xamena and H. Garcia, Semiconductor behavior of a metal-organic framework (MOF), *Chem. – Eur. J.*, 2007, **13**, 5106–5112, DOI: **10.1002/chem.200601003**.

2 T. Tachikawa, J. R. Choi, M. Fujitsuka and T. Majima, Photoinduced charge-transfer processes on MOF-5 nanoparticles: Elucidating differences between metal-organic frameworks and semiconductor metal oxides, *J. Phys. Chem. C*, 2008, **112**, 14090–14101, DOI: **10.1021/jp803620v**.

3 C. A. Kent, D. Liu, L. Ma, J. M. Papanikolas, T. J. Meyer and W. Lin, Light harvesting in microscale metal-organic frameworks by energy migration and interfacial electron transfer quenching, *J. Am. Chem. Soc.*, 2011, **133**, 12940–12943, DOI: **10.1021/ja204214t**.

4 X. Han, Q. Cheng, X. Meng, Z. Shao, K. Ma, D. Wei, J. Ding and H. Hou, Unique structural micro-adjustments in a new benzothiadiazole-derived Zn(II) metal organic framework: Via simple photochemical decarboxylation, *Chem. Commun.*, 2017, **53**, 10314–10317, DOI: **10.1039/c7cc06125k**.

5 S. Subudhi, S. P. Tripathy and K. Parida, Metal oxide integrated metal organic frameworks (MO@MOF): Rational design, fabrication strategy, characterization and emerging photocatalytic applications, *Inorg. Chem. Front.*, 2021, **8**, 1619–1636, DOI: **10.1039/d0qi01117g**.

6 G. Swain, S. Sultana and K. Parida, One-Pot-Architectured Au-Nanodot-Promoted $MoS_2/ZnIn_2S_4$: A Novel p-n Heterojunction Photocatalyst for Enhanced Hydrogen Production and Phenol Degradation, *Inorg. Chem.*, 2019, **58**, 9941–9955, DOI: **10.1021/acs.inorgchem.9b01105**.

7 S. Patnaik, A. Behera and K. Parida, A review on g-C_3N_4/graphene nanocomposites: multifunctional roles of graphene in the nanohybrid photocatalyst toward photocatalytic applications, *Catal. Sci. Technol.*, 2021, **11**, 6018–6040, DOI: **10.1039/d1cy00784j**.

8 J. Sahu, D. Prusty, S. Mansingh and K. Parida, A review on alloyed quantum dots and their applications as photocatalysts, *Int. J. Hydrogen Energy*, 2023, **48**, 29097–29118, DOI: **10.1016/j.ijhydene.2023.04.109**.

9 S. Nayak and K. Parida, Superlative photoelectrochemical properties of 3D MgCr-LDH nanoparticles influencing towards photoinduced water splitting reactions, *Sci. Rep.*, 2022, **12**, 9264, DOI: **10.1038/s41598-022-13457-x**.

10 A. Mishra, N. Priyadarshini, S. Mansingh and K. Parida, Recent advancement in $LaFeO_3$-mediated systems towards photocatalytic and photoelectrocatalytic hydrogen evolution reaction: A comprehensive review, *Adv. Colloid Interface Sci.*, 2024, **333**, 103300, DOI: **10.1016/j.cis.2024.103300**.

11 L. Li, Q. Yin, H. F. Li, T. F. Liu and R. Cao, Rational design of phosphonocarboxylate metal-organic frameworks for light hydrocarbon separations, *Mater. Chem. Front.*, 2018, **2**, 1436–1440, DOI: **10.1039/c8qm00029h**.

12 S. Wu, H. Min, W. Shi and P. Cheng, Multicenter Metal–Organic Framework-Based Ratiometric Fluorescent Sensors, *Adv. Mater.*, 2020, **32**(3), 1805871, DOI: **10.1002/adma.201805871**.

13 P. Priyadarshini and K. Parida, Two-dimensional metal-organic frameworks and their derived materials: Properties, synthesis and application in supercapacitors field, *J. Energy Storage*, 2024, **87**, 111379, DOI: **10.1016/j.est.2024.111379**.

14 L. Li, X. Wang, J. Liang, Y. Huang, H. Li, Z. Lin and R. Cao, Water-Stable Anionic Metal-Organic Framework for Highly Selective Separation of Methane from Natural Gas and Pyrolysis Gas, *ACS Appl. Mater. Interfaces*, 2016, **8**, 9777–9781, DOI: **10.1021/acsami.6b00706**.

15 L. Chen, D. Liu, J. Peng, Q. Du and H. He, Ratiometric fluorescence sensing of metal-organic frameworks: Tactics and perspectives, *Coord. Chem. Rev.*, 2020, **404**, 213113, DOI: **10.1016/j.ccr.2019.213113**.

16 X. Zhao, Y. Wang, D. S. Li, X. Bu and P. Feng, Metal–Organic Frameworks for Separation, *Adv. Mater.*, 2018, **30**, 1705189, DOI: **10.1002/adma.201705189**.

17 S. Wang and X. Wang, Multifunctional Metal-Organic Frameworks for Photocatalysis, *Small*, 2015, **11**, 3097–3112, DOI: **10.1002/smll.201500084**.

18 S. T. Meek, J. A. Greathouse and M. D. Allendorf, Metal-organic frameworks: A rapidly growing class of versatile nanoporous materials, *Adv. Mater.*, 2011, **23**, 249–267, DOI: **10.1002/adma.201002854**.

19 W. Tu, Y. Xu, S. Yin and R. Xu, Rational Design of Catalytic Centers in Crystalline Frameworks, *Adv. Mater.*, 2018, **30**, 1707582, DOI: **10.1002/adma.201707582**.

20 T. Yoshino Furukawa, H. Nakayama, A. Kikuchi, K. Imazumi, H. Yamakuni, H. Sogabe, S. Yamasaki, K. Takeshita, M. Matsuo, T. Manda and W. Uchida, *Antiemetic Effects of a Potent and Selective Neurokinin-1 Receptor Antagonist, FK886, on Cisplatin-and Apomorphine-Induced Emesis in Dogs*, 2013.

21 J. Qin, S. Wang and X. Wang, Visible-light reduction CO_2 with dodecahedral zeolitic imidazolate framework ZIF-67 as an efficient co-catalyst, *Appl. Catal., B*, 2017, **209**, 476–482, DOI: **10.1016/j.apcatb.2017.03.018**.

22 Y. Fang, Y. Ma, M. Zheng, P. Yang, A. M. Asiri and X. Wang, Metal–organic frameworks for solar energy con-

version by photoredox catalysis, *Coord. Chem. Rev.*, 2018, **373**, 83–115, DOI: 10.1016/j.ccr.2017.09.013.

23 S. Wang, W. Yao, J. Lin, Z. Ding and X. Wang, Cobalt imidazolate metal-organic frameworks photosplit CO_2 under mild reaction conditions, *Angew. Chem., Int. Ed.*, 2014, **53**, 1034–1038, DOI: 10.1002/anie.201309426.

24 A. H. Chughtai, N. Ahmad, H. A. Younus, A. Laypkov and F. Verpoort, Metal-organic frameworks: Versatile heterogeneous catalysts for efficient catalytic organic transformations, *Chem. Soc. Rev.*, 2015, **44**, 6804–6849, DOI: 10.1039/c4cs00395k.

25 P. Behera, S. Subudhi, S. P. Tripathy and K. Parida, MOF derived nano-materials: A recent progress in strategic fabrication, characterization and mechanistic insight towards divergent photocatalytic applications, *Coord. Chem. Rev.*, 2022, **456**, 214392, DOI: 10.1016/j.ccr.2021.214392.

26 W. Meng, Y. Zeng, Z. Liang, W. Guo, C. Zhi, Y. Wu, R. Zhong, C. Qu and R. Zou, Tuning Expanded Pores in Metal–Organic Frameworks for Selective Capture and Catalytic Conversion of Carbon Dioxide, *ChemSusChem*, 2018, **11**, 3751–3757, DOI: 10.1002/cssc.201801585.

27 S. P. Tripathy, S. Subudhi and K. Parida, Inter-MOF hybrid (IMOFH): A concise analysis on emerging core–shell based hierarchical and multifunctional nanoporous materials, *Coord. Chem. Rev.*, 2021, **434**, 213786, DOI: 10.1016/j.ccr.2021.213786.

28 J. D. Xiao and H. L. Jiang, Metal-Organic Frameworks for Photocatalysis and Photothermal Catalysis, *Acc. Chem. Res.*, 2019, **52**, 356–366, DOI: 10.1021/acs.accounts.8b00521.

29 X. Han, X. Yang, G. Liu, Z. Li and L. Shao, Boosting visible light photocatalytic activity via impregnation-induced RhB-sensitized MIL-125(Ti), *Chem. Eng. Res. Des.*, 2019, **143**, 90–99, DOI: 10.1016/j.cherd.2019.01.010.

30 J. D. Xiao, L. Han, J. Luo, S. H. Yu and H. L. Jiang, Integration of Plasmonic Effects and Schottky Junctions into Metal–Organic Framework Composites: Steering Charge Flow for Enhanced Visible-Light Photocatalysis, *Angew. Chem., Int. Ed.*, 2018, **57**, 1103–1107, DOI: 10.1002/anie.201711725.

31 J. J. Low, A. I. Benin, P. Jakubczak, J. F. Abrahamian, S. A. Faheem and R. R. Willis, Virtual high throughput screening confirmed experimentally: Porous coordination polymer hydration, *J. Am. Chem. Soc.*, 2009, **131**, 15834–15842, DOI: 10.1021/ja9061344.

32 T. Devic and C. Serre, High valence 3p and transition metal based MOFs, *Chem. Soc. Rev.*, 2014, **43**, 6097–6115, DOI: 10.1039/c4cs00081a.

33 J. H. Cavka, S. Jakobsen, U. Olsbye, N. Guillou, C. Lamberti, S. Bordiga and K. P. Lillerud, A new zirconium inorganic building brick forming metal organic frameworks with exceptional stability, *J. Am. Chem. Soc.*, 2008, **130**, 13850–13851, DOI: 10.1021/ja8057953.

34 A. Schaate, P. Roy, A. Godt, J. Lippke, F. Waltz, M. Wiebcke and P. Behrens, Modulated synthesis of Zr-based metal-organic frameworks: From nano to single crystals, *Chem. – Eur. J.*, 2011, **17**, 6643–6651, DOI: 10.1002/chem.201003211.

35 G. Mouchaham, L. Cooper, N. Guillou, C. Martineau, E. Elkaïm, S. Bourrelly, P. L. Llewellyn, C. Allain, G. Clavier, C. Serre and T. Devic, A Robust Infinite Zirconium Phenolate Building Unit to Enhance the Chemical Stability of Zr MOFs, *Angew. Chem.*, 2015, **127**, 13495–13499, DOI: 10.1002/ange.201507058.

36 Y. Bai, Y. Dou, L. H. Xie, W. Rutledge, J. R. Li and H. C. Zhou, Zr-based metal-organic frameworks: Design, synthesis, structure, and applications, *Chem. Soc. Rev.*, 2016, **45**, 2327–2367, DOI: 10.1039/c5cs00837a.

37 Z. Wei, W. Xu, P. Peng, Q. Sun, Y. Li, N. Ding, C. Zhao, S. Li and S. Pang, Covalent synthesis of Ti-MOF for enhanced photocatalytic CO_2 reduction, *Mol. Catal.*, 2024, **558**, 114042, DOI: 10.1016/j.mcat.2024.114042.

38 Q. Yao, X. Pan, X. Si, X. Wang, X. Zhang, J. Hou, J. Su, Y. Qiu and J. Li, A porous and photoactive Ti-MOF based on a novel tetranuclear $[Ti_2Tb_2]$ cluster, *Chem. Commun.*, 2024, **60**, 2188–2191, DOI: 10.1039/d3cc06114k.

39 H. Z. Li, S. Li, F. Wang and J. Zhang, A chelating coordination modulation method for the synthesis of Ti-MOF single crystals, *Inorg. Chem. Front.*, 2024, **11**, 2876–2883, DOI: 10.1039/d4qi00436a.

40 A. García-Baldoví, R. Del Angel, G. Mouchaham, S. Liu, D. Fan, G. Maurin, S. Navalón, C. Serre and H. Garcia, Active site imprinting on Ti oxocluster metal-organic frameworks for photocatalytic hydrogen release from formic acid, *Energy Environ. Sci.*, 2022, **16**, 167–177, DOI: 10.1039/d2ee02258c.

41 X. He, Y. Ding, Z. Huang, M. Liu, M. Chi, Z. Wu, C. U. Segre, C. Song, X. Wang and X. Guo, Engineering a Self-Grown TiO_2/Ti-MOF Heterojunction with Selectively Anchored High-Density Pt Single-Atomic Cocatalysts for Efficient Visible-Light-Driven Hydrogen Evolution, *Angew. Chem., Int. Ed.*, 2023, **135**(25), e202217439, DOI: 10.1002/anie.202217439.

42 L. Zhao, J. Bian, X. Zhang, L. Bai, L. Xu, Y. Qu, Z. Li, Y. Li and L. Jing, Construction of Ultrathin S-Scheme Heterojunctions of Single Ni Atom Immobilized Ti-MOF and $BiVO_4$ for CO_2 Photoconversion of nearly 100% to CO by Pure Water, *Adv. Mater.*, 2022, **34**, 2205303, DOI: 10.1002/adma.202205303.

43 R. X. Bi, X. Liu, L. Lei, Z. H. Peng, X. X. Wang, L. Zhang, R. P. Liang and J. D. Qiu, Core-shell MOF@COF photocatalysts for synergistic enhanced U(VI) and tetracycline cleanup through space and carrier separation, *Chem. Eng. J.*, 2024, **485**, 150026, DOI: 10.1016/j.cej.2024.150026.

44 V. Guillerm, F. Ragon, M. Dan-Hardi, T. Devic, M. Vishnuvarthan, B. Campo, A. Vimont, G. Clet, Q. Yang, G. Maurin, G. Férey, A. Vittadini, S. Gross and C. Serre, A series of isoreticular, highly stable, porous zirconium oxide based metal-organic frameworks, *Angew. Chem., Int. Ed.*, 2012, **51**, 9267–9271, DOI: 10.1002/anie.201204806.

45 M. Kim and S. M. Cohen, Discovery, development, and functionalization of Zr(iv)-based metal-organic frame-

works, *CrystEngComm*, 2012, **14**, 4096–4104, DOI: 10.1039/c2ce06491j.

46 J. Schneider, M. Matsuoka, M. Takeuchi, J. Zhang, Y. Horiuchi, M. Anpo and D. W. Bahnemann, Understanding TiO_2 photocatalysis: Mechanisms and materials, *Chem. Rev.*, 2014, **114**, 9919–9986, DOI: 10.1021/cr5001892.

47 Y. Fu, D. Sun, Y. Chen, R. Huang, Z. Ding, X. Fu and Z. Li, An amine-functionalized titanium metalorganic framework photocatalyst with visible-light-induced activity for CO_2 reduction, *Angew. Chem., Int. Ed.*, 2012, **51**, 3364–3367, DOI: 10.1002/anie.201108357.

48 H. Wang, X. Yuan, Y. Wu, G. Zeng, X. Chen, L. Leng and H. Li, Synthesis and applications of novel graphitic carbon nitride/metal-organic frameworks mesoporous photocatalyst for dyes removal, *Appl. Catal., B*, 2015, **174–175**, 445–454, DOI: 10.1016/j.apcatb.2015.03.037.

49 Y. Zhang, F. Mao, L. Wang, H. Yuan, P. F. Liu and H. G. Yang, Recent Advances in Photocatalysis over Metal–Organic Frameworks-Based Materials, *Sol. RRL*, 2020, **4**, 1900438, DOI: 10.1002/solr.201900438.

50 Y. Fu, D. Sun, Y. Chen, R. Huang, Z. Ding, X. Fu and Z. Li, An amine-functionalized titanium metal-organic framework photocatalyst with visible-light-induced activity for CO_2 reduction, *Angew. Chem., Int. Ed.*, 2012, **51**, 3364–3367, DOI: 10.1002/anie.201108357.

51 Z. Wu, X. Huang, H. Zheng, P. Wang, G. Hai, W. Dong and G. Wang, Aromatic heterocycle-grafted NH_2-MIL-125 (Ti) via conjugated linker with enhanced photocatalytic activity for selective oxidation of alcohols under visible light, *Appl. Catal., B*, 2018, **224**, 479–487, DOI: 10.1016/j.apcatb.2017.10.034.

52 S. Subudhi, G. Swain, S. P. Tripathy and K. Parida, UiO-66-NH_2Metal-Organic Frameworks with Embedded MoS_2Nanoflakes for Visible-Light-Mediated $H_2$and O_2Evolution, *Inorg. Chem.*, 2020, **59**, 9824–9837, DOI: 10.1021/acs.inorgchem.0c01030.

53 S. Subudhi, S. Mansingh, G. Swain, A. Behera, D. Rath and K. Parida, HPW-Anchored UiO-66 Metal-Organic Framework: A Promising Photocatalyst Effective toward Tetracycline Hydrochloride Degradation and H_2 Evolution via Z-Scheme Charge Dynamics, *Inorg. Chem.*, 2019, **58**, 4921–4934, DOI: 10.1021/acs.inorgchem.8b03544.

54 S. Yin, Y. Chen, M. Li, Q. Hu, Y. Ding, Y. Shao, J. Di, J. Xia and H. Li, Construction of NH_2-MIL-125(Ti)/Bi_2WO_6 composites with accelerated charge separation for degradation of organic contaminants under visible light irradiation, *Green Energy Environ.*, 2020, **5**, 203–213, DOI: 10.1016/j.gee.2020.03.008.

55 K. Dai, L. Lu, Q. Liu, G. Zhu, X. Wei, J. Bai, L. Xuan and H. Wang, Sonication assisted preparation of graphene oxide/graphitic-C_3N_4 nanosheet hybrid with reinforced photocurrent for photocatalyst applications, *Dalton Trans.*, 2014, **43**, 6295–6299, DOI: 10.1039/c3dt53106f.

56 Y. Horiuchi, T. Toyao, M. Saito, K. Mochizuki, M. Iwata, H. Higashimura, M. Anpo and M. Matsuoka, Visible-light-promoted photocatalytic hydrogen production by using an amino-functionalized Ti(IV) metal-organic framework, *J. Phys. Chem. C*, 2012, **116**, 20848–20853, DOI: 10.1021/jp3046005.

57 Z. Su, B. Zhang, J. Shi, D. Tan, F. Zhang, L. Liu, X. Tan, D. Shao, G. Yang and J. Zhang, An NH_2-MIL-125 (Ti)/Pt/g-C_3N_4 catalyst promoting visible-light photocatalytic H_2 production, *Sustainable Energy Fuels*, 2019, **3**, 1233–1238, DOI: 10.1039/c9se00118b.

58 Y. Zhao, W. Cai, J. Chen, Y. Miao and Y. Bu, A Highly Efficient Composite Catalyst Constructed From NH_2-MIL-125(Ti) and Reduced Graphene Oxide for CO_2 Photoreduction, *Front. Chem.*, 2019, **7**, 789, DOI: 10.3389/fchem.2019.00789.

59 G. Wen and Z. G. Guo, Facile modification of NH_2-MIL-125(Ti) to enhance water stability for efficient adsorptive removal of crystal violet from aqueous solution, *Colloids Surf., A*, 2018, **541**, 58–67, DOI: 10.1016/j.colsurfa.2018.01.011.

60 R. Zhang, G. Li and Y. Zhang, Photochemical synthesis of CdS-MIL-125(Ti) with enhanced visible light photocatalytic performance for the selective oxidation of benzyl alcohol to benzaldehyde, *Photochem. Photobiol. Sci.*, 2017, **16**, 996–1002, DOI: 10.1039/c7pp00073a.

61 P. Karthik, E. Balaraman and B. Neppolian, Efficient solar light-driven H_2 production: Post-synthetic encapsulation of a Cu_2O co-catalyst in a metal-organic framework (MOF) for boosting the effective charge carrier separation, *Catal. Sci. Technol.*, 2018, **8**, 3286–3294, DOI: 10.1039/c8cy00604k.

62 M. Wang, L. Yang, J. Yuan, L. He, Y. Song, H. Zhang, Z. Zhang and S. Fang, Heterostructured Bi_2S_3@NH_2-MIL-125(Ti) nanocomposite as a bifunctional photocatalyst for Cr(vi) reduction and rhodamine B degradation under visible light, *RSC Adv.*, 2018, **8**, 12459–12470, DOI: 10.1039/c8ra00882e.

63 X. Li, Y. Pi, Q. Hou, H. Yu, Z. Li, Y. Li and J. Xiao, Amorphous TiO_2@NH_2-MIL-125(Ti) homologous MOF-encapsulated heterostructures with enhanced photocatalytic activity, *Chem. Commun.*, 2018, **54**, 1917–1920, DOI: 10.1039/c7cc09072b.

64 J. Qiu, X. Zhang, Y. Feng, X. Zhang, H. Wang and J. Yao, Modified metal-organic frameworks as photocatalysts, *Appl. Catal., B*, 2018, **231**, 317–342, DOI: 10.1016/j.apcatb.2018.03.039.

65 W. Da Oh, L. W. Lok, A. Veksha, A. Giannis and T. T. Lim, Enhanced photocatalytic degradation of bisphenol A with Ag-decorated S-doped g-C_3N_4 under solar irradiation: Performance and mechanistic studies, *Chem. Eng. J.*, 2018, **333**, 739–749, DOI: 10.1016/j.cej.2017.09.182.

66 J. Zhu, P. Z. Li, W. Guo, Y. Zhao and R. Zou, Titanium-based metal–organic frameworks for photocatalytic applications, *Coord. Chem. Rev.*, 2018, **359**, 80–101, DOI: 10.1016/j.ccr.2017.12.013.

67 H. Assi, G. Mouchaham, N. Steunou, T. Devic and C. Serre, Titanium coordination compounds: From discrete metal complexes to metal-organic frameworks, *Chem. Soc. Rev.*, 2017, **46**, 3431–3452, DOI: **10.1039/c7cs00001d**.

68 S. Yuan, J. S. Qin, C. T. Lollar and H. C. Zhou, Stable Metal-Organic Frameworks with Group 4 Metals: Current Status and Trends, *ACS Cent. Sci.*, 2018, **4**, 440–450, DOI: **10.1021/acscentsci.8b00073**.

69 J. A. Mason, L. E. Darago, W. W. Lukens and J. R. Long, Synthesis and O_2 Reactivity of a Titanium(III) Metal-Organic Framework, *Inorg. Chem.*, 2015, **54**, 10096–10104, DOI: **10.1021/acs.inorgchem.5b02046**.

70 P. G. Yot, K. Yang, F. Ragon, V. Dmitriev, T. Devic, P. Horcajada, C. Serre and G. Maurin, Exploration of the mechanical behavior of metal organic frameworks UiO-66 (Zr) and MIL-125(Ti) and their NH_2 functionalized versions, *Dalton Trans.*, 2016, **45**, 4283–4288, DOI: **10.1039/c5dt03621f**.

71 S. Cassaignon, M. Koelsch and J. P. Jolivet, Selective synthesis of brookite, anatase and rutile nanoparticles: Thermolysis of $TiCl_4$ in aqueous nitric acid, *J. Mater. Sci.*, 2007, **42**, 6689–6695, DOI: **10.1007/s10853-007-1496-y**.

72 L. Li, X. S. Wang, T. F. Liu and J. Ye, Titanium-Based MOF Materials: From Crystal Engineering to Photocatalysis, *Small Methods*, 2020, **4**, 2000486, DOI: **10.1002/smtd.202000486**.

73 M. Eddaoudi, D. B. Moler, H. Li, B. Chen, T. M. Reineke, M. O'Keeffe and O. M. Yaghi, Modular chemistry: Secondary building units as a basis for the design of highly porous and robust metal-organic carboxylate frameworks, *Acc. Chem. Res.*, 2001, **34**, 319–330, DOI: **10.1021/ar000034b**.

74 C. Zlotea, D. Phanon, M. Mazaj, D. Heurtaux, V. Guillerm, C. Serre, P. Horcajada, T. Devic, E. Magnier, F. Cuevas, G. Férey, P. L. Llewellyn and M. Latroche, Effect of NH_2 and CF_3 functionalization on the hydrogen sorption properties of MOFs, *J. Chem. Soc., Dalton Trans.*, 2011, **40**, 4879–4881, DOI: **10.1039/c1dt10115c**.

75 C. Serre and G. Férey, Hybrid open frameworks. 8. Hydrothermal synthesis, crystal structure, and thermal behavior of the first three-dimensional titanium(IV) diphosphonate with an open structure: $Ti_3O_2(H_2O)_2(O_3P\text{-}(CH_2)\text{-}PO_3)_2\cdot(H_2O)_2$, or MIL-22, *Inorg. Chem.*, 1999, **38**, 5370–5373, DOI: **10.1021/ic990345m**.

76 C. Serre and G. Férey, Hydrothermal synthesis and structure determination from powder data of new three-dimensional titanium(IV) diphosphonates Ti(O3P-(CH2)n-PO3) or MIL-25n (n=2, 3), *Inorg. Chem.*, 2001, **40**, 5350–5353, DOI: **10.1021/ic010260x**.

77 C. Serre, J. A. Groves, P. Lightfoot, A. M. Z. Slawin, P. A. Wright, N. Stock, T. Bein, M. Haouas, F. Taulelle and G. Férey, Synthesis, structure and properties of related microporous N,N′-piperazinebismethylenephosphonates of aluminum and titanium, *Chem. Mater.*, 2006, **18**, 1451–1457, DOI: **10.1021/cm052149l**.

78 Y. Fu, Y. Liu, Z. Shi, B. Li and W. Pang, Hydrothermal synthesis and characterization of four oxalatotitanates with Ti4O4(C2O4)8 tetramers as basic building blocks, *J. Solid State Chem.*, 2002, **163**, 427–435, DOI: **10.1006/jssc.2001.9422**.

79 S. Hu, M. Liu, K. Li, Y. Zuo, A. Zhang, C. Song, G. Zhang and X. Guo, Solvothermal synthesis of NH2-MIL-125(Ti) from circular plate to octahedron, *CrystEngComm*, 2014, **16**, 9645–9650, DOI: **10.1039/c4ce01545b**.

80 S. N. Kim, J. Kim, H. Y. Kim, H. Y. Cho and W. S. Ahn, Adsorption/catalytic properties of MIL-125 and NH2-MIL-125, *Catal. Today*, 2013, **204**, 85–93, DOI: **10.1016/j.cattod.2012.08.014**.

81 P. George, N. R. Dhabarde and P. Chowdhury, Rapid synthesis of Titanium based Metal Organic framework (MIL-125) via microwave route and its performance evaluation in photocatalysis, *Mater. Lett.*, 2017, **186**, 151–154, DOI: **10.1016/j.matlet.2016.09.099**.

82 Y. Han, L. Han, L. Zhang and S. Dong, Ultrasonic synthesis of highly dispersed Au nanoparticles supported on Ti-based metal-organic frameworks for electrocatalytic oxidation of hydrazine, *J. Mater. Chem. A*, 2015, **3**, 14669–14674, DOI: **10.1039/c5ta03090k**.

83 Y. R. Lee, S. M. Cho, S. H. Baeck, W. S. Ahn and W. S. Cho, Ti-NH2-MIL-125 membrane grown on a TiO2 disc by combined microwave/ultrasonic heating: Facile synthesis for catalytic application, *RSC Adv.*, 2016, **6**, 63286–63290, DOI: **10.1039/c6ra09438d**.

84 Y. H. Fan, S. W. Zhang, S. Bin Qin, X. S. Li and S. H. Qi, An enhanced adsorption of organic dyes onto NH2 functionalization titanium-based metal-organic frameworks and the mechanism investigation, *Microporous Mesoporous Mater.*, 2018, **263**, 120–127, DOI: **10.1016/j.micromeso.2017.12.016**.

85 C. C. Wang, X. D. Du, J. Li, X. X. Guo, P. Wang and J. Zhang, Photocatalytic Cr(VI) reduction in metal-organic frameworks: A mini-review, *Appl. Catal., B*, 2016, **193**, 198–216, DOI: **10.1016/j.apcatb.2016.04.030**.

86 K. Wang, J. Gu and N. Yin, Efficient Removal of Pb(II) and Cd(II) Using NH2-Functionalized Zr-MOFs via Rapid Microwave-Promoted Synthesis, *Ind. Eng. Chem. Res.*, 2017, **56**, 1880–1887, DOI: **10.1021/acs.iecr.6b04997**.

87 S. Yang, J. Yu, G. Lu, G. Song, G. Shi, Y. Wang, X. Xie, H. Yuan, X. Ren and J. Sun, Effect of NH2-functionalization of MIL-125 on photocatalytic degradation of o-xylene and acetaldehyde, *Chem. Eng. J.*, 2024, **498**, 155251, DOI: **10.1016/j.cej.2024.155251**.

88 J. Long, S. Wang, Z. Ding, S. Wang, Y. Zhou, L. Huang and X. Wanga, Amine-functionalized zirconium metal–organic framework as efficient visible-light photocatalyst for aerobic organic transformations, *Chem. Commun.*, 2012, **48**, 11656–11658, DOI: **10.1039/c2cc34620f**.

89 H. N. Rubin and M. M. Reynolds, Functionalization of Metal-Organic Frameworks To Achieve Controllable Wettability, *Inorg. Chem.*, 2017, **56**, 5266–5274, DOI: **10.1021/acs.inorgchem.7b00373**.

90 Q. Zha, X. Sang, D. Liu, D. Wang, G. Shi and C. Ni, Modification of hydrophilic amine-functionalized metal-organic frameworks to hydrophobic for dye adsorption, *J. Solid State Chem.*, 2019, **275**, 23–29, DOI: **10.1016/j.jssc.2019.04.001**.

91 L. Feng, K. Y. Wang, G. S. Day, M. R. Ryder and H. C. Zhou, Destruction of Metal-Organic Frameworks: Positive and Negative Aspects of Stability and Lability, *Chem. Rev.*, 2020, **120**, 13087–13133, DOI: **10.1021/acs.chemrev.0c00722**.

92 M. A. Baluk, A. Pieczyńska, M. Kroczewska, J. Łuczak, K. Matus, K. Nikiforow and A. Zaleska-Medynska, Efficient method for octahedral NH2-MIL-125 (Ti) synthesis: Fast and mild conditions, *Chem. Eng. J.*, 2024, **492**, 152313, DOI: **10.1016/j.cej.2024.152313**.

93 Y. Liu, X. Xin, Y. Shi, Z. Zhao, J. Tan, D. Yang and Z. Jiang, Three-ligand Ti-MOFs for high-efficient photocatalytic H2 evolution, *Chem. Eng. J.*, 2024, **482**, 149193, DOI: **10.1016/j.cej.2024.149193**.

94 Y. Kondo, Y. Kuwahara, K. Mori and H. Yamashita, Design of metal-organic framework catalysts for photocatalytic hydrogen peroxide production, *Chem*, 2022, **8**, 2924–2938, DOI: **10.1016/j.chempr.2022.10.007**.

95 H. Sepehrmansourie, H. Alamgholiloo, N. Noroozi Pesyan and M. A. Zolfigol, A MOF-on-MOF strategy to construct double Z-scheme heterojunction for high-performance photocatalytic degradation, *Appl. Catal., B*, 2023, **321**, 122082, DOI: **10.1016/j.apcatb.2022.122082**.

96 P. H. M. Andrade, C. Volkringer, T. Loiseau, A. Tejeda, M. Hureau and A. Moissette, Band gap analysis in MOF materials: Distinguishing direct and indirect transitions using UV–vis spectroscopy, *Appl. Mater. Today*, 2024, **37**, 102094, DOI: **10.1016/j.apmt.2024.102094**.

97 X. Y. Ji, Y. Y. Wang and J. Tao, Metal-organic frameworks for the photocatalytic oxygen reduction reaction to hydrogen peroxide, *Mater. Chem. Front.*, 2023, **7**, 5120–5139, DOI: **10.1039/d3qm00468f**.

98 H. Wang, J. Yu, S. Wei, M. Lin, Y. Song and L. Wu, Surface coordination enhanced visible-light photocatalytic coupling of benzylamine to N-benzylidene benzylamine over the Pd/NH2-MIL-125(Ti) nanosheets, *Chem. Eng. J.*, 2022, **441**, 136020, DOI: **10.1016/j.cej.2022.136020**.

99 P. Qiu, X. Liao, Y. Jiang, Y. Yao, L. Shi, S. Lu and Z. Li, Unraveling the photocatalytic electron transfer mechanism in a Ti-MOF/g-C3N4 heterojunction for high-efficient coupling performance of primary amines, *New J. Chem.*, 2022, **46**, 20711–20722, DOI: **10.1039/d2nj04200b**.

100 V. Muelas-Ramos, C. Belver, J. J. Rodriguez and J. Bedia, Synthesis of noble metal-decorated NH2-MIL-125 titanium MOF for the photocatalytic degradation of acetaminophen under solar irradiation, *Sep. Purif. Technol.*, 2021, **272**, 118896, DOI: **10.1016/j.seppur.2021.118896**.

101 X. Guo, X. Tian, X. Xu and J. He, Enhancing visible-light-activity of Ti-based MOFs based on extending the conjugated degree of organic ligands and photocatalytic degradation process and mechanism in real industrial textile wastewaters, *J. Environ. Chem. Eng.*, 2021, **9**, 106428, DOI: **10.1016/j.jece.2021.106428**.

102 M. De Miguel, F. Ragon, T. Devic, C. Serre, P. Horcajada and H. García, Evidence of photoinduced charge separation in the metal-organic framework MIL-125(Ti)-NH2, *ChemPhysChem*, 2012, **13**, 3651–3654, DOI: **10.1002/cphc.201200411**.

103 J. Yang, D. Wang, H. Han and C. Li, Roles of cocatalysts in photocatalysis and photoelectrocatalysis, *Acc. Chem. Res.*, 2013, **46**, 1900–1909, DOI: **10.1021/ar300227e**.

104 M. A. Syzgantseva, C. P. Ireland, F. M. Ebrahim, B. Smit and O. A. Syzgantseva, Metal Substitution as the Method of Modifying Electronic Structure of Metal-Organic Frameworks, *J. Am. Chem. Soc.*, 2019, **141**, 6271–6278, DOI: **10.1021/jacs.8b13667**.

105 C. H. Hendon, D. Tiana, M. Fontecave, C. Sanchez, L. D'Arras, C. Sassoye, L. Rozes, C. Mellot-Draznieks and A. Walsh, Engineering the optical response of the titanium-MIL-125 metal-organic framework through ligand functionalization, *J. Am. Chem. Soc.*, 2013, **135**, 10942–10945, DOI: **10.1021/ja405350u**.

106 F. Mohammadnezhad, S. Kampouri, S. K. Wolff, Y. Xu, M. Feyzi, J. H. Lee, X. Ji and K. C. Stylianou, Tuning the Optoelectronic Properties of Hybrid Functionalized NH2-MIL-125for Photocatalytic Hydrogen Evolution, *ACS Appl. Mater. Interfaces*, 2021, **13**, 5044–5051, DOI: **10.1021/acsami.0c19345**.

107 F. Guo, J. H. Guo, P. Wang, Y. S. Kang, Y. Liu, J. Zhao and W. Y. Sun, Facet-dependent photocatalytic hydrogen production of metal-organic framework NH2-MIL-125(Ti), *Chem. Sci.*, 2019, **10**, 4834–4838, DOI: **10.1039/c8sc05060k**.

108 T. Musho, J. Li and N. Wu, Band gap modulation of functionalized metal-organic frameworks, *Phys. Chem. Chem. Phys.*, 2014, **16**, 23646–23653, DOI: **10.1039/c4cp03110e**.

109 E. Flage-Larsen, A. Røyset, J. H. Cavka and K. Thorshaug, Band gap modulations in UiO metal-organic frameworks, *J. Phys. Chem. C*, 2013, **117**, 20610–20616, DOI: **10.1021/jp405335q**.

110 K. Hendrickx, D. E. P. Vanpoucke, K. Leus, K. Lejaeghere, A. Van Yperen-De Deyne, V. Van Speybroeck, P. Van Der Voort and K. Hemelsoet, Understanding Intrinsic Light Absorption Properties of UiO-66 Frameworks: A Combined Theoretical and Experimental Study, *Inorg. Chem.*, 2015, **54**, 10701–10710, DOI: **10.1021/acs.inorgchem.5b01593**.

111 D. Sun, Y. Fu, W. Liu, L. Ye, D. Wang, L. Yang, X. Fu and Z. Li, Studies on photocatalytic CO2 reduction over NH_2-uio-66(Zr) and its derivatives: Towards a better understanding of photocatalysis on metal-organic frameworks, *Chem. – Eur. J.*, 2013, **19**, 14279–14285, DOI: **10.1002/chem.201301728**.

112 J. G. Santaclara, M. A. Nasalevich, S. Castellanos, W. H. Evers, F. C. M. Spoor, K. Rock, L. D. A. Siebbeles, F. Kapteijn, F. Grozema, A. Houtepen, J. Gascon, J. Hunger and M. A. Van Der Veen, Organic Linker

Defines the Excited-State Decay of Photocatalytic MIL-125 (Ti)-Type Materials, *ChemSusChem*, 2016, **9**, 388–395, DOI: 10.1002/cssc.201501353.

113 Y. He, Y. Tan, M. Song, Q. Tu, M. Fu, L. Long, J. Wu, M. Xu and X. Liu, Switching on photocatalytic NO oxidation and proton reduction of NH2-MIL-125(Ti) by convenient linker defect engineering, *J. Hazard. Mater.*, 2022, **430**, 128468, DOI: 10.1016/j.jhazmat.2022.128468.

114 T. R. Nelson, S. Fernandez-Alberti, A. E. Roitberg and S. Tretiak, *Electronic Delocalization, Vibrational Dynamics and Energy Transfer in Organic Chromophores*, 2017. https://pubs.acs.org.

115 S. Li, S. Sun, H. Wu, C. Wei and Y. Hu, Effects of electron-donating groups on the photocatalytic reaction of MOFs, *Catal. Sci. Technol.*, 2018, **8**, 1696–1703, DOI: 10.1039/c7cy02622f.

116 M. W. Logan, S. Ayad, J. D. Adamson, T. Dilbeck, K. Hanson and F. J. Uribe-Romo, Systematic variation of the optical bandgap in titanium based isoreticular metal-organic frameworks for photocatalytic reduction of CO2 under blue light, *J. Mater. Chem. A*, 2017, **5**, 11854–11863, DOI: 10.1039/c7ta00437k.

117 L. Jiao, Y. Wang, H. L. Jiang and Q. Xu, Metal–Organic Frameworks as Platforms for Catalytic Applications, *Adv. Mater.*, 2018, **30**, 1703663, DOI: 10.1002/adma.201703663.

118 C. Xu, R. Fang, R. Luque, L. Chen and Y. Li, Functional metal–organic frameworks for catalytic applications, *Coord. Chem. Rev.*, 2019, **388**, 268–292, DOI: 10.1016/j.ccr.2019.03.005.

119 F. Zhang, B. Zhang, J. Feng, X. Tan, L. Liu, L. Liu, B. Han, L. Zheng, J. Zhang, J. Tai and J. Zhang, Highly Mesoporous Ru-NH2-MIL-125 Produced by Supercritical Fluid for Efficient Photocatalytic Hydrogen Production, *ACS Appl. Energy Mater.*, 2019, **2**, 4964–4970, DOI: 10.1021/acsaem.9b00649.

120 . The absolute energy positions of conduction and valence bands of selected semiconducting minerals.

121 Z. Helali, A. Jedidi, O. A. Syzgantseva, M. Calatayud and C. Minot, Scaling reducibility of metal oxides, *Theor. Chem. Acc.*, 2017, **136**, 1–16, DOI: 10.1007/s00214-017-2130-y.

122 H. Li, X. Liu, H. Feng, J. Zhao, P. Lu, M. Fu, W. Guo, Y. Zhao and Y. He, NH2-MIL-125(Ti) with transient metal centers: Via novel electron transfer routes for enhancing photocatalytic NO removal and H2evolution, *Catal. Sci. Technol.*, 2021, **11**, 6225–6233, DOI: 10.1039/d1cy01008e.

123 M. A. Nasalevich, R. Becker, E. V. Ramos-Fernandez, S. Castellanos, S. L. Veber, M. V. Fedin, F. Kapteijn, J. N. H. Reek, J. I. Van Der Vlugt and J. Gascon, Co@NH2-MIL-125(Ti): Cobaloxime-derived metal-organic framework-based composite for light-driven H2 production, *Energy Environ. Sci.*, 2015, **8**, 364–375, DOI: 10.1039/c4ee02853h.

124 Z. Li, J. D. Xiao and H. L. Jiang, Encapsulating a Co(II) Molecular Photocatalyst in Metal-Organic Framework for Visible-Light-Driven H2 Production: Boosting Catalytic Efficiency via Spatial Charge Separation, *ACS Catal.*, 2016, **6**, 5359–5365, DOI: 10.1021/acscatal.6b01293.

125 D. Sun, W. Liu, Y. Fu, Z. Fang, F. Sun, X. Fu, Y. Zhang and Z. Li, Noble metals can have different effects on photocatalysis over metal-organic frameworks (MOFs): A case study on M/NH2-MIL-125(Ti) (M=Pt and Au), *Chem. – Eur. J.*, 2014, **20**, 4780–4788, DOI: 10.1002/chem.201304067.

126 M. A. Nasalevich, M. G. Goesten, T. J. Savenije, F. Kapteijn and J. Gascon, Enhancing optical absorption of metal-organic frameworks for improved visible light photocatalysis, *Chem. Commun.*, 2013, **49**, 10575–10577, DOI: 10.1039/c3cc46398b.

127 N. Tian, Z. Y. Zhou, S. G. Sun, Y. Ding and L. W. Zhong, Synthesis of tetrahexahedral platinum nanocrystals with high-index facets and high electro-oxidation activity, *Science*, 2007, **316**, 732–735, DOI: 10.1126/science.1140484.

128 S. Amirjalayer, M. Tafipolsky and R. Schmid, Surface termination of the metal-organic framework HKUST-1: A theoretical investigation, *J. Phys. Chem. Lett.*, 2014, **5**, 3206–3210, DOI: 10.1021/jz5012065.

129 S. Ghosh, P. Roy, N. Karmodak, E. D. Jemmis and G. Mugesh, Nanoisozymes: Crystal-Facet-Dependent Enzyme-Mimetic Activity of V2O5 Nanomaterials, *Angew. Chem., Int. Ed.*, 2018, **57**, 4510–4515, DOI: 10.1002/anie.201800681.

130 H. Hou, X. Zeng and X. Zhang, Production of Hydrogen Peroxide by Photocatalytic Processes, *Angew. Chem., Int. Ed.*, 2020, **59**, 17356–17376, DOI: 10.1002/anie.201911609.

131 Y. Isaka, Y. Kawase, Y. Kuwahara, K. Mori and H. Yamashita, Two-Phase System Utilizing Hydrophobic Metal–Organic Frameworks (MOFs) for Photocatalytic Synthesis of Hydrogen Peroxide, *Angew. Chem., Int. Ed.*, 2019, **58**, 5402–5406, DOI: 10.1002/anie.201901961.

132 Y. Kawase, Y. Isaka, Y. Kuwahara, K. Mori and H. Yamashita, Ti cluster-Alkylated hydrophobic MOFs for photocatalytic production of hydrogen peroxide in two-phase systems, *Chem. Commun.*, 2019, **55**, 6743–6746, DOI: 10.1039/c9cc02380a.

133 H. Wang, X. Yuan, Y. Wu, G. Zeng, X. Chen, L. Leng, Z. Wu, L. Jiang and H. Li, Facile synthesis of amino-functionalized titanium metal-organic frameworks and their superior visible-light photocatalytic activity for Cr(VI) reduction, *J. Hazard. Mater.*, 2015, **286**, 187–194, DOI: 10.1016/j.jhazmat.2014.11.039.

134 Y. Gu, Y. N. Wu, L. Li, W. Chen, F. Li and S. Kitagawa, Controllable Modular Growth of Hierarchical MOF-on-MOF Architectures, *Angew. Chem., Int. Ed.*, 2017, **56**, 15658–15662, DOI: 10.1002/anie.201709738.

135 Y. Isaka, Y. Kondo, Y. Kawase, Y. Kuwahara, K. Mori and H. Yamashita, Photocatalytic production of hydrogen peroxide through selective two-electron reduction of dioxygen utilizing amine-functionalized MIL-125 deposited with nickel oxide nanoparticles, *Chem. Commun.*, 2018, **54**, 9270–9273, DOI: 10.1039/c8cc02679c.

136 Y. Zhang, Z. Luo, T. Zhou, H. Huang and H. Tang, Structure determines performance: isomeric Ti-MOFs for photocatalytic synthesis of hydrogen peroxide, *Chem. Commun.*, 2024, **60**, 1920–1923, DOI: **10.1039/d3cc05845j**.

137 J. Qiu, L. Yang, M. Li and J. Yao, Metal nanoparticles decorated MIL-125-NH_2 and MIL-125 for efficient photocatalysis, *Mater. Res. Bull.*, 2019, **112**, 297–306, DOI: **10.1016/j.materresbull.2018.12.038**.

138 J. N. Choe, X. Yang, J. H. Yu, K. J. Jang, M. B. Kim and K. C. An, Visible- light responsive PPynt@NH2-MIL-125 nanocomposite for efficient reduction of Cr(VI), *Colloids Surf., A*, 2022, **636**, 128147, DOI: **10.1016/j.colsurfa.2021.128147**.

139 Y. Fu, M. Tan, Z. Guo, D. Hao, Y. Xu, H. Du, C. Zhang, J. Guo, Q. Li and Q. Wang, Fabrication of wide-spectra-responsive NA/NH2-MIL-125(Ti) with boosted activity for Cr(VI) reduction and antibacterial effects, *Chem. Eng. J.*, 2023, **452**, 139417, DOI: **10.1016/j.cej.2022.139417**.

140 Y. Fu, D. Sun, Y. Chen, R. Huang, Z. Ding, X. Fu and Z. Li, An Amine–Functionalized Titanium Metal–Organic Framework Photocatalyst with Visible–Light–Induced Activity for CO_2 Reduction, *Angew. Chem.*, 2012, **124**, 3420–3423, DOI: **10.1002/ange.201108357**.

141 Y. Fu, H. Yang, R. Du, G. Tu, C. Xu, F. Zhang, M. Fan and W. Zhu, Enhanced photocatalytic CO2 reduction over Co-doped NH2-MIL-125(Ti) under visible light, *RSC Adv.*, 2017, **7**, 42819–42825, DOI: **10.1039/c7ra06324e**.

142 S. Chen, G. Hai, H. Gao, X. Chen, A. Li, X. Zhang and W. Dong, Modulation of the charge transfer behavior of Ni(II)-doped NH2-MIL-125(Ti): Regulation of Ni ions content and enhanced photocatalytic CO2 reduction performance, *Chem. Eng. J.*, 2021, **406**, 42819–42825, DOI: **10.1016/j.cej.2020.126886**.

143 H. Wang, Q. Zhang, J. J. Li, J. Y. Zhang, Y. Liu, M. Zhou, N. Zhang, Y. Z. Fang and Q. Ke, The covalent Coordination-driven Bi2S3@NH2-MIL-125(Ti)-SH heterojunction with boosting photocatalytic CO2 reduction and dye degradation performance, *J. Colloid Interface Sci.*, 2022, **606**, 1745–1757, DOI: **10.1016/j.jcis.2021.08.135**.

144 J. Zhou, Q. Jia, L. Gong, S. Zhang, X. Zhou and H. Song, Enhanced Z-scheme ZnS/NH2−MIL-125(Ti) photocatalysts with biomass-derived carbon quantum dots for CO2 reduction, *Mol. Catal.*, 2024, **552**, 113715, DOI: **10.1016/j.mcat.2023.113715**.

145 J. O. Olowoyo, U. Saini, M. Kumar, H. Valdés, H. Singh, M. O. Omorogie, J. O. Babalola, A. V. Vorontsov, U. Kumar and P. G. Smirniotis, Reduced graphene oxide/NH2-MIL-125(Ti) composite: Selective CO2photoreduction to methanol under visible light and computational insights into charge separation, *J. CO2 Util.*, 2020, **42**, 101300, DOI: **10.1016/j.jcou.2020.101300**.

146 Q. Jia, J. Zhou, L. Gong, L. Wang, X. Ma and Y. Zhao, Z-scheme heterostructure of Cu2O/Pt/NH2-MIL-125(Ti) for photocatalytic CO2 reduction, *Mol. Catal.*, 2022, **530**, 112599, DOI: **10.1016/j.mcat.2022.112599**.

147 Y. Huang, D. Wei, Z. Li, Y. Mao, Y. Huang, B. Jin, X. Luo and Z. Liang, A highly efficient and stable TiO2@NH2-MIL-125 material for enhanced photocatalytic conversion of CO2 and CH4, *Sep. Purif. Technol.*, 2023, **310**, 123174, DOI: **10.1016/j.seppur.2023.123174**.

148 H. Huang, X. S. Wang, D. Philo, F. Ichihara, H. Song, Y. Li, D. Li, T. Qiu, S. Wang and J. Ye, Toward visible-light-assisted photocatalytic nitrogen fixation: A titanium metal organic framework with functionalized ligands, *Appl. Catal., B*, 2020, **267**, 118686, DOI: **10.1016/j.apcatb.2020.118686**.

149 Z. Hou, Y. Wang, X. Zhao, J. Qiu, G. Liu, Y. Zhang, X. Wu, Y. Wang and L. Wang, Synergistic Effect of bimetallic active sites on NH2-MIL-125 for promoting photocatalytic conversion of nitrogen to NH3, **https://ssrn.com/abstract=4752135**.

150 Y. Zhou, X. Zhao, Q. Liang, M. Zhou, X. Li, S. Xu and Z. Li, In situ growth of CdIn2S4 on NH2-MIL-125 as efficient photocatalysts for H2 production under visible-light irradiation, *J. Phys. Chem. Solids*, 2023, **173**, 111096, DOI: **10.1016/j.jpcs.2022.111096**.

151 X. Zhang, Z. Chen, Y. Luo, X. Han, Q. Jiang, T. Zhou, H. Yang and J. Hu, Construction of NH2-MIL-125(Ti)/CdS Z-scheme heterojunction for efficient photocatalytic H2 evolution, *J. Hazard. Mater.*, 2021, **405**, 124128, DOI: **10.1016/j.jhazmat.2020.124128**.

152 M. Zhang, K. Li, Z. Yin, Z. Zhang, Q. Luo, B. Tang, G. Yu, T. Hu and S. Shan, Unique ternary Pd/NH2-MIL-125/CdIn2S4 composite expands the absorption range of visible light and improves H2 evolution efficiency, *J. Environ. Chem. Eng.*, 2024, **12**, 111640, DOI: **10.1016/j.jece.2023.111640**.

153 H. Liu, J. Zhang and D. Ao, Construction of heterostructured ZnIn2S4@NH2-MIL-125(Ti) nanocomposites for visible-light-driven H2 production, *Appl. Catal., B*, 2018, **221**, 433–442, DOI: **10.1016/j.apcatb.2017.09.043**.

154 S. Zhang, M. Du, Z. Xing, Z. Li, K. Pan and W. Zhou, Defect-rich and electron-rich mesoporous Ti-MOFs based NH2-MIL-125(Ti)@ZnIn2S4/CdS hierarchical tandem heterojunctions with improved charge separation and enhanced solar-driven photocatalytic performance, *Appl. Catal., B*, 2020, **262**, 118202, DOI: **10.1016/j.apcatb.2019.118202**.

155 S. Liu, X. Jiang, G. I. N. Waterhouse, Z. M. Zhang and L. min Yu, A novel Z-scheme NH2-MIL-125(Ti)/Ti3C2 QDs/ZnIn2S4 photocatalyst with fast interfacial electron transfer properties for visible light-driven antibiotic degradation and hydrogen evolution, *Sep. Purif. Technol.*, 2022, **294**, 121094, DOI: **10.1016/j.seppur.2022.121094**.

156 T. N. Nguyen, S. Kampouri, B. Valizadeh, W. Luo, D. Ongari, O. M. Planes, A. Züttel, B. Smit and K. C. Stylianou, Photocatalytic Hydrogen Generation from a Visible-Light-Responsive Metal-Organic Framework System: Stability versus Activity of Molybdenum Sulfide Cocatalysts, *ACS Appl. Mater. Interfaces*, 2018, **10**, 30035–30039, DOI: **10.1021/acsami.8b10010**.

157 S. Kampouri, T. N. Nguyen, M. Spodaryk, R. G. Palgrave, A. Züttel, B. Smit and K. C. Stylianou, Concurrent Photocatalytic Hydrogen Generation and Dye Degradation Using NH2-MIL-125 under Visible Light Irradiation, *Adv. Funct. Mater.*, 2018, **28**, 1806368, DOI: **10.1002/adfm.201806368**.

158 B. Zhang, J. Zhang, X. Tan, D. Shao, J. Shi, L. Zheng, J. Zhang, G. Yang and B. Han, NH2-MIL-125@TiO2 Core-Shell Particles Produced by a Post-Solvothermal Route for High-Performance Photocatalytic H2 Production, *ACS Appl. Mater. Interfaces*, 2018, **10**, 16418–16423, DOI: **10.1021/acsami.8b01462**.

159 S. Li, Y. Fang, J. Mu, X. Sun, H. He, Y. Cao and B. Liu, Photocatalytic removal of Cr(VI) and efficient degradation of tetracycline by oxygen-enriched vacancy pie-like NH2-MIL-125(Ti), *Colloids Surf., A*, 2024, **680**, 132734, DOI: **10.1016/j.colsurfa.2023.132734**.

160 H. Hu, J. Jin, M. Xu, C. Xu, Y. Cheng, W. Ji, Z. Ding, M. Shao and Y. Wan, Novel Z-scheme Bi3O4Br/NH2-MIL-125(Ti) composite for efficient photocatalytic degradation of tetracycline, *Opt. Mater.*, 2023, **135**, 113262, DOI: **10.1016/j.optmat.2022.113262**.

161 V. Muelas-Ramos, M. J. Sampaio, C. G. Silva, J. Bedia, J. J. Rodriguez, J. L. Faria and C. Belver, Degradation of diclofenac in water under LED irradiation using combined g-C3N4/NH2-MIL-125 photocatalysts, *J. Hazard. Mater.*, 2021, **416**, 126199, DOI: **10.1016/j.jhazmat.2021.126199**.

162 H. A. Younes, M. Taha, R. Khaled, H. M. Mahmoud and R. M. Abdelhameed, Perovskite/metal-organic framework photocatalyst: A novel nominee for eco-friendly uptake of pharmaceuticals from wastewater, *J. Alloys Compd.*, 2023, **930**, 167322, DOI: **10.1016/j.jallcom.2022.167322**.

163 L. Yuan, C. Zhang, Y. Zou, T. Bao, J. Wang, C. Tang, A. Du, C. Yu and C. Liu, A S-Scheme MOF-on-MOF Heterostructure, *Adv. Funct. Mater.*, 2023, **33**, 2214627, DOI: **10.1002/adfm.202214627**.

164 T. Gao, H. Zhang, X. Zhao, S. Xiao, Z. Zhang and S. Yu, Efficient removal of tetracycline from MOF-on-MOF heterojunctions driven by visible light: Evaluation of photocatalytic mechanisms and degradation pathway, *Appl. Surf. Sci.*, 2024, **651**, 159227, DOI: **10.1016/j.apsusc.2023.159227**.

165 X. Zheng, Y. Li, J. Yang and S. Cui, Z-Scheme heterojunction Ag/NH2-MIL-125(Ti)/CdS with enhanced photocatalytic activity for ketoprofen degradation: Mechanism and intermediates, *Chem. Eng. J.*, 2021, **422**, 130105, DOI: **10.1016/j.cej.2021.130105**.

166 Z. Zhang, C. Xu, X. Xiong, C. Wang, Q. Zhang, Z. Fan and Y. Wang, Controlled fabrication of Au@NH2-MIL-125(Ti)/CdS with enhanced photocatalytic ability for the degradation of MB, *J. Alloys Compd.*, 2023, **934**, 167910, DOI: **10.1016/j.jallcom.2022.167910**.

167 R. Nivetha, K. Gothandapani, V. Raghavan, G. Jacob, R. Sellapan, A. M. Kannan, S. Pitchaimuthu, S. Pandiaraj, A. H. Almuqrin, A. Alodhayb, M. Muthuramamoorthy, Q. Van Le, S. K. Jeong and A. N. Grace, NH2-MIL-125(Ti) doped CdS/Graphene composite as electro and photo catalyst in basic medium under light irradiation, *Environ. Res.*, 2021, **200**, 111719, DOI: **10.1016/j.envres.2021.111719**.

168 Y. Zhang, W. Cao, B. Zhu, J. Cai, X. Li, J. Liu, Z. Chen, M. Li and L. Zhang, Fabrication of NH2-MIL-125(Ti) nanodots on carbon fiber/MoS2-based weavable photocatalysts for boosting the adsorption and photocatalytic performance, *J. Colloid Interface Sci.*, 2022, **611**, 706–717, DOI: **10.1016/j.jcis.2021.12.073**.

169 S. R. Zhu, P. F. Liu, M. K. Wu, W. N. Zhao, G. C. Li, K. Tao, F. Y. Yi and L. Han, Enhanced photocatalytic performance of BiOBr/NH_2-MIL-125(Ti) composite for dye degradation under visible light, *Dalton Trans.*, 2016, **45**, 17521–17529, DOI: **10.1039/c6dt02912d**.

170 B. Fu, H. Sun, J. Liu, T. Zhou, M. Chen, Z. Cai, D. Hao and X. Zhu, Construction of NH2-MIL-125@BiVO4Composites for Efficient Photocatalytic Dye Degradation, *ACS Omega*, 2022, **7**, 26201–26210, DOI: **10.1021/acsomega.2c01862**.

171 R. M. Abdelhameed, D. M. Tobaldi and M. Karmaoui, Engineering highly effective and stable nanocomposite photocatalyst based on NH2-MIL-125 encirclement with Ag3PO4 nanoparticles, *J. Photochem. Photobiol., A*, 2018, **351**, 50–58, DOI: **10.1016/j.jphotochem.2017.10.011**.

172 H. E. Emam, H. B. Ahmed, E. Gomaa, M. H. Helal and R. M. Abdelhameed, Doping of silver vanadate and silver tungstate nanoparticles for enhancement the photocatalytic activity of NH2-MIL-125 in dye degradation, *J. Photochem. Photobiol., A*, 2019, **383**, 111986, DOI: **10.1016/j.jphotochem.2019.111986**.

173 D. Wu and L. Han, Fabrication of novel Ag/AgBr/NH2-MIL-125(Ti) nanocomposites with enhanced visible-light photocatalytic activity, *Mater. Res. Express*, 2019, **6**, 125501, DOI: **10.1088/2053-1591/ab540a**.

174 W. C. Hsiao, C. H. Tseng and C. W. Huang, A facile reflux method to produce ternary CQDs/P25/NH2–MIL-125 for photocatalytic degradation of methylene blue under simulated solar light, *J. Taiwan Inst. Chem. Eng.*, 2024, **154**, 105286, DOI: **10.1016/j.jtice.2023.105286**.

175 P. Zhang, Z. Wang, L. Zhao, L. Li, N. Li, X. Su and Q. Su, Construction of a novel 0D–3D boron nitride quantum dots /NH2-MIL-125(Ti) composite for photodegradation of Rhodamine B, *Mater. Sci. Semicond. Process.*, 2023, **167**, 107793, DOI: **10.1016/j.mssp.2023.107793**.

176 S. Kato, J. Jung, T. Suenobu and S. Fukuzumi, Production of hydrogen peroxide as a sustainable solar fuel from water and dioxygen, *Energy Environ. Sci.*, 2013, **6**, 3756–3764, DOI: **10.1039/c3ee42815j**.

177 D. Tsukamoto, A. Shiro, Y. Shiraishi, Y. Sugano, S. Ichikawa, S. Tanaka and T. Hirai, Photocatalytic H_2O_2 production from ethanol/O_2 system using TiO_2 loaded with Au-Ag bimetallic alloy nanoparticles, *ACS Catal.*, 2012, **2**, 599–603, DOI: **10.1021/cs2006873**.

178 H. Hirakawa, S. Shiota, Y. Shiraishi, H. Sakamoto, S. Ichikawa and T. Hirai, Au Nanoparticles Supported on

BiVO4: Effective Inorganic Photocatalysts for H_2O_2 Production from Water and O2 under Visible Light, *ACS Catal.*, 2016, **6**, 4976–4982, DOI: **10.1021/acscatal.6b01187**.

179 Y. Xie, Y. Li, Z. Huang, J. Zhang, X. Jia, X. S. Wang and J. Ye, Two types of cooperative nitrogen vacancies in polymeric carbon nitride for efficient solar-driven H_2O_2 evolution, *Appl. Catal., B*, 2020, **265**, 118581, DOI: **10.1016/j.apcatb.2019.118581**.

180 Y. Zhang, M. Xu, H. Li, H. Ge and Z. Bian, The enhanced photoreduction of Cr(VI) to Cr(III) using carbon dots coupled TiO2 mesocrystals, *Appl. Catal., B*, 2018, **226**, 213–219, DOI: **10.1016/j.apcatb.2017.12.053**.

181 J. J. Testa, M. A. Grela and M. I. Litter, Experimental evidence in favor of an initial one-electron-transfer process in the heterogeneous photocatalytic reduction of chromium(VI) over TiO2, *Langmuir*, 2002, **17**, 3515–3517, DOI: **10.1021/la010100y**.

182 J. J. Testa, M. A. Grela and M. I. Litter, Heterogeneous Photocatalytic Reduction of Chromium(VI) over TiO_2 Particles in the Presence of Oxalate: Involvement of Cr(V) Species, *Environ. Sci. Technol.*, 2004, **38**, 1589–1594, DOI: **10.1021/es0346532**.

183 D. Chen and A. K. Ray, *Removal of toxic metal ions from wastewater by semiconductor photocatalysis*, 2001.

184 M. Valari, A. Antoniadis, D. Mantzavinos and I. Poulios, Photocatalytic reduction of Cr(VI) over titania suspensions, *Catal. Today*, 2015, **252**, 190–194, DOI: **10.1016/j.cattod.2014.10.014**.

185 J. Di, J. Xia, M. F. Chisholm, J. Zhong, C. Chen, X. Cao, F. Dong, Z. Chi, H. Chen, Y. X. Weng, J. Xiong, S. Z. Yang, H. Li, Z. Liu and S. Dai, Defect-Tailoring Mediated Electron–Hole Separation in Single-Unit-Cell Bi3O4Br Nanosheets for Boosting Photocatalytic Hydrogen Evolution and Nitrogen Fixation, *Adv. Mater.*, 2019, **31**, 1807576, DOI: **10.1002/adma.201807576**.

186 J. Di, C. Zhu, M. Ji, M. Duan, R. Long, C. Yan, K. Gu, J. Xiong, Y. She, J. Xia, H. Li and Z. Liu, Defect-Rich Bi12O17Cl2 Nanotubes Self-Accelerating Charge Separation for Boosting Photocatalytic CO2 Reduction, *Angew. Chem., Int. Ed.*, 2018, **57**, 14847–14851, DOI: **10.1002/anie.201809492**.

187 Y. Li, L. Ding, Z. Liang, Y. Xue, H. Cui and J. Tian, Synergetic effect of defects rich MoS2 and Ti3C2 MXene as cocatalysts for enhanced photocatalytic H2 production activity of TiO2, *Chem. Eng. J.*, 2020, **383**, 123178, DOI: **10.1016/j.cej.2019.123178**.

188 G. Mo, L. Wang and J. Luo, Controlled thermal treatment of NH2-MIL-125(Ti) for drastically enhanced photocatalytic reduction of Cr(VI), *Sep. Purif. Technol.*, 2021, **277**, 119643, DOI: **10.1016/j.seppur.2021.119643**.

189 F. J. Rodriguez, L. A. García de la Rosa, A. Alatorre, J. Ibañez, L. Godinez, S. Gutierrez and P. Herrasti, Analysis of the effect of polypyrrole synthesis conditions on its capacity to reduce hexavalent chromium, *Prog. Org. Coat.*, 2007, **60**, 297–302, DOI: **10.1016/j.porgcoat.2007.07.031**.

190 X. Gao, G. Huang, H. Gao, C. Pan, H. Wang, J. Yan, Y. Liu, H. Qiu, N. Ma and J. Gao, Facile fabrication of Bi2S3/SnS2 heterojunction photocatalysts with efficient photocatalytic activity under visible light, *J. Alloys Compd.*, 2016, **674**, 98–108, DOI: **10.1016/j.jallcom.2016.03.031**.

191 J. Zhou, Z. Zhang, X. Kong, F. He, R. Zhao, R. Wu, T. Wei, L. Wang and J. Feng, A novel P-N heterojunction with staggered energy level based on ZnFe2O4 decorating SnS2 nanosheet for efficient photocatalytic degradation, *Appl. Surf. Sci.*, 2020, **510**, 145442, DOI: **10.1016/j.apsusc.2020.145442**.

192 C. Liu, Z. Dong, C. Yu, J. Gong, Y. Wang, Z. Zhang and Y. Liu, Study on photocatalytic performance of hexagonal SnS2/g-C3N4 nanosheets and its application to reduce U (VI) in sunlight, *Appl. Surf. Sci.*, 2021, **537**, 147754, DOI: **10.1016/j.apsusc.2020.147754**.

193 L. Sun, S. Dong, S. Chen, H. Chen, M. Luan and T. Huang, Efficient reduction of hexavalent chromium by nubbly mesoporous NH2-MIL-125(Ti)/SnS2 Z-scheme heterostructures with enhanced visible photocatalytic activity, *J. Environ. Chem. Eng.*, 2023, **11**, 110192, DOI: **10.1016/j.jece.2023.110192**.

194 I. Ganesh, Conversion of carbon dioxide into methanol - A potential liquid fuel: Fundamental challenges and opportunities (a review), *Renewable Sustainable Energy Rev.*, 2014, **31**, 221–257, DOI: **10.1016/j.rser.2013.11.045**.

195 R. N. Compton, P. W. Reinhardt and C. D. Cooper, Collisional ionization of Na, K, and Cs by CO2, COS, and CS_2: Molecular electron affinities, *J. Chem. Phys.*, 1975, **63**, 3821–3827, DOI: **10.1063/1.431875**.

196 A. Corma and H. Garcia, Photocatalytic reduction of CO2 for fuel production: Possibilities and challenges, *J. Catal.*, 2013, **308**, 168–175, DOI: **10.1016/j.jcat.2013.06.008**.

197 C. C. Yang, J. Vernimmen, V. Meynen, P. Cool and G. Mul, Mechanistic study of hydrocarbon formation in photocatalytic CO2 reduction over Ti-SBA-15, *J. Catal.*, 2011, **284**, 1–8, DOI: **10.1016/j.jcat.2011.08.005**.

198 J. Mao, T. Peng, X. Zhang, K. Li and L. Zan, Selective methanol production from photocatalytic reduction of CO_2 on $BiVO_4$ under visible light irradiation, *Catal. Commun.*, 2012, **28**, 38–41, DOI: **10.1016/j.catcom.2012.08.008**.

199 S. Wang and X. Wang, Photocatalytic CO2 reduction by CdS promoted with a zeolitic imidazolate framework, *Appl. Catal., B*, 2015, **162**, 494–500, DOI: **10.1016/j.apcatb.2014.07.026**.

200 E. Karamian and S. Sharifnia, On the general mechanism of photocatalytic reduction of CO2, *J. CO_2 Util.*, 2016, **16**, 194–203, DOI: **10.1016/j.jcou.2016.07.004**.

201 R. R. Ikreedeegh and M. Tahir, Indirect Z-scheme heterojunction of NH2-MIL-125(Ti) MOF/g-C3N4nanocomposite with RGO solid electron mediator for efficient photocatalytic CO2reduction to CO and CH4, *J. Environ. Chem. Eng.*, 2021, **9**, 105600, DOI: **10.1016/j.jece.2021.105600**.

202 H. Hirakawa, M. Hashimoto, Y. Shiraishi and T. Hirai, Photocatalytic Conversion of Nitrogen to Ammonia with

Water on Surface Oxygen Vacancies of Titanium Dioxide, *J. Am. Chem. Soc.*, 2017, **139**, 10929–10936, DOI: **10.1021/jacs.7b06634**.

203 S. Kaur, S. Sharma and S. K. Kansal, Synthesis of ZnS/CQDs nanocomposite and its application as a photocatalyst for the degradation of an anionic dye, ARS, *Superlattices Microstruct.*, 2016, **98**, 86–95, DOI: **10.1016/j.spmi.2016.08.011**.

204 P. Baláž, M. Baláž, E. Dutková, A. Zorkovská, J. Kováč, P. Hronec, J. Kováč, M. Čaplovičová, J. Mojžiš, G. Mojžišová, A. Eliyas and N. G. Kostova, CdS/ZnS nanocomposites: From mechanochemical synthesis to cytotoxicity issues, *Mater. Sci. Eng., C*, 2016, **58**, 1016–1023, DOI: **10.1016/j.msec.2015.09.040**.

205 N. Dixit, J. V. Vaghasia, S. S. Soni, M. Sarkar, M. Chavda, N. Agrawal and H. P. Soni, Photocatalytic activity of Fe doped ZnS nanoparticles and carrier mediated ferromagnetism, *J. Environ. Chem. Eng.*, 2015, **3**, 1691–1701, DOI: **10.1016/j.jece.2015.06.010**.

206 M. Li, L. X. Zhong, W. Chen, Y. Huang, Z. Chen, D. Xiao, R. Zou, L. Chen, Q. Hao, Z. Liu, R. Sun and X. Peng, Regulating the electron–hole separation to promote selective oxidation of biomass using ZnS@Bi2S3 nanosheet catalyst, *Appl. Catal., B*, 2021, **292**, 120180, DOI: **10.1016/j.apcatb.2021.120180**.

207 F. Guo, Y. P. Wei, S. Q. Wang, X. Y. Zhang, F. M. Wang and W. Y. Sun, Pt nanoparticles embedded in flowerlike NH2-UiO-68 for enhanced photocatalytic carbon dioxide reduction, *J. Mater. Chem. A*, 2019, **7**, 26490–26495, DOI: **10.1039/c9ta10575a**.

208 W. Chen, J. Xiong, Z. Wen, R. Chen and G. Cheng, Synchronistic embedding of oxygen vacancy and Ag nanoparticles into potholed TiO2 nanoparticles-assembly for collaboratively promoting photocatalytic CO2 reduction, *Mol. Catal.*, 2023, **542**, 113138, DOI: **10.1016/j.mcat.2023.113138**.

209 L. Wang, N. Zuo, M. Sun, Y. Ma, N. Mominou, W. Jiang, S. Li and C. Jing, Deep desulfurization and denitrogenation of diesel fuel over Ir/Pr-N-CQDs-TiO2 under ultraviolet radiation, *Sep. Purif. Technol.*, 2021, **272**, 118861, DOI: **10.1016/j.seppur.2021.118861**.

210 J. Zhao, Y. Liu, Y. Wang, Y. Lian, Q. Wang, Q. Yang, D. Wang, G. J. Xie, G. Zeng, Y. Sun, X. Li and B. J, Ni, Clarifying the Role of Free Ammonia in the Production of Short-Chain Fatty Acids from Waste Activated Sludge Anaerobic Fermentation, *ACS Sustainable Chem. Eng.*, 2018, **6**, 14104–14113, DOI: **10.1021/acssuschemeng.8b02670**.

211 S. Ghosh, I. Calizo, D. Teweldebrhan, E. P. Pokatilov, D. L. Nika, A. A. Balandin, W. Bao, F. Miao and C. N. Lau, Extremely high thermal conductivity of graphene: Prospects for thermal management applications in nanoelectronic circuits, *Appl. Phys. Lett.*, 2008, **92**, DOI: **10.1063/1.2907977**.

212 A. K. Geim and K. S. Novoselov, The rise of graphene, **https://www.nature.com/naturematerials**.

213 W. Wang, P. Serp, P. Kalck and J. L. Faria, Visible light photodegradation of phenol on MWNT-TiO2 composite catalysts prepared by a modified sol-gel method, *J. Mol. Catal. A: Chem.*, 2005, **235**, 194–199, DOI: **10.1016/j.molcata.2005.02.027**.

214 E. T. Thostenson, Z. Ren and T.-W. Chou, Advances in the science and technology of carbon nanotubes and their composites: a review, **https://www.elsevier.com/locate/compscitech**.

215 K. I. Bolotin, K. J. Sikes, Z. Jiang, M. Klima, G. Fudenberg, J. Hone, P. Kim and H. L. Stormer, Ultrahigh electron mobility in suspended graphene, *Solid State Commun.*, 2008, **146**, 351–355, DOI: **10.1016/j.ssc.2008.02.024**.

216 A. A. Balandin, S. Ghosh, W. Bao, I. Calizo, D. Teweldebrhan, F. Miao and C. N. Lau, Superior thermal conductivity of single-layer graphene, *Nano Lett.*, 2008, **8**, 902–907, DOI: **10.1021/nl0731872**.

217 Z. Liu, J. T. Robinson, X. Sun and H. Dai, PEGylated nanographene oxide for delivery of water-insoluble cancer drugs, *J. Am. Chem. Soc.*, 2008, **130**, 10876–10877, DOI: **10.1021/ja803688x**.

218 Q. Wang, X. Chen, K. Yu, Y. Zhang and Y. Cong, Synergistic photosensitized removal of Cr(VI) and Rhodamine B dye on amorphous TiO2 under visible light irradiation, *J. Hazard. Mater.*, 2013, **246–247**, 135–144, DOI: **10.1016/j.jhazmat.2012.12.017**.

219 J. Hu, J. Ding and Q. Zhong, In situ fabrication of amorphous TiO2/NH2-MIL-125(Ti) for enhanced photocatalytic CO2 into CH4 with H_2O under visible-light irradiation, *J. Colloid Interface Sci.*, 2020, **560**, 857–865, DOI: **10.1016/j.jcis.2019.11.003**.

220 I. H. Tseng, L. H. Kang, P. Y. Chang, M. H. Tsai, J. M. Yeh and T. I. Yang, Biomimetic Polyimide-Supported Cuprous Oxide Photocatalytic Film with Tunable Hydrophobicity, Improved Thermal Stability, and Photocatalytic Activity toward CO2 Reduction, *ACS Omega*, 2019, **4**, 1636–1644, DOI: **10.1021/acsomega.8b03247**.

221 X. M. Cheng, X. Y. Dao, S. Q. Wang, J. Zhao and W. Y. Sun, Enhanced Photocatalytic CO2 Reduction Activity over NH2-MIL-125(Ti) by Facet Regulation, *ACS Catal.*, 2021, **11**, 650–658, DOI: **10.1021/acscatal.0c04426**.

222 X. M. Cheng, P. Wang, S. Q. Wang, J. Zhao and W. Y. Sun, Ti(IV)-MOF with Specific Facet-Ag Nanoparticle Composites for Enhancing the Photocatalytic Activity and Selectivity of CO2Reduction, *ACS Appl. Mater. Interfaces*, 2022, **14**, 32350–32359, DOI: **10.1021/acsami.2c05037**.

223 F. Guo, M. Yang, R. X. Li, Z. Z. He, Y. Wang and W. Y. Sun, Nanosheet-Engineered NH2-MIL-125 with Highly Active Facets for Enhanced Solar CO2Reduction, *ACS Catal.*, 2022, **12**, 9486–9493, DOI: **10.1021/acscatal.2c02789**.

224 X. M. Cheng, Y. Gu, X. Y. Zhang, X. Y. Dao, S. Q. Wang, J. Ma, J. Zhao and W. Y. Sun, Crystallographic facet heterojunction of NH2-MIL-125(Ti) for carbon dioxide photoreduction, *Appl. Catal., B*, 2021, **298**, 120524, DOI: **10.1016/j.apcatb.2021.120524**.

225 X. M. Cheng, X. Y. Zhang, X. Y. Dao, S. Q. Wang, J. Zhao and W. Y. Sun, High-index facets exposed on metal–organic framework for boosting photocatalytic carbon dioxide reduction, *Chem. Eng. J.*, 2022, **431**, 134125, DOI: 10.1016/j.cej.2021.134125.

226 M. H. Vu, M. Sakar and T. O. Do, Insights into the recent progress and advanced materials for photocatalytic nitrogen fixation for ammonia (NH3) production, *Catalysts*, 2018, **8**, 621, DOI: 10.3390/catal8120621.

227 L. M. Azofra, N. Li, D. R. Macfarlane and C. Sun, Promising prospects for 2D d2-d4 M3C2 transition metal carbides (MXenes) in N2 capture and conversion into ammonia, *Energy Environ. Sci.*, 2016, **9**, 2545–2549, DOI: 10.1039/c6ee01800a.

228 S. X. Wu, Z. C. Gao, L. Y. Li, W. J. Gao, Y. Q. Huang and J. Yang, High-efficient visible light photocatalytic degradation by nano-Ag-doped NH2-MIL-125(Ti) composites, *Inorg. Chim. Acta*, 2023, **544**, 121233, DOI: 10.1016/j.ica.2022.121233.

229 H. Li, J. Zhang, X. Deng, Y. Wang, G. Meng, R. Liu, J. Huang, M. Tu, C. Xu, Y. Peng, B. Wang and Y. Hou, Structure and Defect Engineering Synergistically Boost High Solar-to-Chemical Conversion Efficiency of Cerium oxide/Au Hollow Nanomushrooms for Nitrogen Photofixation, *Angew. Chem., Int. Ed.*, 2024, **63**, e202316384, DOI: 10.1002/anie.202316384.

230 Y. Shi, A. F. Yang, C. S. Cao and B. Zhao, Applications of MOFs: Recent advances in photocatalytic hydrogen production from water, *Coord. Chem. Rev.*, 2019, **390**, 50–75, DOI: 10.1016/j.ccr.2019.03.012.

231 X. Fang, Q. Shang, Y. Wang, L. Jiao, T. Yao, Y. Li, Q. Zhang, Y. Luo and H. L. Jiang, Single Pt Atoms Confined into a Metal–Organic Framework for Efficient Photocatalysis, *Adv. Mater.*, 2018, **30**, 1705112, DOI: 10.1002/adma.201705112.

232 C. Acar, I. Dincer and G. F. Naterer, Review of photocatalytic water-splitting methods for sustainable hydrogen production, *Int. J. Energy Res.*, 2016, **40**, 1449–1473, DOI: 10.1002/er.3549.

233 B. B. Kale, J. O. Baeg, S. M. Lee, H. Chang, S. J. Moon and C. W. Lee, CdIn2S4 nanotubes and "marigold" nanostructures: A visible-light photocatalyst, *Adv. Funct. Mater.*, 2006, **16**, 1349–1354, DOI: 10.1002/adfm.200500525.

234 A. Bhirud, N. Chaudhari, L. Nikam, R. Sonawane, K. Patil, J. O. Baeg and B. Kale, Surfactant tunable hierarchical nanostructures of $CdIn2S_4$ and their photohydrogen production under solar light, *Int. J. Hydrogen Energy*, 2011, **36**, 11628–11639, DOI: 10.1016/j.ijhydene.2011.06.061.

235 D. Song, J. Bae, H. Ji, M.-B. Kim, Y.-S. Bae, K. S. Park, D. Moon and N. C. Jeong, Coordinative Reduction of Metal Nodes Enhances the Hydrolytic Stability of a Paddlewheel Metal-Organic Framework Coordinative Reduction of Metal Nodes Enhances the Hydrolytic Stability of a Paddlewheel Metal-Organic Framework, 2019. https://pubs.acs.org.

236 A. Gómez-Avilés, M. Peñas-Garzón, J. Bedia, D. D. Dionysiou, J. J. Rodríguez and C. Belver, Mixed Ti-Zr metal-organic-frameworks for the photodegradation of acetaminophen under solar irradiation, *Appl. Catal., B*, 2019, **253**, 253–262, DOI: 10.1016/j.apcatb.2019.04.040.

237 X. Li, C. Garlisi, Q. Guan, S. Anwer, K. Al-Ali, G. Palmisano and L. Zheng, A review of material aspects in developing direct Z-scheme photocatalysts, *Mater. Today*, 2021, **47**, 75–107, DOI: 10.1016/j.mattod.2021.02.017.

238 P. Zhou, J. Yu and M. Jaroniec, All-solid-state Z-scheme photocatalytic systems, *Adv. Mater.*, 2014, **26**, 4920–4935, DOI: 10.1002/adma.201400288.

239 L. Biswal, R. Mohanty, S. Nayak and K. Parida, Review on MXene/TiO2 nanohybrids for photocatalytic hydrogen production and pollutant degradations, *J. Environ. Chem. Eng.*, 2022, **10**, 107211, DOI: 10.1016/j.jece.2022.107211.

240 K. Li, S. Zhang, Y. Li, J. Fan and K. Lv, MXenes as noble-metal-alternative co-catalysts in photocatalysis, *Chin. J. Catal.*, 2020, **42**, 3–14, DOI: 10.1016/S1872-2067(20)63630-0.

241 D. Wang, B. Su, Y. Jiang, L. Li, B. K. Ng, Z. Wu and F. Liu, Polytype 1T/2H MoS2 heterostructures for efficient photoelectrocatalytic hydrogen evolution, *Chem. Eng. J.*, 2017, **330**, 102–108, DOI: 10.1016/j.cej.2017.07.126.

242 Y. Yu, G. H. Nam, Q. He, X. J. Wu, K. Zhang, Z. Yang, J. Chen, Q. Ma, M. Zhao, Z. Liu, F. R. Ran, X. Wang, H. Li, X. Huang, B. Li, Q. Xiong, Q. Zhang, Z. Liu, L. Gu, Y. Du, W. Huang and H. Zhang, High phase-purity 1T′-MoS2- and 1T′-MoSe2-layered crystals, *Nat. Chem.*, 2018, **10**, 638–643, DOI: 10.1038/s41557-018-0035-6.

243 X. Chen, Y. K. Bai, X. Shen, H. J. Peng and Q. Zhang, Sodiophilicty/potassiophilicity chemistry in sodium/potassium metal anodes, *J. Energy Chem.*, 2020, **51**, 1–6, DOI: 10.1016/j.jechem.2020.03.051.

244 K. Meyer, S. Bashir, J. Llorca, H. Idriss, M. Ranocchiari and J. A. van Bokhoven, Photocatalyzed Hydrogen Evolution from Water by a Composite Catalyst of NH2-MIL-125(Ti) and Surface Nickel(II) Species, *Chem. – Eur. J.*, 2016, **22**, 13894–13899, DOI: 10.1002/chem.201601988.

245 J. Ding, X. Li, L. Chen, X. Zhang, S. Sun, J. Bao, C. Gao and X. Tian, Au-Pt alloy nanoparticles site-selectively deposited on CaIn2S4 nanosteps as efficient photocatalysts for hydrogen production, *J. Mater. Chem. A*, 2016, **4**, 12630–12637, DOI: 10.1039/c6ta04468a.

246 X. Wei, C. Shao, X. Li, N. Lu, K. Wang, Z. Zhang and Y. Liu, Facile: In situ synthesis of plasmonic nanoparticles-decorated g-C3N4/TiO2 heterojunction nanofibers and comparison study of their photosynergistic effects for efficient photocatalytic H2 evolution, *Nanoscale*, 2016, **8**, 11034–11043, DOI: 10.1039/c6nr01491g.

247 A. K. Singh and Q. Xu, Synergistic Catalysis over Bimetallic Alloy Nanoparticles, *ChemCatChem*, 2013, **5**, 652–676, DOI: 10.1002/cctc.201200591.

248 J. Xu, J. Gao, C. Wang, Y. Yang and L. Wang, NH2-MIL-125 (Ti)/graphitic carbon nitride heterostructure decorated with NiPd co-catalysts for efficient photocatalytic hydrogen production, *Appl. Catal., B*, 2017, **219**, 101–108, DOI: 10.1016/j.apcatb.2017.07.046.

249 T. Velempini, E. Prabakaran and K. Pillay, Recent developments in the use of metal oxides for photocatalytic degradation of pharmaceutical pollutants in water—a review, *Mater. Today Chem.*, 2021, **19**, 100380, DOI: 10.1016/j.mtchem.2020.100380.

250 K. Qin, Q. Zhao, H. Yu, X. Xia, J. Li, S. He, L. Wei and T. An, A review of bismuth-based photocatalysts for antibiotic degradation: Insight into the photocatalytic degradation performance, pathways and relevant mechanisms, *Environ. Res.*, 2021, **199**, 111360, DOI: 10.1016/j.envres.2021.111360.

251 Y. Li, Y. Fu and M. Zhu, Green synthesis of 3D tripyramid TiO2 architectures with assistance of aloe extracts for highly efficient photocatalytic degradation of antibiotic ciprofloxacin, *Appl. Catal., B*, 2020, **260**, 118149, DOI: 10.1016/j.apcatb.2019.118149.

252 X. Chen, J. Yao, B. Xia, J. Gan, N. Gao and Z. Zhang, Influence of pH and DO on the ofloxacin degradation in water by UVA-LED/TiO2 nanotube arrays photocatalytic fuel cell: mechanism, ROSs contribution and power generation, *J. Hazard. Mater.*, 2020, **383**, 121220, DOI: 10.1016/j.jhazmat.2019.121220.

253 I. B. S. Will, J. E. F. Moraes, A. C. S. C. Teixeira, R. Guardani and C. A. O. Nascimento, Photo-Fenton degradation of wastewater containing organic compounds in solar reactors, *Sep. Purif. Technol.*, 2004, **34**, 51–57, DOI: 10.1016/S1383-5866(03)00174-6.

254 M. H. Habibi and H. Vosooghian, Photocatalytic degradation of some organic sulfides as environmental pollutants using titanium dioxide suspension, *J. Photochem. Photobiol., A*, 2005, **174**, 45–52, DOI: 10.1016/j.jphotochem.2005.02.012.

255 S. Bustos-Guadarrama, A. Nieto-Maldonado, L. Z. Flores-López, H. Espinoza-Gomez and G. Alonso-Nuñez, Photocatalytic degradation of azo dyes by ultra-small green synthesized silver nanoparticles, *J. Taiwan Inst. Chem. Eng.*, 2023, **142**, 104663, DOI: 10.1016/j.jtice.2022.104663.

256 M. Gao, Y. Song, Y. Liu, W. Jiang, J. Peng, L. Shi, R. Jia, Y. Muhammad and L. Huang, Controlled fabrication of Au@MnO_2 core/shell assembled nanosheets by localized surface plasmon resonance, *Appl. Surf. Sci.*, 2021, **537**, 147912, DOI: 10.1016/j.apsusc.2020.147912.

257 J. Liu, H. Lin, Y. He, Y. Dong, E. Rose and G. Y. Menzembere, Novel CoS2/MoS2@Zeolite with excellent adsorption and photocatalytic performance for tetracycline removal in simulated wastewater, *J. Cleaner Prod.*, 2020, **260**, 121047, DOI: 10.1016/j.jclepro.2020.121047.

258 F. Meng, J. Li, S. K. Cushing, M. Zhi and N. Wu, Solar hydrogen generation by nanoscale p-n junction of p-type molybdenum disulfide/n-type nitrogen-doped reduced graphene oxide, *J. Am. Chem. Soc.*, 2013, **135**, 10286–10289, DOI: 10.1021/ja404851s.

259 Y. Li, L. Huang, B. Li, X. Wang, Z. Zhou, J. Li and Z. Wei, Co-nucleus 1D/2D Heterostructures with Bi2S3 Nanowire and MoS2 Monolayer: One-Step Growth and Defect-Induced Formation Mechanism, *ACS Nano*, 2016, **10**, 8938–8946, DOI: 10.1021/acsnano.6b04952.

260 L. Pan, J. Liu and J. Shi, Intranuclear photosensitizer delivery and photosensitization for enhanced photodynamic therapy with ultralow irradiance, *Adv. Funct. Mater.*, 2014, **24**, 7318–7327, DOI: 10.1002/adfm.201402255.

261 W. Zhao, J. Li, B. Dai, Z. Cheng, J. Xu, K. Ma, L. Zhang, N. Sheng, G. Mao, H. Wu, K. Wei and D. Y. C. Leung, Simultaneous removal of tetracycline and Cr(VI) by a novel three-dimensional AgI/BiVO4 p-n junction photocatalyst and insight into the photocatalytic mechanism, *Chem. Eng. J.*, 2019, **369**, 716–725, DOI: 10.1016/j.cej.2019.03.115.

262 Y. Sang, X. Cao, G. Dai, L. Wang, Y. Peng and B. Geng, Facile one-pot synthesis of novel hierarchical Bi2O3/Bi2S3 nanoflower photocatalyst with intrinsic p-n junction for efficient photocatalytic removals of RhB and Cr(VI), *J. Hazard. Mater.*, 2020, **381**, 120942, DOI: 10.1016/j.jhazmat.2019.120942.

263 S. R. Zhu, P. F. Liu, M. K. Wu, W. N. Zhao, G. C. Li, K. Tao, F. Y. Yi and L. Han, Enhanced photocatalytic performance of BiOBr/NH2-MIL-125(Ti) composite for dye degradation under visible light, *Dalton Trans.*, 2016, **45**, 17521–17529, DOI: 10.1039/c6dt02912d.

264 Q. Hu, J. Di, B. Wang, M. Ji, Y. Chen, J. Xia, H. Li and Y. Zhao, *In situ* preparation of NH_2-MIL-125(Ti)/BiOCl composite with accelerating charge carriers for boosting visible light photocatalytic activity, *Appl. Surf. Sci.*, 2019, **466**, 525–534, DOI: 10.1016/j.apsusc.2018.10.020.

265 A. Qayum, J. Wei, Q. Li, D. Chen, X. Jiao and Y. Xia, Efficient decontamination of multi-component wastewater by hydrophilic electrospun PAN/AgBr/Ag fibrous membrane, *Chem. Eng. J.*, 2019, **361**, 1255–1263, DOI: 10.1016/j.cej.2018.12.161.

266 C. Tang, H. Bai, L. Liu, X. Zan, P. Gao, D. D. Sun and W. Yan, A green approach assembled multifunctional Ag/AgBr/TNF membrane for clean water production & disinfection of bacteria through utilizing visible light, *Appl. Catal., B*, 2016, **196**, 57–67, DOI: 10.1016/j.apcatb.2016.05.023.

267 M. Rana, B. Hao, L. Mu, L. Chen and P. C. Ma, Development of multi-functional cotton fabrics with Ag/AgBr-TiO2 nanocomposite coating, *Compos. Sci. Technol.*, 2016, **122**, 104–112, DOI: 10.1016/j.compscitech.2015.11.016.

268 J. Dai, Y. Sun and Z. Liu, Efficient degradation of tetracycline in aqueous solution by Ag/AgBr catalyst under solar irradiation, *Mater. Res. Express*, 2019, **6**, 085512, DOI: 10.1088/2053-1591/ab1db3.

269 X. Yan, X. Wang, W. Gu, M. M. Wu, Y. Yan, B. Hu, G. Che, D. Han, J. Yang, W. Fan and W. Shi, Single-crystalline AgIn(MoO4)2 nanosheets grafted Ag/AgBr composites with enhanced plasmonic photocatalytic activity for degradation of tetracycline under visible light, *Appl. Catal., B*, 2015, **164**, 297–304, DOI: 10.1016/j.apcatb.2014.09.046.

270 Q. Wang, G. Wang, X. Liang, X. Dong and X. Zhang, Supporting carbon quantum dots on NH_2-MIL-125 for enhanced photocatalytic degradation of organic pollutants under a broad spectrum irradiation, *Appl. Surf. Sci.*, 2019, **467–468**, 320–327, DOI: 10.1016/j.apsusc.2018.10.165.

271 Q. Liu, C. Hu and X. Wang, One-pot solvothermal synthesis of water-soluble boron nitride nanosheets and fluorescent boron nitride quantum dots, *Mater. Lett.*, 2019, **234**, 306–310, DOI: 10.1016/j.matlet.2018.09.031.

272 E. Budak, S. Aykut, M. E. Paşaoğlu and C. Ünlü, Microwave assisted synthesis of boron and nitrogen rich graphitic quantum dots to enhance fluorescence of photosynthetic pigments, *Mater. Today Commun.*, 2020, **24**, 100975, DOI: 10.1016/j.mtcomm.2020.100975.

273 X. Yu, L. Wang and S. M. Cohen, Photocatalytic metal-organic frameworks for organic transformations, *CrystEngComm*, 2017, **19**, 4126–4136, DOI: 10.1039/c7ce00398f.

274 P. Wu, C. He, J. Wang, X. Peng, X. Li, Y. An and C. Duan, Photoactive chiral metal-organic frameworks for light-driven asymmetric α-alkylation of aldehydes, *J. Am. Chem. Soc.*, 2012, **134**, 14991–14999, DOI: 10.1021/ja305367j.

275 C. Wang, Z. Xie, K. E. Dekrafft and W. Lin, Doping metal-organic frameworks for water oxidation, carbon dioxide reduction, and organic photocatalysis, *J. Am. Chem. Soc.*, 2011, **133**, 13445–13454, DOI: 10.1021/ja203564w.

276 X. Zhao, Y. Zhang, P. Wen, G. Xu, D. Ma and P. Qiu, NH2-MIL-125(Ti)/TiO2 composites as superior visible-light photocatalysts for selective oxidation of cyclohexane, *Mol. Catal.*, 2018, **452**, 175–183, DOI: 10.1016/j.mcat.2018.04.004.

277 S. Gao, W. Cen, Q. Li, J. Li, Y. Lu, H. Wang and Z. Wu, A mild one-step method for enhancing optical absorption of amine-functionalized metal-organic frameworks, *Appl. Catal., B*, 2018, **227**, 190–197, DOI: 10.1016/j.apcatb.2018.01.007.

278 G. Lu, X. Huang, Y. Li, G. Zhao, G. Pang and G. Wang, Covalently integrated core-shell MOF@COF hybrids as efficient visible-light-driven photocatalysts for selective oxidation of alcohols, *J. Energy Chem.*, 2020, **43**, 8–15, DOI: 10.1016/j.jechem.2019.07.014.

279 T. Toyao, M. Saito, Y. Horiuchi, K. Mochizuki, M. Iwata, H. Higashimura and M. Matsuoka, Efficient hydrogen production and photocatalytic reduction of nitrobenzene over a visible-light-responsive metal-organic framework photocatalyst, *Catal. Sci. Technol.*, 2013, **3**, 2092–2097, DOI: 10.1039/c3cy00211j.

280 Y. Fu, L. Sun, H. Yang, L. Xu, F. Zhang and W. Zhu, Visible-light-induced aerobic photocatalytic oxidation of aromatic alcohols to aldehydes over Ni-doped NH2-MIL-125(Ti), *Appl. Catal., B*, 2016, **187**, 212–217, DOI: 10.1016/j.apcatb.2016.01.038.

281 D. Sun, L. Ye and Z. Li, Visible-light-assisted aerobic photocatalytic oxidation of amines to imines over NH2-MIL-125(Ti), *Appl. Catal., B*, 2015, **164**, 428–432, DOI: 10.1016/j.apcatb.2014.09.054.

282 S. Abedi and A. Morsali, Improved photocatalytic activity in a surfactant-assisted synthesized Ti-containing MOF photocatalyst under blue LED irradiation, *New J. Chem.*, 2015, **39**, 931–937, DOI: 10.1039/c4nj01536c.

283 Q. Xu, Y. Wang, G. Jin, D. Jin, K. Li, A. Mao and X. Hu, Photooxidation assisted sensitive detection of trace Mn^{2+} in tea by NH2-MIL-125 (Ti) modified carbon paste electrode, *Sens. Actuators, B*, 2014, **201**, 274–280, DOI: 10.1016/j.snb.2014.05.017.

284 D. Jin, A. Gong and H. Zhou, Visible-light-activated photoelectrochemical biosensor for the detection of the pesticide acetochlor in vegetables and fruit based on its inhibition of glucose oxidase, *RSC Adv.*, 2017, **7**, 17489–17496, DOI: 10.1039/C7RA00164A.

285 X. Lian and B. Yan, A postsynthetic modified MOF hybrid as heterogeneous photocatalyst for α-phenethyl alcohol and reusable fluorescence sensor, *Inorg. Chem.*, 2016, **55**, 11831–11838, DOI: 10.1021/acs.inorgchem.6b01928.

286 D. Jin, Q. Xu, L. Yu and X. Hu, Photoelectrochemical detection of the herbicide clethodim by using the modified metal-organic framework amino-MIL-125(Ti)/TiO2, *Microchim. Acta*, 2015, **182**, 1885–1892, DOI: 10.1007/s00604-015-1505-9.